TÉCNICO LISBOA

Phenomenology of the minimal inverse-seesaw model with Abelian flavour symmetries

Henrique Pedro Fernandes de Noronha Brito Câmara

Thesis to obtain the Master of Science Degree in

Engineering Physics

Supervisors: Prof. Doutor Filipe Rafael Joaquim
Prof. Doutor Ricardo González Felipe

Examination Committee

Chairperson: Prof. Doutor Mário João Martins Pimenta
Supervisor: Prof. Doutor Filipe Rafael Joaquim
Member of the Committee: Prof.ª Doutora Maria Margarida Nesbitt Rebelo da Silva

December 2020

"Ce monde en lui-même n'est pas raisonnable,
c'est tout ce qu'on peut en dire.
Mais ce qui est absurde,
c'est la confrontation de cet irrationnel et
de ce désir éperdu de clarté
dont l'appel résonne au plus profond de l'homme. "

Albert Camus, Le mythe de Sisyphe (1942)

Acknowledgments

First and foremost, I would like to thank my supervisors, Professors Filipe Rafael Joaquim and Ricardo González Felipe. For their unconditional support, patience and the fact that they were always there, without exception, to answer my questions and provide constructive feedback. This helped me to learn and improve my knowledge in the world of particle physics research and, ultimately, pushed me to perform this work to the best of my abilities.

I am additionally indebted to *Fundação para a Ciência e Tecnologia* (FCT, Portugal) for the financial support through the *Centro de Física Teórica de Partículas* (CFTP) projects UIDB/00777/2020 and UIDP/00777/2020.

I thank my parents and family, for their support and encouragement. For allowing me to pursue my passion for Physics without boundaries.

Last but not least, I thank my friends for listening to my monologues about Physics. For the moments we had together in this utterly immense Universe.

Resumo

O Modelo Padrão da física de partículas descreve com uma precisão notável múltiplos fenómenos relacionados com as interações entre os constituintes fundamentais da matéria. Porém, as observações das oscilações de neutrinos implicam a existência de neutrinos massivos e mistura leptónica, os quais têm de ser explicados em extensões do Modelo Padrão.

Nesta tese, consideramos uma implementação a baixa escala do mecanismo de *seesaw*. De facto, realizamos um estudo aprofundado do cenário mínimo do *inverse seesaw* constituído por dois "neutrinos de direita" e dois singletos fermiónicos estéreis. Começamos por uma análise de texturas de zero para determinar os conjuntos de matrizes de massas de leptões maximamente restritivas compatíveis com os dados das oscilações de neutrinos. De seguida, trabalhando com um sector escalar mínimo composto por dois dubletos de Higgs e dois escalares neutros complexos, conseguimos implementar alguns dos conjuntos de texturas através de simetrias Abelianas de sabor. Para as texturas realizáveis dedicamos o restante deste trabalho aos estudos fenomenológicos. Começamos por mostrar que a violação espontânea de CP é possível e que é comunicada com sucesso ao sector leptónico, o que fornece uma origem comum para os efeitos de violação de CP leptónicos no modelo, codificados nas fases de CP de Majorana e de Dirac. Adicionalmente, estudamos diversos processos de violação do sabor leptónico, sendo obtidas as regiões de exclusão estabelecidas por limites experimentais atuais, bem como as sensibilidades projetadas por futuras procuras. Finalmente, consideram-se constrangimentos experimentais adicionais traduzidos em termos da mistura entre neutrinos leves e pesados.

Palavras-chave: Física de neutrinos; *inverse seesaw*; texturas zero; simetrias Abelianas de sabor; violação espontânea de CP; violação do sabor leptónico.

Abstract

The Standard Model of particle physics describes with remarkable precision numerous phenomena related to the interactions amongst the fundamental constituents of matter. However, the observations of neutrino oscillations imply the existence of massive neutrinos and lepton mixing, which must be accounted through extensions of the Standard Model.

In this thesis, we consider a low-scale implementation of the seesaw mechanism. In fact, we perform a thorough study of the minimal inverse seesaw scenario containing two "right-handed neutrinos" and two sterile fermion singlets. We start with a texture-zero analysis in order to determine the maximally-restrictive sets of lepton mass matrices compatible with neutrino oscillation data. Next, working within the framework of a minimal scalar sector composed of two Higgs doublets and two complex neutral scalar singlets, we are able to realise some of the texture sets through Abelian flavour symmetries. For these realisable sets we dedicate the rest of this work to phenomenological studies. We start by showing that spontaneous CP violation is possible and can be successfully communicated to the lepton sector. This provides a common origin for leptonic CPV effects in the model encoded in the Majorana and Dirac CP phases. Additionally, we study several lepton flavour-violating processes to obtain the exclusion regions set by the current experimental limits as well as the projected sensitivities of future searches. Lastly, we consider additional experimental constraints translated in terms of active-sterile mixing.

Keywords: Neutrino physics; inverse seesaw; texture zeros; Abelian flavour symmetries; spontaneous CP violation; Lepton flavour violation.

Contents

List of Tables

List of Figures

List of Abbreviations

2HDM	Two-Higgs-doublet model
BR	Branching ratio
BSM	Beyond the standard model
CC	Charged current
CKM	Cabibbo-Kobayashi-Maskawa
CL	Confidence level
cLFV	Charged lepton flavour violation
CP	Charge-conjugation and parity
CPV	Charge-conjugation and parity violation
CR	Conversion rate
EW	Electroweak
EWSB	Electroweak symmetry breaking
EWPD	Electroweak precision data
FCNC	Flavour changing neutral current
GUT	Grand unified theory
H.c.	Hermitian conjugate
IO	Inverted ordering
ISS	Inverse seesaw
LCPV	Leptonic charge-conjugation and parity violation
LFV	Lepton flavour violation
LH	Left-handed
LHC	Large hadron collider
LNV	Lepton number violation
NC	Neutral current
NO	Normal ordering
RH	Right-handed
SCPV	Spontaneous charge-conjugation and parity violation
SM	Standard Model
SNF	Smith normal form
SSB	Spontaneous symmetry breaking
VEV	Vacuum expectation value

Chapter 1

Introduction

The last missing piece of the Standard Model (SM) of particle physics [1–3], the famous Higgs boson [4], was discovered in 2012 by the ATLAS and CMS collaborations at the CERN Large Hadron Collider (LHC). This further reaffirmed the success of the SM which describes the electromagnetic (EM), weak and strong interactions amongst the fundamental constituents of matter. From an elegant theoretical framework, the SM allows to explain with remarkable precision a substantial number of phenomena and has successfully stood the tests of numerous experiments. However, the picture does not end here, and the work moving forward for particle physicists is an endless journey of understanding the surrounding phenomena in the Universe. In fact, some theoretical aspects lack explanation within the SM, for example, the strong charge-conjugation and parity (CP) problem, the colour confinement in quantum chromodynamics (QCD), the hierarchy problem, the number of fermion generations and hierarchy among their different masses, the origin of symmetries, the *flavour puzzle*, and the list goes on. Furthermore, there is experimental evidence pointing to new physics, namely, the amount of dark matter/energy, the baryon asymmetry of the Universe or matter-antimatter asymmetry, and the phenomenon of neutrino oscillations [5, 6] that imply massive neutrinos and lepton mixing. From the theoretical viewpoint, addressing these questions requires going beyond the SM (BSM) scope.

The numerous neutrino oscillation experiments performed in the last decades have measured neutrino observables with increased precision, among which the mass-squared differences and the mixing angles parameterising the lepton mixing matrix. Several global data analyses of oscillation phenomena in a three-neutrino mixing scheme [7–9] are able to establish up to date best-fit values for these observables. These analyses take into account experiments with a variety of neutrinos sources, namely, the solar, atmospheric, reactor and accelerator neutrinos. The implications of these experiments is the existence of at least two massive active neutrinos and lepton mixing, constituting evidence of BSM physics. Nevertheless, oscillation experiments cannot provide information on the absolute neutrino mass scale nor the mass ordering, which remain unknown. Moreover, neutrino masses are six orders of magnitude smaller than the mass of the electron, making them abnormally small. Since neutrinos are the only known neutral fermions, they can possibly be their own antiparticle, as proposed by Ettore Majorana in 1937 [10], while the remaining fermions are Dirac particles. This question is still unanswered and searches for the

lepton number violating (LNV) process of neutrinoless double beta decay [11] aim at determining the nature of neutrinos. Furthermore, controversial results from current neutrino oscillation experiments like LSND [12] and MiniBooNE [13] may be hinting at the existence of sterile neutrinos with masses in the eV range. To accommodate all data, more general active-sterile neutrino mixing schemes would then be required. This inspired several analyses of oscillation data beyond the three-neutrino paradigm (see, for instance, Refs. [14–18]).

The most popular extensions of the SM providing an appealing and elegant framework for the explanation of neutrino masses and lepton mixing are those based on the so-called seesaw mechanisms [11, 19–32]. In these models, new particles with a typical mass scale Λ are introduced. Depending on the magnitude of Λ, one can have high-energy models with $\Lambda \gg v$, where v is the electroweak (EW) scale, or low-energy scenarios allowing $\Lambda \simeq v$. As an example of the former type, in the canonical Type-I seesaw scenario [19–23], very heavy right-handed (RH) neutrinos with masses near the grand unified theory (GUT) scale or unnaturally tiny Yukawa couplings are required to generate small neutrino masses, leaving aside any viable experimental search for direct new physics signals. In this work we will focus on the latter type of models and specifically on the so-called inverse seesaw (ISS) [30–32]. In this case, neutrino mass suppression is triggered by small LNV mass parameters. Hence, the lightness of neutrinos stems from an approximate lepton-number symmetry which is restored when those parameters are set to zero. Therefore, the ISS provides a natural neutrino-mass generation mechanism in the 't Hooft sense [33]. A crucial feature of the ISS (not shared by the canonical type I seesaw) is that small Majorana neutrino masses can be generated with RH neutrino masses at the TeV scale (or below) and $\mathcal{O}(1)$ Yukawa coupling parameters. As a result, the mixing between the (active) light neutrinos and the new (sterile) states can be sizeable for sterile neutrino masses lying not far from the EW scale. The presence of new neutral fermions interacting with SM leptons and gauge bosons motivates phenomenological studies BSM, making the ISS a perfect theoretical framework to guide new physics probes. In particular, experimental searches for charged lepton flavour violating (cLFV) processes like $\mu \to e\gamma$ [34, 35], $\mu \to eee$ [36] and $\mu - e$ conversion in nuclei [37–41] have been studied in the ISS framework [42–49] with the purpose of understanding at which extent our current knowledge on those processes is able to constrain the ISS parameter space. Depending on their masses and mixing with the SM degrees of freedom, sterile neutrinos may also lead to interesting signals potentially observable at the LHC, as well as at other experiments sensitive to new physics effects induced by the presence of those particles [50–54]. As turns out, it is possible to construct several ISS low-scale models that are compatible with neutrino oscillation data and, simultaneously, satisfy all phenomenological constraints. In particular, it has been shown that the minimal ISS realisation corresponds to extending the SM with two RH neutrinos and two sterile singlet fermions [43], to which we will refer as the ISS(2,2) model.

A longstanding and challenging issue in particle physics is the lack of a guiding principle to explain the flavour structure of the SM, i.e., the observed fermion mass spectra and mixing patterns. This *flavour puzzle* provides a strong motivation for building models with additional particle content and extended continuous and/or discrete symmetries. Once such symmetries are explicitly or spontaneously broken, they will lead to the required fermion mass and mixing structures. Several frameworks have been put

forward to tackle this puzzle (for reviews on neutrino mass and mixing models see e.g. [55–59]). One of the simplest approaches consists on the implementation of texture zeros in the Yukawa coupling and mass matrices, imposed by continuous U(1) and/or discrete $\mathbb{Z}_N$ transformations (see, for instance, Refs. [60–72]). In the SM extended with RH neutrinos, the realisation of texture zeros with such symmetries is not compatible with data since, in general, they lead to massless charged leptons, massless neutrinos or vanishing lepton mixing angles [72, 73]. This is due to the fact that all fermions in the SM couple to the same Higgs field. Thus, enlarging the Higgs sector is a viable solution to surmount this difficulty, being the two-Higgs doublet model (2HDM) [74] the most economical one.

Inspired by the above ideas, in this work we consider the ISS(2,2) within the 2HDM supplemented with Abelian symmetries to ensure maximal predictability, i.e., to impose the most constraining flavour structure, so that the charged-lepton masses and current neutrino data can be accommodated, while fulfilling all relevant phenomenological constraints. This can be realised by adding to the scalar sector of the SM another scalar doublet and two complex scalar singlets which, upon spontaneous symmetry breaking, generate all relevant mass terms required to implement the ISS(2,2). Moreover, we will show that CP can be spontaneously broken by the complex vacuum expectation value (VEV) of one of the singlets, and that such CP violation (CPV) can be communicated to the neutrino sector via neutrino-scalar interactions.

The thesis is organised as follows. In Chapter 2, we start by briefly reviewing the main aspects of the SM, focusing on the EW sector and show its limitations in what concerns neutrino masses and lepton mixing. Furthermore, we discuss the description for massive Majorana neutrinos and lepton mixing and we present the neutrino oscillation observables as well as the experimental constraints on the effective Majorana mass. Additionally, we succinctly describe the Type-I, II and III canonical seesaw mechanisms as minimal extensions of the SM that tackle neutrino masses and mixing. In Chapter 3, we build the minimal ISS model to which this thesis is dedicated. We start by reviewing general aspects of the ISS mechanism, paying special attention to the comparison between the effective and full treatment of neutrino masses and mixing. The most restrictive flavour structures for the mass matrices in the ISS(2,2) framework are then identified in Section 3.2.1 by performing a systematic search of all possible texture-zero combinations leading to low-energy neutrino parameters compatible with global analyses of neutrino oscillation data. After setting the successful cases, in Section 3.2.2 we select those which can be realised by Abelian horizontal symmetries. The phenomenological analysis is presented in Chapter 4. In Section 4.1, we analyse leptonic CPV where spontaneous CPV (SCPV) is considered and the relation between the Dirac and Majorana phases is established in light of present neutrino data. Predictions for the effective neutrino mass parameter relevant for neutrinoless double beta decay are also discussed in that section. The impact of radiative corrections on light-neutrino masses is analysed in Section 4.2, while the constraints imposed by cLFV decays on the model parameter space are investigated in Section 4.3. Possibilities of testing the ISS(2,2) with Abelian flavour symmetries at other experiments as, for instance, the LHC, future colliders, beam-dump experiments and cLFV searches are discussed in Section 4.4. Finally, our concluding remarks are presented in Chapter 5. Details regarding the scalar sector and the computations of cLFV decay rates are collected in the appendices.

Chapter 2

Neutrino masses in minimal extensions of the Standard Model

In this chapter, we briefly introduce the SM, focusing on the EW sector. We then address its limitations with regard to neutrino masses and lepton mixing, which requires to extend the SM, amongst which are the canonical seesaw models.

2.1 The Standard Model of particle physics

The SM of particle physics was constructed through the work of many physicists during the second half of the 20^{th} century. In 1954, Yang and Mills [75] pioneered work on non-Abelian theories, which are the fundamental mathematical building blocks of the SM. The unification of the electromagnetic (EM) and weak interactions was first proposed by S.L. Glashow in 1961 [1]. A few years later, in 1964-66, the famous Brout-Englert-Higgs (BEH) mechanism [76–79] was formulated and it was shown that spontaneous symmetry breaking (SSB) of a local gauge symmetry could generate massive vector bosons together with massless unphysical scalars, the so-called Nambu-Golstone bosons [80–83], ensuring gauge invariance. In 1967-68, S. Weinberg and A. Salam [2, 3] implemented the BEH mechanism in a non-Abelian gauge theory of EW interactions based on the $\mathrm{SU}(2)_L \times \mathrm{U}(1)_Y$ group. Furthermore, the quark model was proposed independently by Gell-Mann and Zweig in 1964 [84, 85], addressing some properties of hadrons and strong interactions. Finally, the renomalisability of the theory of EW interactions was proved in 1971-72 by 't Hooft and Veltman [86, 87]. Hence, these various ground-breaking works constitute the SM, one of the greatest achievements in theoretical physics, whose wide acceptance was established throughout the years due to numerous experiments that successfully tested the model.

2.1.1 Particle content and electroweak interactions

The SM is a non-abelian gauge quantum field theory (QFT) based on the symmetry group

$$G_{\text{SM}} = \mathrm{SU}(3)_c \times \mathrm{SU}(2)_L \times \mathrm{U}(1)_Y, \tag{2.1}$$

described by the following Lagrangian locally invariant under $G_{\rm SM}$,

$$\mathcal{L}_{\rm SM} = \mathcal{L}_{\rm QCD} + \mathcal{L}_{\rm Gauge} + \mathcal{L}_{\rm fermions} + \mathcal{L}_{\Phi} + \mathcal{L}_{\rm gf} + \mathcal{L}_{\rm Yuk.}. \tag{2.2}$$

In Eq. (2.1), $\mathrm{SU}(3)_c$ corresponds to the strong interactions with c standing for colour. Invariance under this group requires the introduction of eight gluons G^a_μ $(a = 1, ..., 8)$ one for each group generator. The associated QFT is QCD, whose interactions are described by $\mathcal{L}_{\rm QCD}$. Throughout the work in this thesis we will focus on leptons. Therefore, we will analyse the EW sector of the SM, being interested only in the remaining terms in $\mathcal{L}_{\rm SM}$. The corresponding gauge group is $\mathrm{SU}(2)_L \otimes \mathrm{U}(1)_Y$, where L stands for left-handedness and Y is the hypercharge. Invariance under this group requires the introduction of four EW gauge bosons: three W^i_μ $(i = 1, 2, 3)$ for $\mathrm{SU}(2)_L$ and one B_μ for $\mathrm{U}(1)_Y$.

In contrast to the gauge bosons, the number of fermions and scalars are not fixed by $G_{\rm SM}$; they are instead determined empirically. In the SM, we have three generations of fermions, comprised of quarks and leptons. Fermion fields ψ are Dirac spinors, decomposable in their chiral left-handed (LH) and right-handed (RH) components as

$$\psi = \psi_L + \psi_R = P_L\ \psi + P_R\ \psi, \tag{2.3}$$

where $P_{L,R} = (1 \mp \gamma_5)/2$ are the chiral projectors. Additionally, there is only one scalar doublet in the theory that generates all the masses of the particles. All fields transform under the SM gauge group, namely quarks transform as triplets **3** under $\mathrm{SU}(3)_c$, all LH fermions q_L, ℓ_L and the Higgs doublet Φ are organised in doublets **2** of $\mathrm{SU}(2)_L$, while RH fermions q_R, e_R are singlets **1** of $\mathrm{SU}(2)_L$. These fields are given by

$$q_{\alpha L} = \begin{pmatrix} u_{\alpha L} \\ d_{\alpha L} \end{pmatrix}\ ,\ \begin{matrix} u_{\alpha R} = u_R, c_R, t_R \\ d_{\alpha R} = d_R, s_R, b_R \end{matrix}\ ;\ \ell_{\alpha L} = \begin{pmatrix} \nu_{\alpha L} \\ e_{\alpha L} \end{pmatrix}\ ,\ e_{\alpha R} = e_R, \mu_R, \tau_R\ ;\ \Phi = \begin{pmatrix} \phi^+ \\ \phi^0 \end{pmatrix}. \tag{2.4}$$

Local gauge invariance is ensured by replacing the ordinary derivative ∂_μ by the covariant derivative

$$D_\mu = \partial_\mu - ig'\frac{Y}{2}B_\mu - ig\sum_{i=1}^{3}\frac{\tau_i}{2}W^i_\mu\,, \tag{2.5}$$

where g' and g are the coupling constants associated to the $\mathrm{U}(1)_Y$ and $\mathrm{SU}(2)_L$ groups, respectively. The generators of these groups are respectively $Y/2$ and $T_i = \tau_i/2$ with τ_i $(i = 1, 2, 3)$ being the Pauli matrices. We now proceed to write the covariant derivative in terms of the physical gauge fields $W^\pm$, Z and A. First, using the raising and lowering operators $T_\pm = (T_1 \pm iT_2)/\sqrt{2}$ of SU(2) we define

$$W^\pm_\mu = \frac{1}{\sqrt{2}}\left(W^1_\mu \mp iW^2_\mu\right) \to T_1W^1_\mu + T_2W^2_\mu = T_+W^+_\mu + T_-W^-_\mu. \tag{2.6}$$

Additionally, the unphysical fields W^3_μ and B_μ mix among themselves through the Weinberg angle θ_W

defined as

$$\tan\theta_W = -\frac{g'}{g}\ ,\ c_W = -\frac{e}{g'}\ ,\ s_W = \frac{e}{g}, \tag{2.7}$$

where e is the electric charge of the positron, $c_W = \cos\theta_W$ and $s_W = \sin\theta_W$. This enables to relate W^3_μ and B_μ to the physical bosons Z_μ and A_μ through the rotation

$$\begin{pmatrix} Z_\mu \\ A_\mu \end{pmatrix} = \begin{pmatrix} c_W & s_W \\ -s_W & c_W \end{pmatrix} \begin{pmatrix} W^3_\mu \\ B_\mu \end{pmatrix} \rightarrow g'\frac{Y}{2}B_\mu + gT_3W^3_\mu = -eQA_\mu + \frac{g}{c_W}\left(T_3 - s^2_W Q\right) Z_\mu, \tag{2.8}$$

with Q being the electric charge operator defined through the Gell-Nishijima formula as $Q = T_3 + Y/2$ [88]. Finally, the covariant derivative can be written as

$$D_\mu = \partial_\mu + ieQA_\mu - \frac{ig}{c_W}\left(T_3 - s^2_W Q\right) Z_\mu - ig\left(W^+_\mu T^+ + W^-_\mu T^-\right). \tag{2.9}$$

The matter fields interact with the gauge bosons through the covariant derivative as we will show below. In Table 2.1, we summarise the SM particle content, including the representation of each field under the gauge group and the values for the weak-isospin T, its third component T_3, the hypercharge Y and the charge Q for each matter field.

Having presented the SM particle content and defined the covariant derivative, we now turn our attention to the terms of $\mathcal{L}_{\rm SM}$ in Eq. (2.2). We start with the Lagrangian that encodes the kinetic terms, triple and quartic self-interactions of the gauge bosons given by

$$\mathcal{L}_{\rm Gauge} = -\frac{1}{4}F^{\mu\nu}F_{\mu\nu} - \frac{1}{4}\sum_{i=1}^{3} F^{\mu\nu}_i F^i_{\mu\nu}, \tag{2.10}$$

where

$$F^{\mu\nu} = \partial^\mu B^\nu - \partial^\nu B^\mu\ ,\ F^{\mu\nu}_i = \partial^\mu W^\nu_i - \partial^\nu W^\mu_i + g\sum_{j,k=1}^{3}\epsilon_{ijk}W^\mu_j W^\nu_k. \tag{2.11}$$

Next, the Lagrangian containing the kinetic terms of the fermions and their interactions with the gauge bosons is written as

$$\mathcal{L}_{\rm fermions} = \overline{q_{\alpha L}}\left(i\not{D}\right)q_{\alpha L} + \overline{u_{\alpha R}}\left(i\not{D}\right)u_{\alpha R} + \overline{d_{\alpha R}}\left(i\not{D}\right)d_{\alpha R} + \overline{\ell_{\alpha L}}\left(i\not{D}\right)\ell_{\alpha L} + \overline{e_{\alpha R}}\left(i\not{D}\right)e_{\alpha R}, \tag{2.12}$$

where we use the slashed notation $\not{D} = \gamma^\mu D_\mu$. The above Lagrangian contains the charged-current (CC) and the EM and weak neutral-current (NC) interactions. In the weak-basis, the CC interactions are given by,

$$\mathcal{L}_{\rm CC} = \frac{g}{\sqrt{2}}W^-_\mu\left(\overline{e_\alpha}\gamma^\mu P_L\nu_\alpha + \overline{d_\alpha}\gamma^\mu P_L u_\alpha\right) + \text{H.c.}, \tag{2.13}$$

where H.c. stands for Hermitian conjugate. Notice that the CC interactions are chiral since they involve only LH fields. Furthermore, the NC Lagrangian terms in the weak basis are

$$\mathcal{L}^{\rm EM}_{\rm NC} = -eA_\mu\sum_f Q_f\overline{\psi_f}\gamma^\mu\psi_f, \tag{2.14}$$

Gauge Fields	Rep. in $G_{\rm SM}$			
G_μ	$(\mathbf{8},\mathbf{1},0)$			
W_μ	$(\mathbf{1},\mathbf{3},0)$			
B_μ	$(\mathbf{1},\mathbf{1},0)$			
Matter Fields	**Rep. in $G_{\rm SM}$**	**T**	**T_3**	**Q**
$q_{\alpha L} = \begin{pmatrix} u_{\alpha L} \\ d_{\alpha L} \end{pmatrix}$	$(\mathbf{3},\mathbf{2},1/3)$	$1/2$	$+1/2$ $-1/2$	$+2/3$ $-1/3$
$u_{\alpha R}$	$(\mathbf{3},\mathbf{1},4/3)$	0	0	$+2/3$
$d_{\alpha R}$	$(\mathbf{3},\mathbf{1},-2/3)$	0	0	$-1/3$
$\ell_{\alpha L} = \begin{pmatrix} \nu_{\alpha L} \\ e_{\alpha L} \end{pmatrix}$	$(\mathbf{1},\mathbf{2},-1)$	$1/2$	$+1/2$ $-1/2$	0 -1
$e_{\alpha R}$	$(\mathbf{1},\mathbf{1},-2)$	0	0	-1
$\Phi = \begin{pmatrix} \phi^+ \\ \phi^0 \end{pmatrix}$	$(\mathbf{1},\mathbf{2},1)$	$1/2$	$+1/2$ $-1/2$	$+1$ 0

Table 2.1: Summary of the SM particle content. The representations of each field under $\mathrm{SU}(3)_c$, $\mathrm{SU}(2)_L$ and the hypercharge under $\mathrm{U}(1)_Y$ are respectively indicated in parenthesis. The values for the weak isospin T and its third component T_3 as well as the electric charge Q are presented for each matter field.

$$\mathcal{L}_{\rm NC}^{\rm Weak} = \frac{g}{c_W} Z_\mu \sum_f \overline{\psi_f} \gamma^\mu \left(g_L^f P_L + g_R^f P_R \right) \psi_f \ , \ g_L^f = T_3^f - Q_f s_W^2 \ , \ g_R^f = -Q_f s_W^2, \tag{2.15}$$

where the sum in f is performed over all fermions ψ_f with charge Q_f and third component of weak isospin T_3^f. The Z-boson fermion couplings are $g_{L,R}^f$.

2.1.2 Electroweak symmetry breaking

The scalar sector of the SM is defined by the Higgs Lagrangian

$$\mathcal{L}_\Phi = (D_\mu \Phi)^\dagger (D^\mu \Phi) - V(\Phi) \ , \ V(\Phi) = \mu^2 \Phi^\dagger \Phi + \lambda (\Phi^\dagger \Phi)^2, \tag{2.16}$$

where $V(\Phi)$ is the most general renormalisable scalar potential invariant under G_{SM} that can be constructed with one doublet. In the above expression, μ has mass dimension and the dimensionless quartic coupling λ is positive in order to have a potential bounded from below.

The $\mathrm{SU}(2)_L \otimes \mathrm{U}(1)_Y$ symmetry is not observed in Nature. In fact, only the symmetry of electromagnetism $\mathrm{U}(1)_{\rm EM}$ is conserved. Therefore, $\mathrm{SU}(2)_L \otimes \mathrm{U}(1)_Y$ should be broken down to $\mathrm{U}(1)_{\rm EM}$. This is known as the electroweak symmetry breaking (EWSB), and it takes place when a field acquires a non-zero vacuum expectation value (VEV). Such a field must be a scalar, in order to preserve Lorentz invariance, and electrically neutral not to break the EM symmetry. The SM adopts the simplest possible choice to achieve spontaneous symmetry breaking (SSB) by introducing a single scalar doublet.

The minimum of $V(\Phi)$ for $\mu^2 < 0$ is given by

$$\left\langle \Phi^\dagger \Phi \right\rangle = \frac{v^2}{2} \ , \ v^2 = -\frac{\mu^2}{\lambda} > 0, \tag{2.17}$$

where the VEV v is taken to be real without loss of generality. Before SSB, the theory consists of four massless gauge bosons, each with two transversal polarisation degrees of freedom (d.o.f), and the scalar doublet with four d.o.f. giving a total of twelve d.o.f.. When, SSB of $\mathrm{SU}(2)_L \otimes \mathrm{U}(1)_Y \to \mathrm{U}(1)_{\mathrm{EM}}$ occurs, the neutral scalar field ϕ^0 in Eq. (2.4) acquires a non-zero VEV. Note that, only the charge operator Q, leaves the vaccum invariant. Therefore, the scalar doublet will be composed of three unphysical Nambu-Goldstone bosons $G^\pm$ and G^0 [82, 83] and there will also be one massive real scalar field – the Higgs boson H^0. The unphysical fields will be respectively absorbed in the longitudinal components of the gauge bosons $W^\pm$ and Z, providing them mass, while the photon A remains massless. Hence, we still maintain the same number of physical d.o.f.. This is known as the Brout-Englert-Higgs mechanism.

The scalar doublet can be parameterised as

$$\Phi = \frac{1}{\sqrt{2}} \begin{pmatrix} \sqrt{2} G^+ \\ v + H^0 + i G^0 \end{pmatrix} \ , \ \langle \Phi \rangle = \frac{1}{\sqrt{2}} \begin{pmatrix} 0 \\ v \end{pmatrix}, \tag{2.18}$$

with the value for the VEV being $v \simeq 246.2$ GeV [89]. The scalar potential in Eq. (2.12) encodes the scalar self-interactions, the remaining kinetic term with the covariant derivative describes the interactions between the scalar d.o.f. and the gauge bosons which, after EWSB, yields the following mass terms:

$$\begin{aligned} &\mathcal{L}_\Phi^{\mathrm{mass}} = -\frac{m_{H^0}^2}{2} {H^0}^2 + \frac{M_Z^2}{2} Z_\mu Z^\mu + M_W^2 W_\mu^- W^{+\mu}, \\ &m_{H^0} = \sqrt{-2\mu^2} \ , \ M_Z = \frac{gv}{2c_W} \ , \ M_W = \frac{gv}{2} \to \rho = \frac{M_W^2}{c_W^2 M_Z^2} = 1. \end{aligned} \tag{2.19}$$

Note that the photon has no mass term, thus remaining masseless; the masses of the $W^\pm$ and Z bosons are $M_W \simeq 80.4$ GeV and $M_Z \simeq 91.2$ GeV [89]. The remaining mass term corresponds to the one for the CP-even Higgs boson H^0 discovered at the LHC by the CMS and ATLAS collaborations in 2012 [4] with mass $m_{H^0} \simeq 125.4$ GeV.

The interaction terms involving the Golstone bosons are very important to be able to perform loop calculations in an arbitrary gauge. In fact, the inverse propagator of the photon A is non-invertible and the ones for the Z and $W^\pm$ bosons are invertible, but can only be used in the unitary gauge, which poses some technical problems in loop-diagram calculations, since they can worsen divergences appearing at one-loop level. To solve these problems, the gauge fixing term

$$\begin{aligned} \mathcal{L}_{\mathrm{gf}} = &-\frac{1}{2\xi_A} \left(\partial^\mu A_\mu\right)^2 - \frac{1}{2\xi_Z} \left(\partial^\mu Z_\mu - \xi_Z M_Z G^0\right)^2 \\ &- \frac{1}{\xi_W} \left(\partial^\mu W_\mu^+ - i\xi_W M_W G^+\right) \left(\partial^\nu W_\nu^- + i\xi_W M_W G^-\right), \end{aligned} \tag{2.20}$$

is usually added to the Lagrangian, where $\xi_{A,Z,W}$ are the real and arbitrary R_ξ gauge parameters, essentially acting as Lagrange multipliers. Hence, no physical quantity such as an amplitude computed

for a given observable depends on these parameters. Furthermore, in the Feynman-'t Hooft gauge we set $\xi_{A,Z,W} = 1$.

2.1.3 Fermion masses and mixing

In the SM, a Dirac mass term given by

$$-m_\psi \overline{\psi}\psi = -m_\psi \left(\overline{\psi_L}\psi_R + \overline{\psi_R}\psi_L\right), \tag{2.21}$$

cannot be constructed consistently from gauge principles. In fact, this term is not invariant under $\mathrm{SU}(2)_L \otimes \mathrm{U}(1)_Y$ since it is not a singlet of $\mathrm{SU}(2)_L$ and the LH and RH fermionic fields have different $\mathrm{U}(1)_Y$ hypercharge values. However, it is invariant under $\mathrm{U}(1)_{\mathrm{EM}}$, which hints at the possibility that this term can be generated through SSB. Therefore, we consider the Yukawa interaction terms among the fermion fields and the Higgs doublet

$$-\mathcal{L}_{\mathrm{Yuk.}} = \overline{\ell_L}\mathbf{Y}_\ell \Phi e_R + \overline{q_L}\mathbf{Y}_u \widetilde{\Phi} u_R + \overline{q_L}\mathbf{Y}_d \Phi d_R + \mathrm{H.c.}, \tag{2.22}$$

where $\widetilde{\Phi} = i\tau_2 \Phi^*$. The Yukawa Lagrangian contains the invariant Higgs couplings to the fermions, encoded in the 3×3 arbitrary complex Yukawa coupling matrices $\mathbf{Y}_{\ell,u,d}$. After EWSB, the scalar doublet acquires a non-zero VEV leading in the weak basis to the fermion mass terms

$$-\mathcal{L}_{\mathrm{mass}} = \overline{e_L}\mathbf{M}_\ell e_R + \overline{u_L}\mathbf{M}_u u_R + \overline{d_L}\mathbf{M}_d d_R + \mathrm{H.c.}\ ,\ \mathbf{M}_{\ell,u,d} = \frac{v}{\sqrt{2}}\mathbf{Y}_{\ell,u,d}. \tag{2.23}$$

Notice that it is not possible to construct a Yukawa term for neutrinos, since there are no RH neutrinos in the SM. Thus, **neutrinos are strictly massless in the SM**.

In order to bring the mass matrices to the mass-eigenstate basis, we perform unitary rotations of the quark and charged-lepton fields, such that the matrices are bidiagonalised as,

$$\begin{aligned}
&u_L \to \mathbf{V}_L^u u_L\ ,\ u_R \to \mathbf{V}_R^u u_R \Rightarrow \mathbf{V}_L^{u\dagger}\mathbf{M}_u\mathbf{V}_R^u = \mathrm{diag}\left(m_u, m_c, m_t\right),\\
&d_L \to \mathbf{V}_L^d d_L\ ,\ d_R\ \to \mathbf{V}_R^d d_R \Rightarrow \mathbf{V}_L^{d\dagger}\mathbf{M}_d\mathbf{V}_R^d = \mathrm{diag}\left(m_d, m_s, m_b\right),\\
&e_L \to \mathbf{V}_L e_L\ ,\ e_R \to \mathbf{V}_R e_R\ \Rightarrow\ \mathbf{V}_L^\dagger\mathbf{M}_\ell\mathbf{V}_R = \mathrm{diag}\left(m_e, m_\mu, m_\tau\right),
\end{aligned} \tag{2.24}$$

where all fermion masses are taken to be real and positive, and their present values are given in Ref. [89]. The field rotations above do not affect the NC interactions, ensuring that there are no flavour-changing neutral currents (FCNC) at tree level in the SM. However, in the quark case, the CC interactions will be described by a 3×3 unitary quark-mixing matrix $\mathbf{V}$, such that

$$\mathcal{L}_{\mathrm{CC}} \supset \frac{g}{\sqrt{2}} W_\mu^+ \overline{u}_L \gamma^\mu \mathbf{V} d_L + \mathrm{H.c.}\ ,\ \mathbf{V} = \mathbf{V}_L^{u\dagger}\mathbf{V}_L^d, \tag{2.25}$$

where $\mathbf{V}$ is the Cabibbo-Kobayashi-Maskawa (CKM) matrix [90, 91]. In general, an $n\times n$ unitary matrix depends on n^2 parameters comprised of $n(n-1)/2$ mixing angles and $n(n+1)/2$ phases. Therefore, the

CKM matrix contains *à priori* nine parameters, among which are three mixing angles and six phases. However, not all the phases are physical since we have the freedom to rephase the LH fields without altering the interactions terms. Thanks to this property, we are able to remove five unphysical phases. Hence, we are left with four physical parameters in the quark mixing matrix: three mixing angles θ_{12}, θ_{13}, θ_{23} and a Dirac charge-conjugation and parity violation (CPV) phase δ. The standard parameterisation of this matrix is given by [92]

$$\mathbf{V} = \begin{pmatrix} c_{12}c_{13} & s_{12}c_{13} & s_{13}e^{-i\delta} \\ -s_{12}c_{23} - c_{12}s_{23}s_{13}e^{i\delta} & c_{12}c_{23} - s_{12}s_{23}s_{13}e^{i\delta} & s_{23}c_{13} \\ s_{12}s_{23} - c_{12}c_{23}s_{13}e^{i\delta} & -c_{12}s_{23} - s_{12}c_{23}s_{13}e^{i\delta} & c_{23}c_{13} \end{pmatrix}, \tag{2.26}$$

where $c_{ij} \equiv \cos\theta_{ij}$, $s_{ij} \equiv \sin\theta_{ij}$ and we take without loss of generality $\theta_{ij} \in [0, \pi/2]$ and $\delta \in [0, 2\pi[$.

In the lepton sector, since we have the freedom to perform the neutrino field rotation $\nu_L \to \mathbf{V}_L \nu_L$ no lepton mixing matrix appears in the leptonic CC interactions. Thus, **there is no lepton mixing in the SM**. Furthermore, there is conservation of lepton number for each flavour and thus the **total lepton number is conserved in the SM**.

2.2 Massive neutrinos

As seen in the previous section, RH neutrinos are missing from the SM. Therefore, we start our study of massive neutrinos by adding three RH neutrino fields ν_R, singlets under the SM gauge group. We recall that adding an arbitrary number of gauge singlets to the SM particle content does not affect the anomaly-cancellation constraints. We can write a Yukawa term for neutrinos, similar to the one of the up-type quarks, leading to a **Dirac mass** term,

$$\mathcal{L}_{\text{Yuk.}} \supset -\overline{\ell_L}\mathbf{Y}_\nu \widetilde{\Phi}\nu_R + \text{H.c.} \xrightarrow{\text{EWSB}} -\overline{\nu_L}\mathbf{M}_\nu\nu_R + \text{H.c.}\,, \; \mathbf{M}_\nu = \frac{v}{\sqrt{2}}\mathbf{Y}_\nu\,, \tag{2.27}$$

where $\mathbf{M}_\nu$ is the 3×3 complex neutrino mass matrix of Dirac type, which can be bidiagonalised as in Eq. (2.24) by performing the following unitary rotations of the flavour neutrinos ν_α ($\alpha = e, \mu, \tau$) relating them to the massive neutrino states ν_i ($i = 1, 2, 3$),

$$\nu_L \to \mathbf{V}_L^\nu \nu_L\,,\; \nu_R \to \mathbf{V}_R^\nu \nu_R \Rightarrow \mathbf{V}_L^{\nu\dagger}\mathbf{M}_\nu\mathbf{V}_R^\nu = \text{diag}\,(m_1, m_2, m_3)\,, \tag{2.28}$$

where $m_{1,2,3}$ are the real and positive neutrino masses. Furthermore, there will be mixing in the leptonic CC interactions as for the quarks. Hence, flavour lepton number is no longer conserved, but the total lepton number remains conserved.

Let us take a look at the order of magnitude of neutrino masses. We quote a couple of recent bounds, the first one is the cosmological constraint $\sum m_\nu < 0.12$ eV (95% CL) on the sum of neutrino masses provided by the Planck collaboration (2018) [93] and the second one is the upper neutrino mass limit of 1.1 eV (90% CL) obtained by the KATRIN collaboration (2019) [94]. Hence, we notice that neutrino

masses are extremely tiny around 10^6 times smaller than the mass of the lightest charged fermion, the electron. Therefore, since $v \simeq 246.2$ GeV, to generate small neutrino masses one has to assume unnaturally small Yukawa couplings $\mathbf{Y}_\nu$ of the order of 10^{-12}. According to 't Hooft's naturalness criterium which goes as *"at any energy scale μ, a physical parameter or set of physical parameters $\alpha_i(\mu)$ is allowed to be very small if the replacement $\alpha_i(\mu) = 0$ would increase the symmetry of the system"* [33], a Dirac mass term for neutrinos is unnatural. Indeed, if we take the limit $\mathbf{Y}_\nu \to 0$, the theory does not exhibit a new symmetry. Nonetheless, there is an alternative way to describe the nature of neutrinos that allows for naturally small couplings, which we discuss in the following section.

2.2.1 Majorana neutrinos

There is the possibility that neutrinos are Majorana particles as first proposed in 1937 by E. Majorana [10]. We start by defining the charged-conjugate fermion field as $\psi^c = C\overline{\psi}^T$ ($\overline{\psi} = \psi^\dagger\gamma_0$), where C is the charge conjugation operator with the following useful properties:

$$C^\dagger = C^{-1}\ ,\ C^T = -C\ ,\ C^* = -C^{-1}\ ,\ C\gamma_0^T C^*\gamma_0^\dagger = \mathbb{1}. \tag{2.29}$$

Notice that the spinor ψ with electric charge q in the presence of an EM field A_μ obeys the following Dirac equation

$$\left(i\partial\!\!\!/ - qA\!\!\!/ - m\right)\psi = 0 \to \left(i\partial\!\!\!/ + qA\!\!\!/ - m\right)\psi^c = 0, \tag{2.30}$$

implying that the spinor ψ^c satisfies the same equation but with opposite charge. In other words, ψ^c represents the antiparticle of ψ. A Majorana fermion is a self-conjugate field, i.e., its own antiparticle and, thus, the Majorana condition reads $\psi^c = \psi$. Consequently, only neutral particles can be of Majorana type. Writing a Majorana field in its chiral components we have

$$\psi = \psi_L + \psi_R = \psi^c \to \psi_L = \psi_R^c\ ,\ \psi_R = \psi_L^c. \tag{2.31}$$

Hence, the spinor ψ_L^c acts as a RH field under Lorentz transformations and vice-versa. We can therefore write a Majorana mass term of the form

$$-m\overline{\psi}\psi = -\frac{m}{2}\overline{\psi}\psi^c + \text{H.c.} = -\frac{m}{2}\overline{\psi}C\overline{\psi}^T + \frac{m^*}{2}\psi^T C^{-1}\psi, \tag{2.32}$$

where the bilinear $\overline{\psi}\psi^c$ is Lorentz invariant. Note that this term is only possible if the field ψ anticommutes since, otherwise, it would vanish. The only anticommuting fields in the SM are fermions. Therefore, the only possible candidate in the SM to be of Majorana type are the neutrinos since they are electrically neutral fermions. Note also that if the fields ψ carry a charge under a U(1) symmetry, $\psi \to e^{iq\phi}\psi$, then the Majorana mass term breaks this symmetry.

Considering an arbitrary number n_R of RH neutrinos ν_R we can assign a **Majorana mass** term for

ν_L and ν_R as follows [95]

$$\mathcal{L}^M_{\text{mass}} = \mathcal{L}^M_L + \mathcal{L}^M_R = -\frac{1}{2}\overline{\nu^c_L}\mathbf{M}_L\nu_L - \frac{1}{2}\overline{\nu_R}\mathbf{M}_R\nu^c_R + \text{H.c.}. \tag{2.33}$$

Due to the anticommuting character of fermionic fields and the antisymmetric property of C as shown in Eq. (2.29), we have $\overline{\nu_{\alpha L}}\nu^c_{\beta L} = \overline{\nu_{\beta L}}\nu^c_{\alpha L}$ (the same for ν_R). Therefore, the Majorana mass matrices $\mathbf{M}_L$ and $\mathbf{M}_R$ are symmetric. In addition, these terms violate the total lepton number by two units. The smallness of a Majorana mass for active neutrinos is natural according to 't-Hooft, since if we take the limit $\mathbf{M}_L \to 0$, we regain total lepton number conservation. Additionally, $\mathcal{L}^M_R$ is invariant under $\text{SU}(2)_L \times \text{U}(1)_Y$ since the RH neutrinos are singlets under the gauge group. However, $\mathcal{L}^M_L$ is not invariant under the SM gauge group since $\overline{\nu^c_L}\nu_L$ belongs to a triplet of $\text{SU}(2)_L$ and has hypercharge $Y = -2$. As we will see later on, to generate a singlet out of this term we would need to extend the SM with the addition of a scalar triplet of hypercharge $Y = +2$ (see Section 2.3.2).

2.2.2 Lepton mixing and observables

We focus on the case where we have the same particle content as in the SM, but ν_L is a Majorana field, with mass term $\mathcal{L}^M_L$ as in Eq. (2.33). Besides the unitary rotations of the charged-lepton fields, we also perform a unitary rotation of the neutrino fields such that the symmetric matrix $\mathbf{M}_L$ is diagonalised as

$$\nu_{\alpha_L} \to (\mathbf{U}_\nu)_{\alpha j}\nu_{j_L} \quad \Rightarrow \quad \mathbf{U}^T_\nu \mathbf{M}_L \mathbf{U}_\nu = \text{diag}(m_1, m_2, m_3), \tag{2.34}$$

where the mass eigenstate Majorana neutrinos ν_j have real and positive masses $m_{1,2,3}$. The field rotation will affect the CC interactions leading to the 3×3 unitary Pontecorvo-Maki-Nakagawa-Sakata **lepton mixing matrix** $\mathbf{U}'$ [5, 96]

$$\mathcal{L}_{\text{CC}} \supset \frac{g}{\sqrt{2}}\overline{e}_L\gamma^\mu \mathbf{U}'\,\nu_L W_\mu + \text{H.c.}\,, \;\; \mathbf{U}' = \mathbf{V}^\dagger_L \mathbf{U}_\nu. \tag{2.35}$$

The matrix $\mathbf{U}'$ contains a total of six parameters: three mixing angles θ_{12}, θ_{23}, and θ_{13}, and three CPV phases: the Dirac-type phase δ and two Majorana-type phases α_{21} and α_{31}. If neutrinos are of Majorana type we cannot rephase the ν_L fields without altering the Lagrangian; hence this leads to two extra physical phases in the mixing matrix. The Dirac neutrino case is similar to what happens for quarks, i.e., we have $\alpha_{21} = \alpha_{31} = 0$. We can parameterise $\mathbf{U}'$ as [25, 97]

$$\mathbf{U}' = \begin{pmatrix} c_{12}c_{13} & s_{12}c_{13} & s_{13} \\ -s_{12}c_{23} - c_{12}s_{23}s_{13}e^{i\delta} & c_{12}c_{23} - s_{12}s_{23}s_{13}e^{i\delta} & s_{23}c_{13}e^{i\delta} \\ s_{12}s_{23} - c_{12}c_{23}s_{13}e^{i\delta} & -c_{12}s_{23} - s_{12}c_{23}s_{13}e^{i\delta} & c_{23}c_{13}e^{i\delta} \end{pmatrix} \begin{pmatrix} 1 & 0 & 0 \\ 0 & e^{i\alpha_{21}} & 0 \\ 0 & 0 & e^{i\alpha_{31}} \end{pmatrix}, \tag{2.36}$$

where without loss of generality $\theta_{ij} \in [0, \pi/2]$, $\delta \in [0, 2\pi[$, and $\alpha_{21,31} \in [0, 2\pi[$. Note that the parameters in the leptonic mixing matrix $\mathbf{U}'$ are completely different from the ones in the CKM matrix in Eq. (2.26), although for the sake of simplicity we keep the same notation.

Parameter	Best Fit $\pm 1\sigma$	3σ range
$\theta_{12}(^\circ)$	34.3 ± 1.0	$31.4 \to 37.4$
$\theta_{23}(^\circ)$[NO]	$48.79^{+0.93}_{-1.25}$	$41.63 \to 51.32$
$\theta_{23}(^\circ)$[IO]	$48.79^{+1.04}_{-1.30}$	$41.88 \to 51.30$
$\theta_{13}(^\circ)$[NO]	$8.58^{+0.11}_{-0.15}$	$8.16 \to 8.94$
$\theta_{13}(^\circ)$[IO]	$8.63^{+0.11}_{-0.15}$	$8.21 \to 8.99$
$\delta(^\circ)$[NO]	216^{+41}_{-25}	$144 \to 360$
$\delta(^\circ)$[IO]	277^{+23}_{-24}	$205 \to 342$
Δm^2_{21} $(\times 10^{-5}$ eV$^2)$	$7.50^{+0.22}_{-0.20}$	$6.94 \to 8.14$
$\lvert\Delta m^2_{31}\rvert$ $(\times 10^{-3}$ eV$^2)$ [NO]	$2.56^{+0.03}_{-0.04}$	$2.46 \to 2.65$
$\lvert\Delta m^2_{31}\rvert$ $(\times 10^{-3}$ eV$^2)$ [IO]	2.46 ± 0.03	$2.37 \to 2.55$

Table 2.2: Current neutrino data obtained from the global fit of three flavour oscillation parameters [8].

Neutrinos can undergo a quantum mechanical phenomenon known as neutrino oscillations [5, 6]. The transition probability, in vacuum, of a neutrino with flavour α created at a source $(0,0)$ with energy E that oscillates through time arriving at a detector (t, L) with different flavour β is given by the well-known expression [95]

$$P\left(\nu_\alpha \to \nu_\beta\right) = \sum_{j,k} \mathbf{U}'^{*}_{\alpha j}\mathbf{U}'_{\beta j}\mathbf{U}'_{\alpha k}\mathbf{U}'^{*}_{\beta k} \exp\left(-i\frac{\Delta m^2_{jk}L}{2E}\right) \ , \ \Delta m^2_{jk} = m^2_j - m^2_k. \tag{2.37}$$

Notice that neutrino oscillations are lepton number conserving; therefore the transition probability above does not involve the Majorana phases. Oscillation experiments cannot determine whether neutrinos are of Dirac or Majorana type. Moreover, these experiments are only sensitive to the neutrino mass-squared differences Δm^2_{jk}, providing no information on the absolute neutrino mass scale. Nevertheless, they do provide information on the mixing angles and the Dirac CPV phase. The current experimental setups that analyse neutrino oscillation phenomena use various types of neutrino sources, namely solar, atmospheric, accelerator and reactor neutrinos. Hence, a common notation for the neutrino observables is $\Delta m^2_{21} \equiv \Delta m^2_{\text{sol}}$, θ_{12} (solar), $\Delta m^2_{31} \equiv \Delta m^2_{\text{atm}}$, θ_{23} (atmospheric) and θ_{13} is the mixing angle obtained from the data analysis of nuclear reactor and accelerator experiments.

Global data analyses of oscillation phenomena in a three-neutrino mixing scheme [7–9] allow to obtain the most up to date values for the neutrino observables. In this thesis, we take as reference the data obtained from the most recent (2020) global fit of neutrino oscillation parameters [8]. The results are presented in Table 2.2 which, among others, include the data from the solar neutrino experiments Sudbury Neutrino Observatory (SNO) [98] and KamLAND [99]; the atmospheric neutrino experiments Super-Kamiokande [100] and IceCube DeepCore [101, 102]; the reactor experiments RENO [103] and Daya Bay [104]; the long-baseline accelerator experiments NOνA [105], T2K [106, 107], MINOS [108] and K2K [109].

Notice from Table 2.2 that, $\Delta m^2_{21} \ll \Delta m^2_{31}$ and the sign of Δm^2_{31} is still unknown, leaving the possibility for two neutrino mass orderings: normal ordering (NO) where $m_1 < m_2 \ll m_3$, and inverted ordering (IO) where $m_3 \ll m_1 < m_2$. For both cases we can write the neutrino mass-squared

Present limit	
Experiment	$m_{\beta\beta}$ (meV)
KamLAND-Zen [110]	$61 - 165$
GERDA [111]	$79 - 180$
CUORE [112]	$73 - 350$
EXO-200 [113]	$93 - 286$

Future sensitivity	
Experiment	$m_{\beta\beta}$ (meV)
AMORE II [114]	$15 - 30$
CUPID [115]	$10 - 15$
LEGEND [116]	$15 - 50$
SNO+ I [117]	$41 - 99$
KamLAND2-Zen [110]	$25 - 70$
nEXO [118]	$8 - 18$
PandaX-III [119]	$20 - 50$

Table 2.3: Present limits and future sensitivities for the effective Majorana mass $m_{\beta\beta}$ of several $\beta\beta_{0\nu}$ experiments.

differences in terms of the lightest neutrino states,

$$\text{NO} : m_2 = \sqrt{m_1^2 + \Delta m_{21}^2}\ ,\ m_3 = \sqrt{m_1^2 + |\Delta m_{31}^2|}, \tag{2.38}$$

$$\text{IO} : m_1 = \sqrt{m_3^2 + |\Delta m_{31}^2|}\ ,\ m_2 = \sqrt{m_3^2 + \Delta m_{21}^2 + |\Delta m_{31}^2|}. \tag{2.39}$$

At this point it is also worthwhile to remark that, since only information on Δm_{jk}^2 is obtained experimentally, there is the possibility for a massless neutrino state. In fact, the work in this thesis will focus on a minimal model where the lightest neutrino state is massless, so that $m_1 = 0$ for NO and $m_3 = 0$ for IO (see Chapter 3).

As mentioned before, the most stringent bound on the absolute neutrino mass scale is the cosmological constraint $\sum m_\nu < 0.12$ eV (95% CL) on the sum of neutrino masses provided by the Planck collaboration (2018) [93]. If one neutrino is massless, we have $\sum m_\nu \simeq 0.059$ eV for NO and $\sum m_\nu \simeq 0.099$ eV for IO, both satisfying the cosmological bound. However, this is an indirect limit since it is model dependent. The most important bounds come from the direct measurements of the β-decay endpoint of tritium ${}^3\text{H} \to {}^3\text{He} + e^- + \overline{\nu_e}$. This provided an upper neutrino mass limit of 1.1 eV (90% CL) obtained by the KATRIN collaboration (2019) [94]. In the upcoming years, KATRIN's goal is to improve this bound up to 0.2 eV.

The determination of the nature of neutrinos has been rather challenging, and no experimental information on the Majorana phases have been obtained so far. However, promising searches for the lepton number violating (LNV) process of neutrinoless double beta decay ($\beta\beta_{0\nu}$) [11] have been made. The amplitude for this rare process is proportional to the effective Majorana mass [95]

$$m_{\beta\beta} = \left| \sum_{j=1}^{3} \mathbf{U}'_{ej} m_j \right| = \left| \left(m_1 c_{12}^2 + m_2 s_{12}^2 e^{2i\alpha_{21}} \right) c_{13}^2 + m_3 s_{13}^2 e^{2i\alpha_{31}} \right|, \tag{2.40}$$

which can be written in terms of the lightest neutrino mass for both spectrum orderings as

$$\text{NO} : m_{\beta\beta} = \left| \left(m_1 c_{12}^2 + \sqrt{m_1^2 + \Delta m_{21}^2}\ s_{12}^2 e^{2i\alpha_{21}} \right) c_{13}^2 + \sqrt{m_1^2 + |\Delta m_{31}^2|}\ s_{13}^2 e^{2i\alpha_{31}} \right|, \tag{2.41}$$

$$\text{IO} : m_{\beta\beta} = \left| \left(\sqrt{m_3^2 + |\Delta m_{31}^2|}\ c_{12}^2 + \sqrt{m_3^2 + \Delta m_{21}^2 + |\Delta m_{31}^2|}\ s_{12}^2 e^{2i\alpha_{21}} \right) c_{13}^2 + m_3 s_{13}^2 e^{2i\alpha_{31}} \right|. \tag{2.42}$$

In the case of a massless neutrino, we immediately conclude that one of the phases is unphysical and

the sole physical Majorana phase is $\alpha = \alpha_{31} - \alpha_{21}$ for NO or $\alpha = \alpha_{21}$ for IO. In Table 2.3 we display the present upper limits on $m_{\beta\beta}$ reported by the KamLAND-Zen [110], GERDA [111], CUORE [112] and EXO-200 [113] collaborations. We also show the future $m_{\beta\beta}$ sensitivities projected by the upcoming experiments AMORE II [114], CUPID [115], LEGEND [116], SNO+ I [117], KamLAND2-Zen [110], nEXO [118] and PandaX-III [119].

In summary, if neutrinos are Majorana particles, the lepton sector contains a total of twelve parameters: three charged lepton masses, three light neutrino masses, three mixing angles and three phases. If one neutrino is massless, the number of parameters is reduced to ten. Any extension of the SM that aim at studying neutrinos must take into account the experimental observables presented in this section.

2.3 Seesaw mechanisms

As mentioned before, a Majorana mass term for the LH neutrinos ν_L as the one presented in Eq. (2.33) is not allowed by the SM symmetries. However, the origin of such term can be explained if we consider the SM as a low-energy effective theory resulting from a more complete theory at a high-energy scale $\Lambda \gg v$. Any given ultraviolet (UV) completion of the SM is composed of additional heavy fields, denoted here by N_i, where i runs over the number of extra particles with mass scale of the order of Λ. Using the path integral formalism these heavy states can be integrated out leading to an effective Lagrangian $\mathcal{L}_{\text{eff}}$. The effective action S_{eff} is defined as [120–122]

$$e^{iS_{\text{eff}}} = \exp\left(i\int d^4x \mathcal{L}_{\text{eff}}(x)\right) \equiv \int \mathcal{D}N\mathcal{D}\overline{N} e^{iS} = e^{iS_{\text{SM}}} \int \mathcal{D}N\mathcal{D}\overline{N} e^{iS_N(N)}, \tag{2.43}$$

where $\mathcal{D}N$ is the integral measure and S is the full action, which we separate in the terms involving the SM fields S_{SM} and the terms involving the heavy fields S_N. Expanding the action $S_N(N)$ around its stationary point, i.e., the minimum energy configuration N_0, we obtain

$$e^{iS_{\text{SM}}} \int \mathcal{D}N\mathcal{D}\overline{N} e^{iS_N(N)} = e^{iS_{\text{SM}}} \int \mathcal{D}N\mathcal{D}\overline{N} e^{i\left[S_N(N_0)+\delta S_N(N_0)+\delta^2 S_N(N_0)+\dots\right]} \simeq e^{i[S_{\text{SM}}+S_N(N_0)]}, \tag{2.44}$$

where the first order term $\delta S_N(N_0)$ vanishes due to the minimum condition and higher-order terms are neglected. This procedure yields the effective action

$$S_{\text{eff}} \simeq \int d^4x \left[\mathcal{L}_{\text{SM}} + \mathcal{L}_N(N_0)\right] = S_{\text{SM}} + S_N(N_0). \tag{2.45}$$

The stationary fields are obtained by solving the classical Euler-Lagrange equations of motion (EOM),

$$\left.\frac{\delta S}{\delta \overline{N_i}}\right|_{\overline{N_i}=\overline{N_{0i}}} = 0\ ,\ \left.\frac{\delta S}{\delta N_i}\right|_{N_i=N_{0i}} = 0. \tag{2.46}$$

Inserting their solutions in the action $S_N(N_0)$ will lead to an effective Lagrangian valid at scales much lower than Λ, which can be written as

$$\mathcal{L}_{\text{eff}} = \mathcal{L}_{\text{SM}} + \mathcal{L}_N(N_0) = \mathcal{L}_{\text{SM}} + \mathcal{L}_{d=5} + \mathcal{L}_{d=6} + \dots\ , \tag{2.47}$$

where $\mathcal{L}_{d=n}$ are non-renormalisable dimension $d = n > 4$ operators, invariant under $G_{\rm SM}$, suppressed by a factor of Λ^{4-n}.

The lowest dimension operator of such kind that can be constructed with the SM particle content is the unique dimension-five **Weinberg operator** [123], which leads, after EWSB, to a Majorana mass term for the LH neutrinos of the form as the one given in Eq. (2.33),

$$\mathcal{L}_{d=5} = \frac{c_{\alpha\beta}^{d=5}}{2}\left(\overline{\ell_{\alpha_L}^c}\widetilde{\Phi}^*\right)\left(\widetilde{\Phi}^\dagger \ell_{\beta_L}\right) + \text{H.c.} \xrightarrow{\text{EWSB}} -\frac{1}{2}\overline{\nu_L^c}\mathbf{M}_{\rm eff}\nu_L + \text{H.c.}\,,\ \mathbf{M}_{\rm eff} = -\frac{v^2}{2}c_{\alpha\beta}^{d=5}. \tag{2.48}$$

In the above expression, the coefficient $c^{d=5}$ is suppressed by Λ^{-1} and $\mathbf{M}_{\rm eff}$ is the effective light-neutrino mass matrix. Note that a Majorana neutrino mass term is the lowest order effect of high-energy physics. Thus, **neutrinos open a new window to physics beyond the SM.** Additionally, the dimension-six operators are numerous and depend on the given UV completion of the SM we work with. These higher-order operators are crucial for the identification of other low-energy effects, such as the non-unitarity of the lepton mixing matrix.

In the following sections, we describe the canonical Type-I, II and III seesaw mechanisms which are minimal extensions of the SM. Note that special emphasis will be given on deriving the effective neutrino mass matrix $\mathbf{M}_{\rm eff}$. Additionally, we will focus in more detail on the Type-I mechanism since the analysis developed for this case will be very helpful to the remaining work in this thesis.

2.3.1 Type-I mechanism

The most common framework to generate small neutrino masses and lepton mixing is the Type-I seesaw mechanism [19–23]. In this case, we add n_R RH neutrinos ν_R to the SM leading to the most general Lagrangian invariant under $G_{\rm SM}$ given by

$$\mathcal{L}_{\rm I} = \mathcal{L}_{\rm SM} + i\overline{\nu_R}\partial\!\!\!/\nu_R - \left(\overline{\ell_L}\widetilde{\Phi}\mathbf{Y}_D^*\nu_R + \frac{1}{2}\overline{\nu_R^c}\mathbf{M}_R\nu_R + \text{H.c.}\right), \tag{2.49}$$

where the $n_R \times n_R$ mass matrix $\mathbf{M}_R$ is of Majorana type and the complex $3 \times n_R$ matrix $\mathbf{Y}_D$ is of Dirac type. In order to obtain the effective neutrino mass matrix two approaches can be adopted: the diagonalisation method and the integration of heavy states.

Diagonalisation method

After EWSB the neutrino mass Lagrangian reads

$$-\mathcal{L}_{\nu,\rm mass}^{\rm I} = \overline{\nu_L}\mathbf{M}_D^*\nu_R + \frac{1}{2}\overline{\nu_R^c}\mathbf{M}_R\nu_R + \text{H.c.}\,,\ \mathbf{M}_D = \frac{v\mathbf{Y}_D}{\sqrt{2}}. \tag{2.50}$$

Organising the neutrino fields in the vector $N_L = (\nu_L, \nu_R^c)^T$ of dimension $n_f = 3 + n_R$, with $\nu_L = (\nu_{eL}, \nu_{\mu L}, \nu_{\tau L})^T$, $\nu_R = (\nu_{R1}, \dots, \nu_{Rn_R})^T$, we obtain the simplified form

$$-\mathcal{L}_{\nu,\rm mass}^{\rm I} = \frac{1}{2}\,\overline{N_L^c}\,\boldsymbol{\mathcal{M}}\,N_L + \text{H.c.}\,,\ \boldsymbol{\mathcal{M}} = \begin{pmatrix} 0 & \mathbf{M}_D \\ \mathbf{M}_D^T & \mathbf{M}_R \end{pmatrix}, \tag{2.51}$$

where $\boldsymbol{\mathcal{M}}$ is the full $n_f \times n_f$ Majorana-type mass matrix. If we assume the mass hierarchy $M_D \ll M_R$ for the mass matrix entries, the full neutrino mass matrix can be block-diagonalised through the unitary matrix $\boldsymbol{\mathcal{U}}_B$ [124], so that

$$\boldsymbol{\mathcal{U}}_B = \begin{pmatrix} \sqrt{\mathbf{1} - \mathbf{F}\mathbf{F}^\dagger} & \mathbf{F} \\ -\mathbf{F}^\dagger & \sqrt{\mathbf{1} - \mathbf{F}^\dagger\mathbf{F}} \end{pmatrix} \Rightarrow \boldsymbol{\mathcal{U}}_B^T \boldsymbol{\mathcal{M}}\, \boldsymbol{\mathcal{U}}_B = \begin{pmatrix} \mathbf{M}_{\rm eff}^{\rm I} & 0 \\ 0 & \mathbf{M}_{\rm heavy} \end{pmatrix}, \tag{2.52}$$

where $\mathbf{M}_{\rm eff}^{\rm I}$ is the 3×3 effective light neutrino mass matrix and $\mathbf{M}_{\rm heavy}$ is the $n_R \times n_R$ heavy neutrino mass matrix. At first order in $\mathbf{F} \sim \mathcal{O}\left(M_R^{-1}\right)$ we obtain the following system of matrix equations:

$$\begin{cases} \mathbf{M}_{\rm eff}^{\rm I} \simeq -\mathbf{F}^*\mathbf{M}_R\mathbf{F}^\dagger - \mathbf{F}^*\mathbf{M}_D^T + \mathbf{M}_D\mathbf{F}^\dagger \,,\; 0 \simeq \mathbf{M}_D - \mathbf{F}^*\mathbf{M}_R - \mathbf{F}^*\mathbf{M}_D^T\mathbf{F}, \\ 0 \simeq \mathbf{M}_D^T - \mathbf{M}_R\mathbf{F}^\dagger - \mathbf{F}^T\mathbf{M}_D\mathbf{F}^\dagger \,,\; \mathbf{M}_{\rm heavy} \simeq \mathbf{M}_R + \mathbf{F}^T\mathbf{M}_D + \mathbf{M}_D^T\mathbf{F}, \end{cases} \Rightarrow \mathbf{F} \simeq \mathbf{M}_D^*(\mathbf{M}_R^*)^{-1}, \tag{2.53}$$

which leads to the light and heavy neutrino mass matrices

$$\mathbf{M}_{\rm eff}^{\rm I} = -\mathbf{F}^*\mathbf{M}_R\mathbf{F}^\dagger = -\mathbf{M}_D\mathbf{M}_R^{-1}\mathbf{M}_D^T \,,\; \mathbf{M}_{\rm heavy} = \mathbf{M}_R \,, \tag{2.54}$$

at first order in the seesaw approximation. Notice that the effective light neutrino mass formula is inversely proportional to the mass of the heavy neutrinos. Therefore, for natural Dirac Yukawa couplings of the order of unity, it is required a mass scale $M_R \sim 10^{14}$ GeV to be able to explain the smallness of neutrino masses. This value is near the GUT scale, not allowing for any potential experimental observations of new physics signals.

The resulting mass matrices in Eq. (2.54) are diagonalised through the following unitary matrices,

$$\nu_L \to \mathbf{U}_\nu\, \nu_L \Rightarrow \mathbf{U}_\nu^T\, \mathbf{M}_{\rm eff}\, \mathbf{U}_\nu = \mathbf{D}_\nu = {\rm diag}\left(\tilde{m}_1, \ldots, \tilde{m}_3\right), \tag{2.55}$$

$$\nu_R^c \to \mathbf{U}_s\, \nu_R^c \Rightarrow \mathbf{U}_s^T\, \mathbf{M}_{\rm heavy}\, \mathbf{U}_s = \mathbf{D}_{\rm heavy} = {\rm diag}\left(\tilde{m}_{3+1}, \ldots, \tilde{m}_{n_f}\right), \tag{2.56}$$

where $\tilde{m}_i$ ($i = 1, \ldots, n_f$) are the real and positive neutrino masses in the seesaw approximation. Therefore, the full $n_f \times n_f$ unitary matrix $\boldsymbol{\mathcal{U}}$ is expressed in the seesaw approximation by

$$\boldsymbol{\mathcal{U}} = \begin{pmatrix} \sqrt{\mathbf{1} - \mathbf{F}\mathbf{F}^\dagger} & \mathbf{F} \\ -\mathbf{F}^\dagger & \sqrt{\mathbf{1} - \mathbf{F}^\dagger\mathbf{F}} \end{pmatrix} \begin{pmatrix} \mathbf{U}_\nu & 0 \\ 0 & \mathbf{U}_s \end{pmatrix} \Rightarrow \boldsymbol{\mathcal{U}}^T \boldsymbol{\mathcal{M}}\, \boldsymbol{\mathcal{U}} = {\rm diag}\left(\tilde{m}_1, \ldots, \tilde{m}_{n_f}\right). \tag{2.57}$$

Due to the additional sterile neutrino states ν_R the lepton mixing matrix $\mathbf{U}$ will be non-unitary [125],

$$\mathbf{U} = \mathbf{V}_L^\dagger\, \sqrt{\mathbf{1} - \mathbf{F}\mathbf{F}^\dagger}\; \mathbf{U}_\nu = (\mathbb{1} - \boldsymbol{\eta})\, \mathbf{U}' \,,\; \mathbf{U}' = \mathbf{V}_L^\dagger \mathbf{U}_\nu, \tag{2.58}$$

where $\mathbf{U}'$ is the unitary lepton mixing matrix and $\boldsymbol{\eta}$ is an Hermitian matrix encoding deviations from unitarity. In the seesaw approximation, if we expand the square root in Eq. (2.58) in a Taylor series up to second order in $\mathbf{F}$, i.e., up to $\mathcal{O}\left(M_R^{-2}\right)$, we will have $\sqrt{\mathbf{1} - \mathbf{F}\mathbf{F}^\dagger} \simeq \mathbf{1} - \frac{1}{2}\mathbf{F}\mathbf{F}^\dagger$, and using Eq. (2.53) we

obtain the following deviations from unitarity:

$$\boldsymbol{\eta} = \frac{1}{2}\mathbf{V}_L^\dagger \mathbf{F}\mathbf{F}^\dagger \mathbf{V}_L \simeq \frac{1}{2}\mathbf{V}_L^\dagger \mathbf{M}_D^* (\mathbf{M}_R^*)^{-1}\mathbf{M}_R^{-1}\mathbf{M}_D^T \mathbf{V}_L. \tag{2.59}$$

Furthermore, since the mass spectrum is composed of light and heavy neutrinos, it becomes clear from Eq. (2.57) that, in the basis where $\mathbf{M}_\ell$ is diagonal, the heavy-light mixing will be given at first order in $\mathbf{F}$ by the $3 \times n_R$ matrix

$$\mathbf{V}_L^\dagger \mathbf{F}\mathbf{U}_s \simeq \mathbf{V}_L^\dagger \mathbf{M}_D^* (\mathbf{M}_R^*)^{-1}\mathbf{U}_s. \tag{2.60}$$

Integration of heavy states method

We now proceed with the second method based on the heavy state integration in order to obtain the effective neutrino mass matrix in Eq. (2.54). We follow the procedure outlined in Eqs. (2.43) - (2.47). Assuming $\mathbf{M}_R$ to be real, we start by defining the heavy fields as $N = \nu_R + \nu_R^c$ and writing (2.49) in the following form

$$\mathcal{L}_{\rm I} = \mathcal{L}_{\rm SM} + \frac{1}{2}\left[\overline{N}\left(i\partial\!\!\!/ - \mathbf{M}_R\right)N - \left(\overline{N}\mathbf{Y}_D^T \widetilde{\Phi}^\dagger \ell_L + \overline{N}\mathbf{Y}_D^\dagger \widetilde{\Phi}^T \ell_L^c + \text{H.c.}\right)\right], \tag{2.61}$$

Hence, from Eq (2.46) we promptly obtain the EOM for the stationary fields N_0,

$$\left(i\partial\!\!\!/ - \mathbf{M}_R\right)N_0 = \left(\mathbf{Y}_D^T \widetilde{\Phi}^\dagger \ell_L + \mathbf{Y}_D^\dagger \widetilde{\Phi}^T \ell_L^c\right). \tag{2.62}$$

Reinserting the solution back into Eq. (2.54) we get

$$\mathcal{L}_{\rm I} = \mathcal{L}_{\rm SM} + \mathcal{L}_N(N_0) = \mathcal{L}_{\rm SM} - \frac{1}{2}\left(\overline{\ell_L}\widetilde{\Phi}\mathbf{Y}_D^* + \overline{\ell_L^c}\widetilde{\Phi}^*\mathbf{Y}_D\right)N_0. \tag{2.63}$$

The higher-order effective operators are obtained by expanding the propagator of the heavy fields. We have

$$\left(i\partial\!\!\!/ - \mathbf{M}_R\right)^{-1} = -\mathbf{M}_R^{-1} - i\partial\!\!\!/\,\mathbf{M}_R^{-2} + \ldots, \tag{2.64}$$

where the first-order term yields the dimension-five operator and the second-order one will provide the dimension-six operators. We do not expand further the propagator since for our purposes it is enough to limit the analysis up to the dimension-six operators.

Using the expansion above, the coefficient of the Weinberg operator will produce the effective neutrino mass matrix as in Eq. (2.54). We obtain

$$c^{d=5} = \mathbf{Y}_D \mathbf{M}_R^{-1}\mathbf{Y}_D^T \xrightarrow{\text{EWSB}} \mathbf{M}_{\rm eff}^{\rm I} = -\frac{v^2}{2}c_{\alpha\beta}^{d=5} = -\mathbf{M}_D\mathbf{M}_R^{-1}\mathbf{M}_D^T. \tag{2.65}$$

For this particular UV completion, which is the Type-I mechanism, there is a single dimension-six operator obtained by using the expansion in Eq. (2.64),

$$\mathcal{L}_{d=6} = c_{\alpha\beta}^{d=6}\left(\overline{\ell_{\alpha L}}\widetilde{\Phi}\right)i\partial\!\!\!/\left(\widetilde{\Phi}^\dagger \ell_{\beta L}\right)\ ,\ c^{d=6} = \mathbf{Y}_D^*\mathbf{M}_R^{-2}\mathbf{Y}_D^T. \tag{2.66}$$

After EWSB, the dimension-six operator essentially modifies the LH neutrinos kinetic term. Notice also that the coefficient $c^{d=6}$ will encode deviations from unitarity as in Eq. (2.59),

$$\mathcal{L}_{d=6} = i\frac{v^2}{2}c^{d=6}_{\alpha\beta}\overline{\nu_{\alpha L}}\partial\!\!\!/\nu_{\beta L} \to \boldsymbol{\eta} = \frac{v^2}{4}\mathbf{V}_L^\dagger c^{d=6}\mathbf{V}_L. \tag{2.67}$$

Furthermore, an important feature of the Type-I seesaw is the fact that both $c^{d=5}$ and $c^{d=6}$ depend quadratically on the Dirac-type mass, and that $c^{d=5}$ is suppressed by $\mathcal{O}\left(M_R^{-1}\right)$, while $c^{d=6}$ is further suppressed by $\mathcal{O}\left(M_R^{-2}\right)$.

As expected, the lepton mixing matrix appears in the leptonic CC interactions and there is also FCNCs. We will reserve the detailed analysis of these effects for the model of interest discussed in the upcoming chapters. Note however that the methods outlined here are quite generic and, therefore, they turn out to be useful as well in Chapter 3.

2.3.2 Type-II mechanism

For the case of the Type-II seesaw mechanism [11, 24–28] we extend the SM particle content with a scalar triplet $\vec{\Delta} = (\Delta_1, \Delta_2, \Delta_3)^T$ with $Y = +2$. The triplet is in the adjoint representation of $\mathrm{SU}(2)_L$ with generators

$$T_1 = \begin{pmatrix} 0 & 0 & 0 \\ 0 & 0 & -i \\ 0 & i & 0 \end{pmatrix}, \; T_2 = \begin{pmatrix} 0 & 0 & i \\ 0 & 0 & 0 \\ -i & 0 & 0 \end{pmatrix}, \; T_3 = \begin{pmatrix} 0 & -i & 0 \\ i & 0 & 0 \\ 0 & 0 & 0 \end{pmatrix}. \tag{2.68}$$

To work with the charge eigenfields we must diagonalise the charge operator Q, this is done by working in a basis where the generator T_3 is diagonal. To achieve this, we perform the similarity transformation $T'_a = \mathbf{K}T_a\mathbf{K}^\dagger$ $(a = 1, 2, 3)$, with the matrix $\mathbf{K}$ relating the flavour fields to the charge eigenstate ones

$$\mathbf{K} = \frac{1}{\sqrt{2}}\begin{pmatrix} -1 & i & 0 \\ 0 & 0 & \sqrt{2} \\ 1 & i & 0 \end{pmatrix} \to \mathbf{K}\vec{\Delta} = \begin{pmatrix} \frac{-\Delta_1 + i\Delta_2}{\sqrt{2}} \\ \Delta_3 \\ \frac{\Delta_1 + i\Delta_2}{\sqrt{2}} \end{pmatrix} = \begin{pmatrix} -\Delta^{++} \\ \Delta^{+} \\ \Delta^{0} \end{pmatrix}, \tag{2.69}$$

where the charge of the field combinations above was determined by applying the diagonal charge operator to $\mathbf{K}\vec{\Delta}$.

Note that we want to obtain an invariant out of a term involving a triplet and two doublets. To see this is actually the case, we look at the product for the representations under $\mathrm{SU}(2)_L$

$$\mathbf{2} \times \mathbf{2} \times \mathbf{3} = (\mathbf{1} + \mathbf{3}) \times \mathbf{3} = \mathbf{3} + (\mathbf{1} + \mathbf{3} + \mathbf{5}). \tag{2.70}$$

We notice that a singlet can be obtained from a term composed of two doublets and a triplet. Moreover, to be able to construct invariant terms involving the SM doublets, we write the fields above in the 2×2

matrix representation as

$$i\tau_2\left(\vec{\tau}\cdot\vec{\Delta}\right)=\begin{pmatrix}\Delta_1+i\Delta_2 & -\Delta_3\\ -\Delta_3 & -\Delta_1+i\Delta_2\end{pmatrix}=\begin{pmatrix}\sqrt{2}\Delta^0 & -\Delta^+\\ -\Delta^+ & -\sqrt{2}\Delta^{++}\end{pmatrix}. \tag{2.71}$$

This matrix allows to write the couplings $\sim \overline{\ell_L^c}\Delta\ell_L$ and $\sim \widetilde{\Phi}^T\Delta\Phi$, which are invariant under all SM gauge transformations since they form a singlet under $\mathrm{SU}(2)_L$ and have zero hypercharge.

Hence, the Type-II Lagrangian is given by

$$\mathcal{L}_{\mathrm{II}}=\mathcal{L}_{\mathrm{SM}}-\left[\overline{\ell_L^c}\mathbf{Y}_\Delta\Delta\ell_L+\mathrm{H.c.}\right]+\frac{1}{2}\mathrm{Tr}\left[\left(D_\mu\Delta\right)^\dagger\left(D^\mu\Delta\right)\right]-V(\Phi,\Delta), \tag{2.72}$$

with the scalar potential

$$\begin{aligned}V(\Phi,\Delta)=&\frac{1}{2}M_\Delta^2\mathrm{Tr}\left(\Delta^\dagger\Delta\right)+\left(\mu_\Delta\widetilde{\Phi}^T\Delta\Phi+\mathrm{H.c.}\right)+\tilde{\lambda}_1\mathrm{Tr}\left(\Delta^\dagger\Delta\right)^2\\&+\tilde{\lambda}_2\mathrm{Tr}\left(\Delta^\dagger\Delta\Delta^\dagger\Delta\right)+\tilde{\lambda}_3\Phi^\dagger\Phi\mathrm{Tr}\left(\Delta^\dagger\Delta\right)+\tilde{\lambda}_4\Phi^\dagger\Delta^\dagger\Delta\Phi,\end{aligned} \tag{2.73}$$

where we assume that the mass matrix for the scalar triplet $\mathbf{M}_\Delta=M_\Delta\mathrm{diag}\,(1,1,1)$, which suffices for the purpose of our discussion, namely to illustrate the Type-II seesaw mechanism. Finally, μ_Δ has mass dimension and $\tilde{\lambda}_{1,2,3,4}$ are the dimensionless quartic couplings.

The core idea of the Type-II seesaw mechanism is that the scalar triplet acquires a very small VEV v_Δ, induced after EWSB by the Higgs doublet VEV v, providing the small neutrino masses. In the matrix representation given in Eq. (2.71), the scalar triplet acquires a VEV as follows

$$\langle\Delta\rangle=\begin{pmatrix}\sqrt{2}\langle\Delta^0\rangle & -\langle\Delta^+\rangle\\ -\langle\Delta^+\rangle & -\sqrt{2}\langle\Delta^{++}\rangle\end{pmatrix}=\begin{pmatrix}v_\Delta & 0\\ 0 & 0\end{pmatrix},\ \frac{v_\Delta}{v}\ll 1, \tag{2.74}$$

since only neutral scalar fields can acquire a non-vanishing VEV. To obtain v_Δ and show it is indeed small in comparison to the EW scale, we must minimise the scalar potential. Such a detailed analysis is out of the scope of this work; thus we simply present the result here:

$$v_\Delta=-\frac{\mu_\Delta^*}{M_\Delta^2+\tilde{\lambda}_3v^2}\simeq-\frac{\mu_\Delta^*}{M_\Delta^2}, \tag{2.75}$$

where the approximate expression is valid for $\tilde{\lambda}_3v^2\ll M_\Delta^2$. The VEV given above is small for heavy scalars with mass $M_\Delta\gg\mu_\Delta$. Hence, from Eqs. (2.72), (2.74) and (2.75), we obtain the effective light neutrino mass matrix for the Type-II seesaw case

$$\mathbf{M}_{\mathrm{eff}}^{\mathrm{II}}=2v_\Delta\mathbf{Y}_\Delta\simeq-\frac{2v^2\mu_\Delta^*}{M_\Delta^2}\mathbf{Y}_\Delta. \tag{2.76}$$

Note an important distinction with the Type-I seesaw. In the Type-II case the effective light neutrino mass matrix is inversely proportional to M_Δ^2. For natural Yukawa couplings of the order of unity and a coupling constant $\mu_\Delta\sim 1$ eV, we would only need the masses of the additional scalars to be $M_\Delta\sim$ TeV in

order to explain the small neutrino masses. Therefore, the Type-II seesaw has a low-scale implementation enabling feasible experimental detection of direct new physics signals.

2.3.3 Type-III mechanism

The Type-III mechanism [29] consists of adding n_Σ fermionic triplets $\vec{\Sigma}_R^i = \left(\Sigma_1^i, \Sigma_2^i, \Sigma_3^i\right)^T$ $(i = 1, \ldots, n_\Sigma)$, with $Y = 0$, to the SM. As explained for the Type-II seesaw mechanism, this triplet flavour isospin pertains to the adjoint representation of $\mathrm{SU}(2)_L$. Furthermore, as outlined in the previous section, we can write the fields above in the 2×2 matrix representation, analogous to Eq. (2.71). We have

$$i\tau_2\left(\vec{\tau}\cdot\vec{\Sigma}_R\right) = \begin{pmatrix} \Sigma_1 + i\Sigma_2 & -\Sigma_3 \\ -\Sigma_3 & -\Sigma_1 + i\Sigma_2 \end{pmatrix} = \begin{pmatrix} \sqrt{2}\Sigma^- & -\Sigma^0 \\ -\Sigma^0 & -\sqrt{2}\Sigma^+ \end{pmatrix}, \tag{2.77}$$

which relates the flavour fields to the charge eigenstates. From the matrix above, we can construct invariant coupling terms with the SM doublets.

The Type-III Lagrangian, in the flavour basis, is given by

$$\mathcal{L}^{\mathrm{III}} = \mathcal{L}^{\mathrm{SM}} + \overline{\vec{\Sigma}_R}\left(i\not{D}\right)\vec{\Sigma}_R - \left[\overline{\vec{\Sigma}_R}\cdot\left(\mathbf{Y}_\Sigma^T\widetilde{\Phi}^\dagger\vec{\tau}\ell_L\right) + \frac{1}{2}\overline{\vec{\Sigma}_R^c}\mathbf{M}_\Sigma^*\vec{\Sigma}_R + \mathrm{H.c.}\right], \tag{2.78}$$

where the $n_\Sigma \times n_\Sigma$ mass matrix $\mathbf{M}_\Sigma$ is of Majorana type and the complex $3 \times n_\Sigma$ matrix $\mathbf{Y}_\Sigma$ is of Dirac type. After EWSB, the neutrino mass Lagrangian reads as

$$-\mathcal{L}_{\nu,\mathrm{mass}}^{\mathrm{III}} = \overline{\nu_L}\mathbf{M}_D^*\Sigma_R^0 + \frac{1}{2}\overline{\Sigma_R^{0c}}\mathbf{M}_\Sigma^*\Sigma_R^0 + \mathrm{H.c.}\,,\ \mathbf{M}_D = \frac{v}{\sqrt{2}}\mathbf{Y}_\Sigma. \tag{2.79}$$

Organising the neutrino fields in the vector $N_L = \left(\nu_L, \Sigma_R^{0c}\right)^T$ of dimension $n_f = 3 + n_\Sigma$, with $\nu_L = \left(\nu_{eL}, \nu_{\mu L}, \nu_{\tau L}\right)^T$, $\Sigma_R^0 = \left(\Sigma_{R1}^0, \ldots, \Sigma_{Rn_\Sigma}^0\right)^T$, the simplified form

$$-\mathcal{L}_{\nu,\mathrm{mass}}^{\mathrm{III}} = \frac{1}{2}\,\overline{N_L^c}\,\boldsymbol{\mathcal{M}}\,N_L + \mathrm{H.c.}\,,\ \boldsymbol{\mathcal{M}} = \begin{pmatrix} 0 & \mathbf{M}_D \\ \mathbf{M}_D^T & \mathbf{M}_\Sigma \end{pmatrix}, \tag{2.80}$$

is obtained. Note that the full neutrino mass matrix has the same form as the one for the Type-I seesaw case in Eq. (2.51). Then, following a similar block-diagonalisation procedure, in the seesaw approximation with the hierarchy $M_D \ll M_\Sigma$ for the mass matrix entries, we obtain the effective light neutrino mass matrix for the Type-III seesaw case,

$$\mathbf{M}_{\mathrm{eff}}^{\mathrm{III}} = -\mathbf{M}_D\mathbf{M}_\Sigma^{-1}\mathbf{M}_D^T. \tag{2.81}$$

Therefore, in both the Type-I and Type-III seesaw mechanisms, the neutrino masses are inversely proportional to the mass of the particles added to the SM. Hence, for natural values of the Yukawa couplings, it is required a mass scale M_Σ near the GUT scale to be able to explain the smallness of neutrino masses, which precludes the possibility of potential experimental probes for detecting direct new physics signals.

Chapter 3

Minimal inverse-seesaw model with Abelian symmetries

As seen in the previous chapter, the canonical Type-I and Type-III seesaw scenarios require very heavy particles or unnaturally tiny Dirac Yukawa couplings in order to generate small neutrino masses and lepton mixing. However, the Type-II seesaw allows for a low-scale implementation where the masses of the additional particles are testable at experiments such as the LHC. This thesis will be anchored in the latter perspective. In fact, we dedicate the rest of this work to the study of a low-scale seesaw implementation which has gained popularity in recent years: the so-called inverse seesaw (ISS) [30–32]. We mention that the remainder of this work follows closely Ref. [126].

3.1 Inverse seesaw mechanism

The ISS mechanism can be implemented by extending the SM particle content with n_R RH neutrinos ν_R and n_s sterile fermion singlets s, leading to what we denote as ISS(n_R, n_s). In this framework, the generic mass Lagrangian for leptons is given in the flavour basis by

$$-\mathcal{L}_{\text{mass}}^{\text{ISS}} = \overline{e_L}\,\mathbf{M}_\ell\, e_R + \overline{\nu_L}\,\mathbf{M}_D \nu_R + \overline{\nu_R}\,\mathbf{M}_R s + \frac{1}{2}\overline{s^c}\,\mathbf{M}_s s + \text{H.c.}\,, \tag{3.1}$$

where $\nu_L = (\nu_{eL}, \nu_{\mu L}, \nu_{\tau L})^T$, $\nu_R = (\nu_{R1}, \dots, \nu_{Rn_R})^T$, $s = (s_1, \dots, s_{n_s})^T$. In the above equation, $\mathbf{M}_\ell$ is the 3×3 charged-lepton mass matrix, $\mathbf{M}_D$ is a $3 \times n_R$ Dirac-type mass matrix, $\mathbf{M}_R$ is a $n_R \times n_s$ matrix, and $\mathbf{M}_s$ is a LNV $n_s \times n_s$ Majorana mass matrix. The latter can be naturally small in the 't Hooft [33] sense, since lepton number conservation is restored in the limit where the last term in Eq. (3.1) vanishes. Furthermore, note that the above mass Lagrangian is not the most general gauge invariant one that can be constructed with the additional particle content of ν_R and s. In fact, the most general one is given by

$$\mathcal{L}_{\text{mass}}^{\text{Gen.}} = \mathcal{L}_{\text{mass}}^{\text{ISS}} - \left(\overline{\nu_L}\,\mathbf{M}_{D_s} s^c + \frac{1}{2}\overline{\nu_R^c}\mathbf{M}_{\mu_R}\nu_R + \text{H.c.}\right). \tag{3.2}$$

In order to obtain the ISS mass Lagrangian two assumptions have to be made, which are $\mathbf{M}_{D_s} = 0$ and $\mathbf{M}_{\mu_R} = 0$. As we will see in the upcoming sections in this chapter, we will forbid the terms involving these two matrices through Abelian symmetries. From now on, our analysis in this section stems from the ISS mass Lagrangian in Eq. (3.1).

Defining $N_L = (\nu_L, \nu_R^c, s)^T$ of dimension $n_f = 3 + n_R + n_s$, we can write $\mathcal{L}_{\text{mass}}^{\text{ISS}}$ in the compact form

$$-\mathcal{L}_{\text{mass}}^{\text{ISS}} = \overline{e_L}\mathbf{M}_\ell\, e_R + \frac{1}{2}\,\overline{N_L^c}\,\boldsymbol{\mathcal{M}}\,N_L + \text{H.c.}\ ,\ \ \boldsymbol{\mathcal{M}} = \begin{pmatrix} 0 & \mathbf{M}_D^* & 0 \\ \mathbf{M}_D^\dagger & 0 & \mathbf{M}_R \\ 0 & \mathbf{M}_R^T & \mathbf{M}_s \end{pmatrix}\,, \tag{3.3}$$

where $\boldsymbol{\mathcal{M}}$ is the full $n_f \times n_f$ neutrino mass matrix.

The charged-lepton mass matrix is bidiagonalised through the unitary transformations $\mathbf{V}_{L,R}$ defined in Eq. (2.24). Theses unitary matrices are obtained by diagonalising the Hermitian matrices $\mathbf{H}_\ell = \mathbf{M}_\ell\mathbf{M}_\ell^\dagger$ and $\mathbf{H}'_\ell = \mathbf{M}_\ell^\dagger\mathbf{M}_\ell$,

$$\mathbf{V}_L^\dagger\mathbf{H}_\ell\mathbf{V}_L = \mathbf{D}_\ell^2 = \text{diag}\left(m_e^2, m_\mu^2, m_\tau^2\right)\ ,\ \mathbf{V}_R^\dagger\mathbf{H}'_\ell\mathbf{V}_R = \mathbf{D}_\ell^2 = \text{diag}\left(m_e^2, m_\mu^2, m_\tau^2\right), \tag{3.4}$$

where $m_{e,\mu,\tau}$ are the charged lepton masses, taken to be real and positive.

The weak-basis states $N_{L,R}$ are related to the mass eigenstates $(\nu_1, ..., \nu_{n_f})^T$ by a $n_f \times n_f$ unitary matrix $\boldsymbol{\mathcal{U}}$

$$N_L = \boldsymbol{\mathcal{U}}\,(\nu_1, \dots\ , \nu_{n_f})_L^T\ ,\ N_R = N_L^c = \boldsymbol{\mathcal{U}}^*\,(\nu_1, \dots\ , \nu_{n_f})_R^T\,, \tag{3.5}$$

such that the full neutrino mass matrix is diagonalised as

$$\boldsymbol{\mathcal{U}}^T\boldsymbol{\mathcal{M}}\,\boldsymbol{\mathcal{U}} = \boldsymbol{\mathcal{D}}_\nu = \text{diag}\,(m_1, \dots\ , m_{n_f})\,, \tag{3.6}$$

where $m_{1,\dots,n_f}$ are the n_f (real and positive) Majorana neutrino masses. Notice that, in general, the light-active (heavy-sterile) neutrino masses are labelled as $m_{1,2,3}$ ($m_{4,\dots,n_f}$).

In the ISS approximation limit where $M_s, M_D \ll M_R$, for the matrix entries, we will derive the effective light neutrino mass matrix, using the diagonalisation method and the integration of heavy states, following a similar procedure as for the Type-I seesaw case (see Section 2.3.1).

Diagonalisation method

The neutrino mass matrix $\boldsymbol{\mathcal{M}}$ of Eq. (3.3) can be block-diagonalised by writing it in the form

$$\boldsymbol{\mathcal{M}} = \left(\begin{array}{c|cc} 0 & \mathbf{M}_D^* & 0 \\ \hline \mathbf{M}_D^\dagger & 0 & \mathbf{M}_R \\ 0 & \mathbf{M}_R^T & \mathbf{M}_s \end{array}\right) \equiv \begin{pmatrix} 0 & \mathbf{M}'_D \\ \mathbf{M}'^T_D & \mathbf{M}'_R \end{pmatrix}, \tag{3.7}$$

where the right-hand-side matrix takes the same form as the full Type-I seesaw matrix in Eq. (2.51).

The full unitary matrix $\boldsymbol{\mathcal{U}}$ of Eq. (3.6) can then be parameterised as [124] [see Eq. (2.57)]

$$\boldsymbol{\mathcal{U}} = \begin{pmatrix} \sqrt{\mathbb{1} - \mathbf{F}\mathbf{F}^\dagger} & \mathbf{F} \\ -\mathbf{F}^\dagger & \sqrt{\mathbb{1} - \mathbf{F}^\dagger\mathbf{F}} \end{pmatrix} \begin{pmatrix} \mathbf{U}_\nu & 0 \\ 0 & \mathbf{U}_s \end{pmatrix}, \tag{3.8}$$

so that

$$\boldsymbol{\mathcal{U}}^T \boldsymbol{\mathcal{M}}\, \boldsymbol{\mathcal{U}} = \begin{pmatrix} \mathbf{U}_\nu^T \mathbf{M}_{\rm eff} \mathbf{U}_\nu & 0 \\ 0 & \mathbf{U}_s^T \mathbf{M}_{\rm heavy} \mathbf{U}_s \end{pmatrix}, \tag{3.9}$$

where $\mathbf{U}_\nu$ and $\mathbf{U}_s$ are 3×3 and $(n_R + n_s)\times(n_R + n_s)$ unitary matrices, respectively; $\mathbf{M}_{\rm eff}$ and $\mathbf{M}_{\rm heavy}$ are the effective light and heavy-neutrino mass matrices. At leading order, $\mathbf{M}_{\rm heavy} \simeq \mathbf{M}'_R$ [see Eq. (2.54)] yielding $n_R + n_s$ heavy neutrinos. In Eq. (3.8), $\mathbf{F}$ is an $3\times(n_R + n_s)$ matrix given at first order in the seesaw approximation by [see Eq. (2.53)],

$$\mathbf{F} \simeq \mathbf{M}'^*_D \left(\mathbf{M}'^*_R\right)^{-1} \simeq \left(0,\ \mathbf{M}_D (\mathbf{M}_R^\dagger)^{-1}\right), \tag{3.10}$$

where the inverse of $\mathbf{M}'_R$ is

$$\mathbf{M}'^{-1}_R = \begin{pmatrix} -\left(\mathbf{M}_R\, \mathbf{M}_S^{-1} \mathbf{M}_R^T\right)^{-1} & (\mathbf{M}_R^T)^{-1} \\ (\mathbf{M}_R)^{-1} & 0 \end{pmatrix}, \tag{3.11}$$

with $\mathbf{M}_R$ and $\mathbf{M}_s$ invertible. This leads to the 3×3 effective light-neutrino mass matrix

$$\mathbf{M}_{\rm eff} = -\mathbf{F}^* \mathbf{M}'_R \mathbf{F}^\dagger = -\mathbf{M}_D^* \left(\mathbf{M}_R\, \mathbf{M}_s^{-1} \mathbf{M}_R^T\right)^{-1} \mathbf{M}_D^\dagger\,. \tag{3.12}$$

We start by comparing the above formula with the Type-I effective mass matrix given in Eq. (2.54). For the latter case the smallness of neutrino masses is explained through the sole suppression M_R^{-1} whereas in the ISS case, thanks to the addition of a second species of sterile fermions, we have two suppressing factors $M_R^{-1} M_D$ and M_s. Hence, for natural Dirac Yukawa couplings, $M_D \sim v/\sqrt{2}$, and having a small LNV parameter $M_s \sim$ eV, we would only need $M_R \sim$ TeV, in order to explain the small neutrino masses. Hence, the ISS can be regarded as a **low-energy scale mechanism**, enabling sizeable experimental observations of new physics signals and LNV processes. This is the reason why the ISS is sometimes dubbed as a low-scale implementation of the Type-I seesaw mechanism. Furthermore, the above matrix can be diagonalised through a unitary rotation of the active neutrino fields, $\nu_L \to \mathbf{U}_\nu\, \nu_L$, satisfying [see Eq. (2.55)]

$$\mathbf{U}_\nu^T\, \mathbf{M}_{\rm eff}\, \mathbf{U}_\nu = \mathbf{D}_\nu = {\rm diag}\left(\tilde{m}_1, \tilde{m}_2, \tilde{m}_3\right), \tag{3.13}$$

where $\tilde{m}_{1,2,3}$ are the real and positive light neutrino masses in the ISS approximation. The unitary matrix $\mathbf{U}_\nu$ is obtained from the diagonalisation of the Hermitian matrix $\mathbf{H}_{\rm eff} = \mathbf{M}_{\rm eff}\mathbf{M}_{\rm eff}^\dagger$,

$$\mathbf{U}_\nu^\dagger \mathbf{H}_{\rm eff} \mathbf{U}_\nu = \mathbf{D}_\nu^2 = {\rm diag}\left(\tilde{m}_1^2, \tilde{m}_2^2, \tilde{m}_3^2\right), \tag{3.14}$$

yielding the unitary lepton mixing matrix [see Eq. (2.58)]

$$\mathbf{U}' = \mathbf{V}_L^\dagger \mathbf{U}_\nu \,, \tag{3.15}$$

after performing the rotation to the charged-lepton mass basis. The matrix $\mathbf{U}'$ can be parameterised in terms of the lepton observables namely the mixing angles and CPV phases given in Section 2.2.2 by Eq. (2.36).

We now characterise active and active-sterile mixing considering the full mixing matrix $\boldsymbol{\mathcal{U}}$ or, more specifically, the rectangular $3 \times n_f$ matrix $\mathbf{W}_{\alpha j} \equiv \boldsymbol{\mathcal{U}}_{\alpha j}$ ($\alpha = e, \mu, \tau$, $j = 1, \ldots, n_f$) which, according to Eq. (3.8), can be decomposed in the form

$$\mathbf{W} = (\sqrt{\mathbb{1} - \mathbf{F}\mathbf{F}^\dagger}\, \mathbf{U}_\nu \,,\, \mathbf{F}\mathbf{U}_s) \equiv (\mathbf{W}_\nu, \mathbf{W}_s) \,, \tag{3.16}$$

where $\mathbf{W}_\nu$ and $\mathbf{W}_s$ are 3×3 and $3 \times (n_R + n_s)$ matrices, respectively. It is clear that $\mathbf{V}_L^\dagger \mathbf{W}_s$ defines the mixing between the three active neutrinos and the $n_R + n_s$ sterile states in the physical charged-lepton basis. Due to the additional fermion states, active-neutrino mixing is determined by the non-unitary matrix [see Eq. (2.58)]

$$\mathbf{U} = \mathbf{V}_L^\dagger \mathbf{W}_\nu = (\mathbb{1} - \boldsymbol{\eta})\, \mathbf{U}', \tag{3.17}$$

where $\mathbf{U}'$ is the unitary mixing matrix given in Eq. (3.15) and $\boldsymbol{\eta}$ is an Hermitian matrix encoding deviations from unitarity of $\mathbf{U}$. Expanding Eq. (3.8) up to second order in $\mathbf{F}$, one has $\sqrt{\mathbb{1} - \mathbf{F}\mathbf{F}^\dagger} \simeq \mathbb{1} - \frac{1}{2}\mathbf{F}\mathbf{F}^\dagger$ which, together with Eqs. (3.10) and (3.17), leads to

$$\boldsymbol{\eta} = \frac{1}{2}\mathbf{V}_L^\dagger \mathbf{F}\mathbf{F}^\dagger \mathbf{V}_L \simeq \frac{1}{2}\mathbf{V}_L^\dagger \mathbf{M}_D (\mathbf{M}_R^\dagger)^{-1} \mathbf{M}_R^{-1} \mathbf{M}_D^\dagger \mathbf{V}_L \,. \tag{3.18}$$

Note that the expression above is very similar to the Type-I seesaw one in Eq. (2.59), the relevant difference lying in the order of magnitude of the mass scale M_R. Active-sterile neutrino mixing is described by $\mathbf{W}_s$ given in Eq. (3.16), which at first order in $\mathbf{F}$ is

$$\mathbf{V}_L^\dagger \mathbf{W}_s = \mathbf{V}_L^\dagger \mathbf{F}\mathbf{U}_s \simeq \mathbf{V}_L^\dagger \big(0,\ \mathbf{M}_D (\mathbf{M}_R^\dagger)^{-1}\big) \mathbf{U}_s, \tag{3.19}$$

in the basis where $\mathbf{M}_\ell$ is diagonal [see Eq. (2.60)].

Furthermore, leptonic mixing will affect the CC and NC interactions. The detailed modified interaction Lagrangians involving the weak bosons and the scalars in our model are presented in Appendix B. We introduce here the matrices $\mathbf{B}$ and $\boldsymbol{\mathcal{C}}$ which will appear in these Lagrangians [127],

$$\mathbf{B}_{\alpha j} = \sum_{k=1}^{3} (\mathbf{V}_L^*)_{k\alpha} \mathbf{W}_{kj}, \quad \boldsymbol{\mathcal{C}}_{ij} = \sum_{k=1}^{3} \mathbf{W}_{ki}^* \mathbf{W}_{kj}, \tag{3.20}$$

which obey the equalities

$$\sum_{k=1}^{n_f}\mathbf{B}_{\alpha k}\mathbf{B}^*_{\beta k}=\delta_{\alpha\beta},\quad \sum_{k=1}^{n_f}\mathbf{B}_{\alpha k}\boldsymbol{\mathcal{C}}_{ki}=\mathbf{B}_{\alpha i},\quad \sum_{k=1}^{n_f}\boldsymbol{\mathcal{C}}_{ik}\boldsymbol{\mathcal{C}}^*_{jk}=\boldsymbol{\mathcal{C}}_{ij},\quad \sum_{\alpha=1}^{3}\mathbf{B}^*_{\alpha i}\mathbf{B}_{\alpha j}=\boldsymbol{\mathcal{C}}_{ij}, \tag{3.21}$$

$$\sum_{k=1}^{n_f}m_k\boldsymbol{\mathcal{C}}_{ik}\boldsymbol{\mathcal{C}}_{jk}=0,\quad \sum_{k=1}^{n_f}m_k\mathbf{B}_{\alpha k}\boldsymbol{\mathcal{C}}^*_{ki}=0,\quad \sum_{k=1}^{n_f}m_k\mathbf{B}_{\alpha k}\mathbf{B}_{\beta k}=0. \tag{3.22}$$

Note that the mixing between the light and sterile neutrinos is given by the matrix elements $\mathbf{B}_{\alpha j}$ for $\alpha=e,\mu,\tau$ and $j=4,\ldots,n_f$, in the charged-lepton physical basis. Furthermore, the parameters $\boldsymbol{\eta}_{\alpha\beta}$ encoding deviations from unitarity [see Eq. (3.17)] can be expressed in terms of $\mathbf{B}$ through the relation

$$\boldsymbol{\eta}_{\alpha\beta}=\frac{1}{2}\sum_{j=4}^{n_f}\mathbf{B}_{\alpha j}\mathbf{B}^*_{\beta j}, \tag{3.23}$$

where we used the first equality in Eq. (3.21) in order to write $\boldsymbol{\eta}_{\alpha\beta}$ solely in terms of the active-sterile mixing.

Integration of heavy states method

We proceed to the heavy-state integration in order to obtain the effective ISS light neutrino mass matrix in Eq. (3.12). In this section, we work with the SM scalar sector of one Higgs doublet and assume that $\mathbf{M}_R$ is real. Defining the heavy fields as $N=\nu_R+\nu_R^c$ and $Z=s+s^c$, we have

$$\mathcal{L}_{\rm ISS}=\mathcal{L}_{\rm SM}+\frac{1}{2}\left[\overline{N}i\partial\!\!\!/N+\overline{Z}\left(i\partial\!\!\!/-\mathbf{M}_S\right)Z-\left(\overline{N}\mathbf{M}_RZ+\overline{N}\mathbf{Y}_D^\dagger\widetilde{\Phi}^\dagger\ell_L+\overline{N}\mathbf{Y}_D^T\widetilde{\Phi}^T\ell_L^c+\text{H.c.}\right)\right], \tag{3.24}$$

where $\mathbf{M}_D=v\mathbf{Y}_D/\sqrt{2}$. Obtaining the EOM for the classical configurations N_0 and Z_0, and reinserting them back in (3.24), we get the ISS effective Lagrangian

$$\begin{cases}(i\partial\!\!\!/-\mathbf{M}_S)Z_0=\mathbf{M}_R^TN_0,\\ i\partial\!\!\!/N_0-\mathbf{M}_RZ_0=\mathbf{Y}_D^\dagger\widetilde{\Phi}^\dagger\ell_L+\mathbf{Y}_D^T\widetilde{\Phi}^T\ell_L^c,\end{cases}\Rightarrow\mathcal{L}_{\rm eff}^{\rm ISS}=\mathcal{L}_{\rm SM}-\frac{1}{2}\overline{\ell_L^c}\widetilde{\Phi}^*\mathbf{Y}_D^*N_0-\frac{1}{2}\overline{\ell_L}\widetilde{\Phi}\mathbf{Y}_DN_0. \tag{3.25}$$

In order to obtain N_0, we must work out the coupled EOM using a Taylor expansion of the propagators as in Eq. (2.64). We start by expanding the Z_0 propagator up to first order in the small LNV parameter M_s which leads to a result of order $\mathcal{O}\left(M_s^{-1}M_R\right)$, then we reinsert the result back into the second coupled equation above in order to obtain N_0 up to $\mathcal{O}\left(M_R^{-2}\right)$. We obtain

$$N_0\simeq-(\mathbf{M}_R^T)^{-1}\mathbf{M}_s\mathbf{M}_R^{-1}\left(\mathbf{Y}_D^\dagger\widetilde{\Phi}^\dagger\ell_L+\mathbf{Y}_D^T\widetilde{\Phi}^T\ell_L^c\right)-(\mathbf{M}_R^T)^{-1}\mathbf{M}_R^{-1}i\partial\!\!\!/\left(\mathbf{Y}_D^\dagger\widetilde{\Phi}^\dagger\ell_L+\mathbf{Y}_D^T\widetilde{\Phi}^T\ell_L^c\right). \tag{3.26}$$

The first term above yields the Weinberg operator in Eq. (2.48), leading to the light neutrino mass matrix in Eq. (3.12),

$$c^{d=5}=\mathbf{Y}_D^*(\mathbf{M}_R^T)^{-1}\mathbf{M}_s\mathbf{M}_R^{-1}\mathbf{Y}_D^\dagger\xrightarrow{\text{EWSB}}\mathbf{M}_{\rm eff}=-\frac{v^2}{2}c^{d=5}=-\mathbf{M}_D^*(\mathbf{M}_R^T)^{-1}\mathbf{M}_s\mathbf{M}_R^{-1}\mathbf{M}_D^\dagger. \tag{3.27}$$

The unique dimension-six effective operator for the ISS case stems from the second term of Eq. (3.26). We obtain

$$\mathcal{L}_{d=6} = c_{\alpha\beta}^{d=6}\left(\overline{\ell_{\alpha L}}\widetilde{\Phi}\right) i\partial\!\!\!/\left(\widetilde{\Phi}^{\dagger}\ell_{\beta L}\right) \ , \ c^{d=6} = \mathbf{Y}_D(\mathbf{M}_R^T)^{-1}\mathbf{M}_R^{-1}\mathbf{Y}_D^{\dagger}. \tag{3.28}$$

After EWSB, the dimension-six operator essentially modifies the LH neutrinos kinetic term and its coefficient will encode deviations from unitarity as in Eq. (3.18),

$$\mathcal{L}_{d=6} = i\frac{v^2}{2}c_{\alpha\beta}^{d=6}\overline{\nu_{\alpha L}}\partial\!\!\!/\nu_{\beta L} \to \boldsymbol{\eta} = \frac{v^2}{4}\mathbf{V}_L^{\dagger}c^{d=6}\mathbf{V}_L. \tag{3.29}$$

Note some important features of the ISS UV completion. First, the dimension-six operator above is independent of the LNV parameter M_s. Furthermore, it is suppressed by $\mathcal{O}(M_R^{-2})$ which is the same suppression as in the dimension-five operator. Hence, both operators have the same high-energy suppression in the ISS [121].

3.2 Maximally-restrictive Abelian flavour symmetries

This section, is divided in two parts. First, we proceed to identify the maximally-restrictive textures for the set of matrices $(\mathbf{M}_\ell, \mathbf{M}_D, \mathbf{M}_R, \mathbf{M}_s)$ compatible with neutrino oscillation data within the minimal ISS(2,2) framework, where two ν_R and two s fermion singlets are added to the SM particle content, i.e., $n_R = n_s = 2$ and $n_f = 7$. By maximally restrictive we mean that no additional texture zero can be placed into any of the mass matrices while keeping compatibility with the charged-lepton masses and neutrino oscillation data. Secondly, we will determine which sets can be realised by imposing discrete or continuous Abelian symmetries. This will be done by exploring the minimal scalar sector needed in order to realise at least one of the texture sets. Then we apply the canonical and Smith normal form (SNF) methods to obtain the minimal Abelian flavour symmetry groups that reproduce the given texture set while forbidding unwanted coupling terms in the Lagrangian.

3.2.1 Maximally-restrictive textures for leptons

Our texture-zero analysis is performed assuming the seesaw approximation given in Eq. (3.12). Later on, we will comment on the validity of this approximation when comparing with the results obtained with the full neutrino mass matrix $\boldsymbol{\mathcal{M}}$. The identification of the compatible textures is based on a standard χ^2-analysis, using the function

$$\chi^2(x) = \sum_i \frac{\left[\mathcal{P}_i(x) - \mathcal{O}_i\right]^2}{\sigma_i^2}, \tag{3.30}$$

where x denotes the input parameters, i.e., the matrix elements of $\mathbf{M}_\ell$, $\mathbf{M}_D$, $\mathbf{M}_R$ and $\mathbf{M}_s$; $\mathcal{P}_i(x)$ is the model prediction for a given observable with best-fit (b.f.) value $\mathcal{O}_i$, and σ_i denotes its 1σ experimental uncertainty. In our search for viable sets $(\mathbf{M}_\ell, \mathbf{M}_D, \mathbf{M}_R, \mathbf{M}_s)$, we require the charged-lepton masses to be at their central values [89], such that the χ^2-function is minimised only with respect to the six neutrino observables, namely the two neutrino mass-squared differences $\Delta m_{21}^2, \Delta m_{31}^2$, the three mixing angles $\theta_{12}, \theta_{23}, \theta_{13}$ and the Dirac CPV phase δ, using the current data reported in Table 2.2 [8]. Notice that, in

$\mathbf{M}_\ell = 6^\ell$			
$\mathbf{M}_D$	$\mathbf{M}_R$	$\mathbf{M}_s$	$\mathbf{M}_{\rm eff}$
T_1	T_{14}	T_{23}	-
T_4	T_{14}	T_{23}	-
T_5	T_{14}	T_{23}	-
T_{14}	T_1	T_{23}	-
T_{16}	T_1	T_{23}	-
T_{23}	T_1	T_{23}	-
T_{25}	T_1	T_{23}	-
T_{36}	T_1	T_{23}	-
T_{45}	T_1	T_{23}	-

$\mathbf{M}_\ell = 5_1^\ell$			
$\mathbf{M}_D$	$\mathbf{M}_R$	$\mathbf{M}_s$	$\mathbf{M}_{\rm eff}$
T_{13}	T_{14}	T_{23}	-
T_{14}	T_{14}	T_{23}	1_4^ν
T_{16}	T_{14}	T_{23}	1_5^ν
T_{35}	T_{14}	T_{23}	-
T_{45}	T_{14}	T_{23}	1_6^ν

$\mathbf{M}_\ell = 4_1^\ell,\, 4_2^\ell,\, 4_3^\ell$			
$\mathbf{M}_D$	$\mathbf{M}_R$	$\mathbf{M}_s$	$\mathbf{M}_{\rm eff}$
T_{124}	T_{14}	T_{23}	3_{11}^ν
T_{125}	T_{14}	T_{23}	3_{11}^ν
T_{134}	T_{14}	T_{23}	3_{16}^ν
T_{136}	T_{14}	T_{23}	2_{15}^ν
T_{145}	T_{14}	T_{23}	2_{14}^ν
T_{146}	T_{14}	T_{23}	2_{13}^ν
T_{156}	T_{14}	T_{23}	3_{19}^ν
T_{345}	T_{14}	T_{23}	3_{16}^ν
T_{456}	T_{14}	T_{23}	3_{19}^ν

Table 3.1: Maximally-restrictive texture sets for $\mathbf{M}_\ell = 6^\ell$ (left), 5_1^ℓ (centre) and $4_{1,2,3}^\ell$ (right).

the ISS(2,2) framework, there is always a massless neutrino ($\tilde{m}_1 = 0$ for NO or $\tilde{m}_3 = 0$ for IO).

For a given set of input matrices, we consider compatibility with data if the deviation of each neutrino observable from its experimental value is at most 3σ at the χ^2-minimum [65, 72, 128, 129]. If this is the case, we also test the compatibility of the textures at 1σ. For the sake of simplicity, we shall use the following sequential notation to label the position of the matrix elements of a given 3×2 and 2×2 texture T, respectively,

$$\begin{pmatrix} 1 & 2 \\ 3 & 4 \\ 5 & 6 \end{pmatrix}, \quad \begin{pmatrix} 1 & 2 \\ 3 & 4 \end{pmatrix}, \tag{3.31}$$

where we denote the position of any vanishing element labelled i with a subscript, i.e., T_i. For instance, in this notation, a matrix with vanishing 11 and 22 elements would be labelled as T_{14}.

It is straightforward to show that the ISS formula in Eq. (3.12) is invariant under the weak-basis permutations

$$\mathbf{M}_D \to \mathbf{M}_D\,\mathbf{P}_R \;\;,\;\; \mathbf{M}_R \to \mathbf{P}_R^T\,\mathbf{M}_R\,\mathbf{P}_s \;\;,\;\; \mathbf{M}_s \to \mathbf{P}_s^T\,\mathbf{M}_s\,\mathbf{P}_s, \tag{3.32}$$

where $\mathbf{P}$ denote the 3×3 (or 2×2) permutation matrices. Furthermore, for a given pair $(\mathbf{M}_\ell, \mathbf{M}_{\rm eff})$, the permutations

$$\mathbf{M}_\ell \to \mathbf{P}_\ell^T\,\mathbf{M}_\ell\,\mathbf{P}_e \;\;,\;\; \mathbf{M}_{\rm eff} \to \mathbf{P}_\ell^T\,\mathbf{M}_{\rm eff}\,\mathbf{P}_\nu, \tag{3.33}$$

leave the lepton mixing matrix in Eq. (3.15) invariant. Therefore, for each weak-basis permutation class, only one representative set of textures needs to be identified. The maximally-restrictive texture zero sets $(\mathbf{M}_\ell, \mathbf{M}_D, \mathbf{M}_R, \mathbf{M}_s)$ compatible with neutrino oscillation data for NO are presented in Table 3.1. It turns out that these sets of matrices are also viable for IO. Moreover, all the sets are compatible with data at 1σ. The labelling used for the charged-lepton mass matrix and the effective neutrino mass matrix follows Ref. [130] and the corresponding textures are presented in Tables 3.2 and 3.3, respectively.

$$4_1^\ell \sim \begin{pmatrix} 0 & 0 & \times \\ 0 & \times & 0 \\ \times & \times & \times \end{pmatrix} \quad 4_2^\ell \sim \begin{pmatrix} 0 & 0 & \times \\ 0 & \times & \times \\ \times & 0 & \times \end{pmatrix} \quad 4_3^\ell \sim \begin{pmatrix} 0 & 0 & \times \\ 0 & \times & \times \\ \times & \times & 0 \end{pmatrix}$$

$$5_1^\ell \sim \begin{pmatrix} 0 & 0 & \times \\ 0 & \times & 0 \\ \times & 0 & \times \end{pmatrix} \quad 6^\ell \sim \begin{pmatrix} \times & 0 & 0 \\ 0 & \times & 0 \\ 0 & 0 & \times \end{pmatrix}$$

Table 3.2: Textures for the charged-lepton mass matrix $\mathbf{M}_\ell$.

$$1_4^\nu \sim \begin{pmatrix} \times & 0 & \times \\ 0 & \times & \times \\ \times & \times & \times \end{pmatrix} \quad 1_5^\nu \sim \begin{pmatrix} \times & \times & 0 \\ \times & \times & \times \\ 0 & \times & \times \end{pmatrix} \quad 1_6^\nu \sim \begin{pmatrix} \times & \times & \times \\ \times & \times & 0 \\ \times & 0 & \times \end{pmatrix}$$

$$2_{13}^\nu \sim \begin{pmatrix} \times & 0 & 0 \\ 0 & \times & \times \\ 0 & \times & \times \end{pmatrix} \quad 2_{14}^\nu \sim \begin{pmatrix} \times & 0 & \times \\ 0 & \times & 0 \\ \times & 0 & \times \end{pmatrix} \quad 2_{15}^\nu \sim \begin{pmatrix} \times & \times & 0 \\ \times & \times & 0 \\ 0 & 0 & \times \end{pmatrix}$$

$$3_{11}^\nu \sim \begin{pmatrix} 0 & 0 & 0 \\ 0 & \times & \times \\ 0 & \times & \times \end{pmatrix} \quad 3_{16}^\nu \sim \begin{pmatrix} \times & 0 & \times \\ 0 & 0 & 0 \\ \times & 0 & \times \end{pmatrix} \quad 3_{19}^\nu \sim \begin{pmatrix} \times & \times & 0 \\ \times & \times & 0 \\ 0 & 0 & 0 \end{pmatrix}$$

Table 3.3: Textures for the effective neutrino mass matrix $\mathbf{M}_{\text{eff}}$.

3.2.2 Abelian symmetry realisation of compatible textures

We start this section by specifying the scalar sector of the model. As mentioned before, maximally-restrictive texture zeros in Yukawa coupling matrices cannot be implemented in the SM with Abelian symmetries, since all fermion fields couple to the same Higgs doublet. Hence, to realise such textures, our minimal setup will require the presence of at least two Higgs doublets Φ_a ($a = 1, 2$). Furthermore, to avoid bare mass terms in the Lagrangian, we also add two complex scalar fields S_a ($a = 1, 2$), so that $\mathbf{M}_s$ and $\mathbf{M}_R$ are dynamically generated through couplings of S_1 and S_2 with $s^T C s$ and $\overline{\nu_R}\, s$, respectively. We parameterise Φ_a and S_a as

$$\Phi_a = \begin{pmatrix} \phi_a^+ \\ \phi_a^0 \end{pmatrix} = \frac{1}{\sqrt{2}} \begin{pmatrix} \sqrt{2}\phi_a^+ \\ v_a e^{i\theta_a} + \rho_a + i\eta_a \end{pmatrix} \ , \ S_a = \frac{1}{\sqrt{2}} \left(u_a e^{i\xi_a} + \rho_{a+2} + i\eta_{a+2} \right) \ , \ a = 1, 2 \,, \tag{3.34}$$

where v_a and u_a are the VEVs of the neutral components of Higgs doublets ϕ_a^0 and the scalar singlet fields, respectively. Note that only the phase difference $\theta = \theta_2 - \theta_1$ is physical (a more detailed analysis of the scalar sector can be found in Appendix A).

Given the minimal fermion and scalar contents described above, the Yukawa Lagrangian relevant for our work is

$$\begin{aligned} -\mathcal{L}_{\text{Yuk.}}^{(1)} = {} & \overline{\ell_L} \left(\mathbf{Y}_\ell^1 \Phi_1 + \mathbf{Y}_\ell^2 \Phi_2 \right) e_R + \overline{\ell_L} \left(\mathbf{Y}_D^1 \tilde{\Phi}_1 + \mathbf{Y}_D^2 \tilde{\Phi}_2 \right) \nu_R \\ & + \frac{1}{2} \overline{s^c} \left(\mathbf{Y}_s^1 S_1 + \mathbf{Y}_s^2 S_1^* \right) s + \overline{\nu_R} \left(\mathbf{Y}_R^1 S_2 + \mathbf{Y}_R^2 S_2^* \right) s + \text{H.c.}. \end{aligned} \tag{3.35}$$

Upon SSB, the scalar fields acquire non-zero VEVs and the above Yukawa interactions yield the generic

mass Lagrangian of Eq. (3.1) for the ISS(2,2). The corresponding mass matrices are given by

$$\begin{aligned}
&\mathbf{M}_\ell = \frac{v_1}{\sqrt{2}}\mathbf{Y}_\ell^1 + \frac{v_2}{\sqrt{2}}\mathbf{Y}_\ell^2\, e^{i\theta},\ \mathbf{M}_D = \frac{v_1}{\sqrt{2}}\mathbf{Y}_D^1 + \frac{v_2}{\sqrt{2}}\mathbf{Y}_D^2\, e^{-i\theta},\\
&\mathbf{M}_s = \frac{u_1}{\sqrt{2}}\left(\mathbf{Y}_s^1\, e^{i\xi_1} + \mathbf{Y}_s^2\, e^{-i\xi_1}\right),\ \mathbf{M}_R = \frac{u_2}{\sqrt{2}}\left(\mathbf{Y}_R^1\, e^{i\xi_2} + \mathbf{Y}_R^2\, e^{-i\xi_2}\right).
\end{aligned} \tag{3.36}$$

Notice that there are other Yukawa interactions invariant under the SM gauge symmetry, beside the ones in Eq. (3.35). In fact, there will be the additional terms displayed in Eq. (3.2) as well as bare mass terms, which are given by

$$\begin{aligned}
-\mathcal{L}^{(2)}_{\text{Yuk.}} = {}& \overline{\ell_L}\left(\mathbf{Y}^1_{D_s}\tilde{\Phi}_1 + \mathbf{Y}^2_{D_s}\tilde{\Phi}_2\right) s^c\\
&+ \frac{1}{2}\overline{\nu_R^c}\mathbf{M}^0_{\mu_R}\nu_R + \frac{1}{2}\overline{\nu_R^c}\left(\mathbf{Y}^1_{\mu_R}S_1 + \mathbf{Y}^2_{\mu_R}S_1^*\right)\nu_R + \frac{1}{2}\overline{\nu_R^c}\left(\mathbf{Y}^3_{\mu_R}S_2 + \mathbf{Y}^4_{\mu_R}S_2^*\right)\nu_R\\
&+ \frac{1}{2}\overline{s^c}\mathbf{M}^0_s s + \frac{1}{2}\overline{s^c}\left(\mathbf{Y}^3_s S_2 + \mathbf{Y}^4_s S_2^*\right) s\\
&+ \overline{\nu_R}\mathbf{M}^0_R s + \overline{\nu_R}\left(\mathbf{Y}^3_R S_1 + \mathbf{Y}^4_R S_1^*\right) s + \text{H.c.}.
\end{aligned} \tag{3.37}$$

The above terms will be forbidden by the Abelian symmetries to be considered next.

To implement Abelian flavour symmetries, we require the full Lagrangian to be invariant under the field transformations

$$\begin{aligned}
&\Phi_a \to \mathbf{X}_{\Phi_a}\Phi_a, \quad S_a \to \mathbf{X}_{S_a}S_a\ ,\\
&\ell_L \to \mathbf{X}_\ell \ell_L,\ e_R \to \mathbf{X}_e e_R\ ,\\
&\nu_R \to \mathbf{X}_R\nu_R,\ s \to \mathbf{X}_s s,
\end{aligned} \tag{3.38}$$

where, for each field component F, $\mathbf{X}_F$ denotes a phase of the form e^{ix_F}. This invariance requirement yields the following constraints on the Yukawa matrices of Eq. (3.35):

$$\begin{aligned}
&\mathbf{Y}^a_\ell = \mathbf{X}^\dagger_\ell \mathbf{Y}^a_\ell \mathbf{X}_e \mathbf{X}_{\Phi_a},\ \mathbf{Y}^a_D = \mathbf{X}^\dagger_\ell \mathbf{Y}^a_D \mathbf{X}_R \mathbf{X}^*_{\Phi_a},\\
&\mathbf{Y}^1_s = \mathbf{X}^T_s \mathbf{Y}^1_s \mathbf{X}_s \mathbf{X}_{S_1},\ \mathbf{Y}^2_s = \mathbf{X}^T_s \mathbf{Y}^2_s \mathbf{X}_s \mathbf{X}^*_{S_1},\\
&\mathbf{Y}^1_R = \mathbf{X}^\dagger_R \mathbf{Y}^1_R \mathbf{X}_s \mathbf{X}_{S_2},\ \mathbf{Y}^2_R = \mathbf{X}^\dagger_R \mathbf{Y}^2_R \mathbf{X}_s \mathbf{X}^*_{S_2}\ ,
\end{aligned} \tag{3.39}$$

which can be translated into relations among the various field-transformation phases x_F. To implement a texture-zero entry in one of the above Yukawa matrices we require that the corresponding phase relation is not fulfilled.

We now proceed to identify which of the maximally-restrictive texture sets compatible with neutrino data (see previous section) can be realised by imposing discrete or continuous Abelian symmetries. To this end, we will apply two methods that complement each other, namely the canonical [131, 132] and the Smith normal form (SNF) [133, 134] methods. Our methodology follows closely the one employed in Refs. [72, 129]. We start with the canonical approach applied to the maximally-restrictive textures presented in Table 3.1 to reduce the scope of realisable textures before employing the SNF method. We recall that the charged-lepton textures 4^ℓ_1 and 4^ℓ_2 cannot be realised through Abelian symmetries in the 2HDM [72]. For the remaining cases, we first write all possible decompositions of the mass matrix textures into the corresponding two Yukawa matrices defined in Eq. (3.36). Afterwards, for a given

$\mathbf{M}_\ell$	$\mathbf{M}_D$	$\mathbf{M}_R$	$\mathbf{M}_s$	$\mathbf{M}_{\rm eff}$
$5^\ell_{1,\rm I}$	T_{45}	T_{14}	T_{23}	1^ν_6
4^ℓ_3	T_{124}	T_{14}	T_{23}	3^ν_{11}
	T_{456}	T_{14}	T_{23}	3^ν_{19}
	$\mathrm{T}_{136,\rm I}$	T_{14}	T_{23}	2^ν_{15}
	$\mathrm{T}_{146,\rm I}$	T_{14}	T_{23}	2^ν_{13}

$\mathbf{M}_\ell$	$\mathbf{Y}^1_\ell$	$\mathbf{Y}^2_\ell$
4^ℓ_3	$\begin{pmatrix} 0 & 0 & \times \\ 0 & \times & 0 \\ \times & 0 & 0 \end{pmatrix}$	$\begin{pmatrix} 0 & 0 & 0 \\ 0 & 0 & \times \\ 0 & \times & 0 \end{pmatrix}$
$5^\ell_{1,\rm I}$	$\begin{pmatrix} 0 & 0 & \times \\ 0 & 0 & 0 \\ \times & 0 & 0 \end{pmatrix}$	$\begin{pmatrix} 0 & 0 & 0 \\ 0 & \times & 0 \\ 0 & 0 & \times \end{pmatrix}$
$5^\ell_{1,\rm II}$	$\begin{pmatrix} 0 & 0 & \times \\ 0 & \times & 0 \\ \times & 0 & 0 \end{pmatrix}$	$\begin{pmatrix} 0 & 0 & 0 \\ 0 & 0 & 0 \\ 0 & 0 & \times \end{pmatrix}$

$\mathbf{M}_R$	$\mathbf{Y}_R$
T_{14}	$\begin{pmatrix} 0 & \times \\ \times & 0 \end{pmatrix}$

$\mathbf{M}_s$	$\mathbf{Y}^1_s$	$\mathbf{Y}^2_s$
T_{23}	$\begin{pmatrix} \times & 0 \\ 0 & 0 \end{pmatrix}$	$\begin{pmatrix} 0 & 0 \\ 0 & \times \end{pmatrix}$

$\mathbf{M}_D$	$\mathbf{Y}^1_D$	$\mathbf{Y}^2_D$
T_{45}	$\begin{pmatrix} \times & 0 \\ 0 & 0 \\ 0 & \times \end{pmatrix}$	$\begin{pmatrix} 0 & \times \\ \times & 0 \\ 0 & 0 \end{pmatrix}$
T_{124}	$\begin{pmatrix} 0 & 0 \\ 0 & 0 \\ \times & 0 \end{pmatrix}$	$\begin{pmatrix} 0 & 0 \\ 0 & 0 \\ 0 & \times \end{pmatrix}$
T_{456}	$\begin{pmatrix} 0 & \times \\ \times & 0 \\ 0 & 0 \end{pmatrix}$	$\begin{pmatrix} \times & 0 \\ 0 & 0 \\ 0 & 0 \end{pmatrix}$
$\mathrm{T}_{136,\rm I}$	$\begin{pmatrix} 0 & 0 \\ 0 & \times \\ 0 & 0 \end{pmatrix}$	$\begin{pmatrix} 0 & \times \\ 0 & 0 \\ \times & 0 \end{pmatrix}$
$\mathrm{T}_{136,\rm II}$	$\begin{pmatrix} 0 & \times \\ 0 & 0 \\ 0 & 0 \end{pmatrix}$	$\begin{pmatrix} 0 & 0 \\ 0 & \times \\ \times & 0 \end{pmatrix}$
$\mathrm{T}_{146,\rm I}$	$\begin{pmatrix} 0 & \times \\ 0 & 0 \\ \times & 0 \end{pmatrix}$	$\begin{pmatrix} 0 & 0 \\ \times & 0 \\ 0 & 0 \end{pmatrix}$
$\mathrm{T}_{146,\rm II}$	$\begin{pmatrix} 0 & \times \\ \times & 0 \\ 0 & 0 \end{pmatrix}$	$\begin{pmatrix} 0 & 0 \\ 0 & 0 \\ \times & 0 \end{pmatrix}$

Table 3.4: [Top] Maximally-restrictive texture-zero sets compatible with neutrino oscillation data and realisable through Abelian symmetries. [Bottom] Decomposition of mass matrices into the Yukawa textures according to Eq. (3.36).

$(\mathbf{M}_\ell, \mathbf{M}_D, \mathbf{M}_R, \mathbf{M}_s)$ combination, and for all decompositions of its matrices, we solve the corresponding system of algebraic relations for the field phases (or charges) stemming from Eq. (3.39). If a solution exists for a set of charges, then that specific $(\mathbf{M}_\ell, \mathbf{M}_D, \mathbf{M}_R, \mathbf{M}_s)$ is realisable by Abelian symmetries with the fields carrying those charges. Note we must also check if no term in Eq. (3.37) is allowed such that we restrict our analysis to the ISS mass Lagrangian. In Table 3.4, we present the realisable mass matrix textures and their corresponding Yukawa decompositions, respectively. Notice that although in some cases two decompositions are possible for a given mass matrix, only one is realisable. We set the ordering for $\mathbf{Y}^{1,2}_\ell$ and $\mathbf{Y}^{1,2}_D$ as the one given in Table 3.4. Also, we use the notation $\mathbf{Y}_R \equiv \mathbf{Y}^1_R$ [see Eq. (3.35)] since $\mathbf{Y}^2_R$ is forbidden by the symmetries as we shall see promptly. Hence, since for all realisable cases $\mathbf{M}_R$ and $\mathbf{M}_s$ are fixed by the textures T_{14} and T_{23}, respectively, from now on we will refer to each case just through the pair notation $(\mathbf{M}_\ell, \mathbf{M}_D)$.

Fields	U(1)	$(5^{\ell}_{1,\mathrm{I}}, \mathrm{T}_{45})$ $\mathbb{Z}_2 \times \mathrm{U}(1)_{\mathrm{F}}$	$(4^{\ell}_{3}, \mathrm{T}_{124})$ $\mathbb{Z}_2 \times \mathrm{U}(1)_{\mathrm{F}}$	$(4^{\ell}_{3}, \mathrm{T}_{456})$ $\mathbb{Z}_2 \times \mathrm{U}(1)_{\mathrm{F}}$	$(4^{\ell}_{3}, \mathrm{T}_{136,\mathrm{I}})$ $\mathbb{Z}_4 \times \mathrm{U}(1)_{\mathrm{F}}$	$(4^{\ell}_{3}, \mathrm{T}_{146,\mathrm{I}})$ $\mathbb{Z}_4 \times \mathrm{U}(1)_{\mathrm{F}}$
Φ_1	0	$(1,1)$	$(0,-5)$	$(1,1)$	$(1,2)$	$(0,1)$
Φ_2	0	$(0,-1)$	$(1,-3)$	$(0,-1)$	$(0,1)$	$(3,0)$
S_1	0	$(0,2)$	$(0,-2)$	$(0,-2)$	$(0,-2)$	$(0,-2)$
S_2	1	$(0,0)$	$(0,0)$	$(1,0)$	$(0,0)$	$(0,0)$
ℓ_{e_L}	1	$(1,0)$	$(0,0)$	$(0,0)$	$(2,0)$	$(2,0)$
ℓ_{μ_L}	1	$(0,2)$	$(1,2)$	$(1,-2)$	$(1,-1)$	$(1,-1)$
ℓ_{τ_L}	1	$(0,-2)$	$(0,4)$	$(0,-4)$	$(0,-2)$	$(0,-2)$
e_R	1	$(1,-3)$	$(0,9)$	$(1,-5)$	$(3,-4)$	$(0,-3)$
μ_R	1	$(0,3)$	$(1,7)$	$(0,-3)$	$(0,-3)$	$(1,-2)$
τ_R	1	$(0,-1)$	$(0,5)$	$(1,-1)$	$(1,-2)$	$(2,-1)$
ν_{R_1}	1	$(0,1)$	$(0,-1)$	$(0,-1)$	$(0,-1)$	$(0,-1)$
ν_{R_2}	1	$(1,-1)$	$(1,1)$	$(1,1)$	$(2,1)$	$(2,1)$
s_1	0	$(1,-1)$	$(1,1)$	$(0,1)$	$(2,1)$	$(2,1)$
s_2	0	$(0,1)$	$(0,-1)$	$(1,-1)$	$(0,-1)$	$(0,-1)$

Table 3.5: Maximally-restrictive texture sets realisable through an Abelian symmetry group. For each texture pair, we provide the $\mathbb{Z}_n$ charges q_n such that the transformation phases are $e^{2\pi i q_n/n}$. The U(1) and $\mathrm{U}(1)_{\mathrm{F}}$ charges are expressed as multiples of the arbitrary charges q_1 and q_{F}, respectively.

Applying the SNF method to the texture sets passing the canonical method test, we find that the minimal Abelian symmetry group $\mathbf{G}$ realising such textures is

$$\mathbf{G} = \mathbb{Z}_n \times [\mathrm{U}(1)]^3\,, \quad n = 2, 4. \tag{3.40}$$

Irrespective of the type of Yukawa textures, the Lagrangian is invariant under the global continuous symmetry $\mathrm{U}(1)_Y$, Y being the SM hypercharge. Since, obviously, that $\mathrm{U}(1)_Y$ does not impose any texture zero, the actual flavour symmetry group $\mathbf{G}_{\mathrm{F}} = \mathbf{G}/\mathrm{U}(1)_Y$ is

$$\mathbf{G}_{\mathrm{F}} = \mathbb{Z}_n \times [\mathrm{U}(1)]^2\,, \quad n = 2, 4. \tag{3.41}$$

Furthermore, the Yukawa Lagrangian (3.35) is also invariant under the following U(1) global symmetry,

$$\ell_L \to e^{iq_1}\,\ell_L,\ e_R \to e^{iq_1}\,e_R,\ \nu_R \to e^{iq_1}\,\nu_R,\ S_2 \to e^{iq_1}\,S_2, \tag{3.42}$$

with the other fields remaining invariant. Note that the term in Eq. (3.35) involving $\mathbf{Y}_R^2$ is forbidden. Furthermore, although this symmetry does not impose any texture zero on the mass matrices, it restricts the possible coupling terms that can appear in the Lagrangian. In fact, all terms in Eq. (3.37) are forbidden except for the bare Majorana mass term of the form $s^T C s$ which is allowed by this symmetry. Nevertheless, it can be shown that the remaining Abelian symmetries forbid such a bare term. The

minimal group that discretises this U(1) symmetry is $\mathbb{Z}_4$, with $q_1 = \pi/2$. Thus, the actual flavour symmetry group is

$$\mathbf{G}_\mathrm{F} = \mathrm{U}(1) \times \mathbb{Z}_n \times \mathrm{U}(1)_\mathrm{F}, \quad n = 2, 4. \tag{3.43}$$

The maximally restrictive texture sets $\left(5^\ell_{1,\mathrm{I}}, \mathrm{T}_{45}\right)$, $\left(4^\ell_3, \mathrm{T}_{124}\right)$ and $\left(4^\ell_3, \mathrm{T}_{456}\right)$ are realised by the flavour symmetry for $n = 2$, while $\left(4^\ell_3, \mathrm{T}_{136,\mathrm{I}}\right)$ and $\left(4^\ell_3, \mathrm{T}_{146,\mathrm{I}}\right)$ are realised by the Abelian symmetry group for $n = 4$. The corresponding $\mathrm{U}(1)_\mathrm{F}$ charges can be determined through the canonical method, while the discrete group charges are obtained resorting to the SNF method. We present in Table 3.5, for each texture set, the Abelian symmetry group that realises the set and the associated transformation charges for each field. In all cases, the full texture decomposition is imposed by the $\mathrm{U}(1)_\mathrm{F}$ symmetry alone. The discrete groups, $\mathbb{Z}_2$ or $\mathbb{Z}_4$, only preserve some of the texture zeros but ultimately fail in imposing them totally. Yet, they are crucial in forbidding the bare Majorana mass term for sterile singlet fermions s. In fact, the $\mathrm{U}(1)_\mathrm{F}$ charges alone only forbid the diagonal elements of the bare mass term, while the charges of the discrete groups forbid the remaining off-diagonal elements. Therefore, the Yukawa Lagrangian remains restricted to the form given in Eq. (3.35) where the term with $\mathbf{Y}^2_R$ is forbidden and $\mathbf{Y}_R \equiv \mathbf{Y}^1_R$. As a final comment, let us note that for the realisable cases the $\mathrm{U}(1)_\mathrm{F}$ symmetry can be discretised into a minimal set of charges corresponding to a $\mathbb{Z}_5$ symmetry.

Chapter 4

Phenomenology

The previous chapter was aimed at building the model for this work. In fact, we showed that the maximally-restrictive textures for the lepton mass and Yukawa matrices, compatible with neutrino oscillation data, can be realised through Abelian symmetries in the context of the minimal ISS mechanism for the sets shown in Table 3.5. For reasons that will become clear later (see Section 4.3), throughout the rest of this thesis we restrict our phenomenological analysis to the combination $\left(5^{\ell}_{1,\mathrm{I}}, \mathrm{T}_{45}\right)$. Hence, in this chapter, we study the phenomenological possibilities stemming from this case. Due to the extended scalar content of our model, we start by showing the common origin of leptonic CPV (LCPV) lying in spontaneous CPV (SCPV) coming from the complex phase of the VEV of the singlet S_1. Next, we comment on the validity of the ISS approximation and the impact of radiative corrections to light neutrino masses. Additionally, we study lepton flavour violation (LFV) focusing on the constraints coming from the charged LFV (cLFV) processes $\ell_\alpha \to \ell_\beta \gamma$, $Z \to \ell^{\pm}_{\alpha}\ell^{\mp}_{\beta}$, $\ell^{-}_{\alpha} \to \ell^{-}_{\beta}\ell^{+}_{\gamma}\ell^{-}_{\delta}$ and coherent $\mu - e$ conversion in nuclei. Finally, we look at further constraints translated in terms of mass and active-sterile mixing, namely the ones coming from beam-dump and collider experiments as well as EW precision data (EWPD). We recall that, the analysis we perform in this chapter follows closely the one realised in Ref. [126].

4.1 Lepton masses, mixing and leptonic CPV

For the case under study $\left(5^{\ell}_{1,\mathrm{I}}, \mathrm{T}_{45}\right)$, the charged-lepton mass matrix can be parameterised as

$$5^{\ell}_{1}: \quad \mathbf{M}_{\ell} = \begin{pmatrix} 0 & 0 & a_1 \\ 0 & a_3 & 0 \\ a_2 & 0 & a_4 \end{pmatrix}, \qquad \begin{aligned} a_1^2 &= \frac{m^2_{\ell_2} m^2_{\ell_3}}{a_2^2}\ ,\ m_{\ell_2} < a_2 < m_{\ell_3}, \\ a_3^2 &= m^2_{\ell_1}\ ,\ a_4^2 = \frac{(a_2^2 - m^2_{\ell_2})(m^2_{\ell_3} - a_2^2)}{a_2^2}, \end{aligned} \tag{4.1}$$

where a_i can always be made real by phase field redefinitions, and $m_{\ell_{1,2,3}}$ are the charged-lepton masses. Note that the charged-lepton state ℓ_1 is decoupled from the remaining ones. The unitary matrices $\mathbf{V}'_L$

and $\mathbf{V}'_R$ that diagonalise the Hermitian matrices $\mathbf{H}_\ell = \mathbf{M}_\ell \mathbf{M}_\ell^\dagger$ and $\mathbf{H}'_\ell = \mathbf{M}_\ell^\dagger \mathbf{M}_\ell$ are given by

$$\mathbf{H}_\ell = \begin{pmatrix} a_1^2 & 0 & a_1 a_4 \\ 0 & a_3^2 & 0 \\ a_1 a_4 & 0 & a_2^2 + a_4^2 \end{pmatrix} \, , \; \mathbf{V}'_L = \begin{pmatrix} c_L & 0 & s_L \\ 0 & 1 & 0 \\ -s_L & 0 & c_L \end{pmatrix} \tag{4.2}$$

$$\mathbf{H}'_\ell = \begin{pmatrix} a_1^2 & 0 & a_2 a_4 \\ 0 & a_3^2 & 0 \\ a_2 a_4 & 0 & a_1^2 + a_4^2 \end{pmatrix} \, , \; \mathbf{V}'_R = \begin{pmatrix} c_R & 0 & s_R \\ 0 & 1 & 0 \\ -s_R & 0 & c_R \end{pmatrix} \, . \tag{4.3}$$

Here, we have used the compact notation $c_{L,R} \equiv \cos\theta_{L,R}$ and $s_{L,R} \equiv \sin\theta_{L,R}$ with the angles $\theta_{L,R}$ given by the following expressions

$$\tan(2\theta_L) = \frac{2 m_{\ell_2} m_{\ell_3} \sqrt{(a_2^2 - m_{\ell_2}^2)(m_{\ell_3}^2 - a_2^2)}}{a_2^2 (m_{\ell_2}^2 + m_{\ell_3}^2) - 2 m_{\ell_2}^2 m_{\ell_3}^2} \, , \; \tan(2\theta_R) = \frac{2\sqrt{(a_2^2 - m_{\ell_2}^2)(m_{\ell_3}^2 - a_2^2)}}{m_{\ell_2}^2 + m_{\ell_3}^2 - 2a_2^2} . \tag{4.4}$$

We consider the three distinct cases of $5_1^{\ell_1}$ textures with $\ell_1 = e, \mu, \tau$, labelled as $5_1^{e,\mu,\tau}$. Since after the diagonalisation of the charged-lepton mass matrix the unitary matrices $\mathbf{V}_{L,R}$ are such that the correct mass ordering is obtained as in Eq. (2.24), we have

$$5_1^e : \mathbf{V}_{L,R} = \mathbf{V}'_{L,R} \mathbf{P}_{12}, \quad 5_1^\mu : \mathbf{V}_{L,R} = \mathbf{V}'_{L,R}, \quad 5_1^\tau : \mathbf{V}_{L,R} = \mathbf{V}'_{L,R} \mathbf{P}_{23}, \tag{4.5}$$

with

$$\mathbf{P}_{12} = \begin{pmatrix} 0 & 1 & 0 \\ 1 & 0 & 0 \\ 0 & 0 & 1 \end{pmatrix} \, , \; \mathbf{P}_{23} = \begin{pmatrix} 1 & 0 & 0 \\ 0 & 0 & 1 \\ 0 & 1 & 0 \end{pmatrix} . \tag{4.6}$$

As seen in the previous section, for $\mathbf{M}_\ell$ of the type 5_1^ℓ, only the $\mathbf{M}_D$, $\mathbf{M}_R$ and $\mathbf{M}_s$ matrices of the type T_{45}, T_{14} and T_{23}, respectively, lead to maximally-restricted neutrino mass matrices. In terms of the Yukawa matrices given in Eq. (3.35), those mass matrices are realised through Abelian symmetries for the decompositions (see Table 3.4)

$$\begin{aligned} \mathbf{Y}_D^1 &= \begin{pmatrix} b_1 & 0 \\ 0 & 0 \\ 0 & b_2 \end{pmatrix} \, , \; \mathbf{Y}_D^2 = \begin{pmatrix} 0 & b_3\, e^{i\beta_1} \\ b_4 & 0 \\ 0 & 0 \end{pmatrix} \, , \\ \mathbf{Y}_R &= \begin{pmatrix} 0 & d_2 \\ d_1 & 0 \end{pmatrix} \, , \; \mathbf{Y}_s^1 = \begin{pmatrix} f_2 & 0 \\ 0 & 0 \end{pmatrix} \, , \; \mathbf{Y}_s^2 = \begin{pmatrix} 0 & 0 \\ 0 & f_1\, e^{i\beta_2} \end{pmatrix} . \end{aligned} \tag{4.7}$$

Notice that we have rephased the fields to remove the unphysical phases such that b_i, d_i and f_i are real and only the phases $\beta_{1,2}$ remain in all Yukawa couplings of Eq. (3.35).

From now on, instead of considering the general case of complex Yukawa couplings, we will consider the scenario in which CP is imposed at the Lagrangian level and, thus, $\beta_{1,2} = 0$. As shown in Appendix A, the scalar potential of the fields Φ and $S_{1,2}$, with the soft breaking of the $\mathrm{U}(1) \times \mathbb{Z}_2 \times \mathrm{U}(1)_{\mathrm{F}}$ symmetry,

allows for a CP-violating vacuum configuration with [1]

$$\langle \phi_1^0 \rangle = v \cos\beta \ , \ \langle \phi_2^0 \rangle = v \sin\beta \ , \ \langle S_1 \rangle = u_1 e^{i\xi} \ , \ \langle S_2 \rangle = u_2 \ , \ \tan\beta = \frac{v_2}{v_1} \, . \tag{4.8}$$

Together with Eqs. (4.7), these VEVs lead to the mass matrices

$$\mathbf{M}_D = \begin{pmatrix} m_{D_1} & m_{D_3} \\ m_{D_4} & 0 \\ 0 & m_{D_2} \end{pmatrix} \ , \ \mathbf{M}_R = \begin{pmatrix} 0 & M \\ qM & 0 \end{pmatrix} \ , \ \mathbf{M}_s = \begin{pmatrix} p\,\mu_s e^{i\xi} & 0 \\ 0 & \mu_s e^{-i\xi} \end{pmatrix} \ , \tag{4.9}$$

being the matrix elements defined as

$$m_{D_{1,2}} = b_{1,2}\, v \cos\beta \ , \ m_{D_{3,4}} = b_{3,4}\, v \sin\beta \ , \ M = d_2 u_2 \ , \ \mu_s = f_1 u_1 \ , \ q = d_1/d_2 \ , \ p = f_2/f_1 \ , \tag{4.10}$$

where p and q are rescaling adimensional parameters, which will be useful for later discussions. Taking into account Eqs. (3.12) and (4.9), the effective neutrino mass matrix in the original symmetry basis reads

$$\mathbf{M}_{\rm eff} = \begin{pmatrix} \dfrac{y^2}{x} + \dfrac{z^2}{w} e^{2i\xi} & y & z e^{2i\xi} \\ y & x & 0 \\ z e^{2i\xi} & 0 & w e^{2i\xi} \end{pmatrix} \ , \quad \begin{array}{l} x = \mu_s \dfrac{m_{D_4}^2}{M^2} \ , \ y = \mu_s \dfrac{m_{D_1} m_{D_4}}{M^2} \ , \\ z = \mu_s \dfrac{m_{D_2} m_{D_3}}{M^2} \dfrac{p}{q^2} \ , \ w = \mu_s \dfrac{m_{D_2}^2}{M^2} \dfrac{p}{q^2} \, , \end{array} \tag{4.11}$$

with all parameters real. Performing the rotation to the charged-lepton mass basis with one of the unitary matrices $\mathbf{V}_L$ given in Eq. (4.5), we obtain for the 5_1^e case:

$$\mathbf{V}_L^T \mathbf{M}_{\rm eff} \mathbf{V}_L = \begin{pmatrix} x & y c_L & y s_L \\ \times & \dfrac{y^2 c_L^2}{x} + \dfrac{(z c_L - w s_L)^2}{w} e^{2i\xi} & \dfrac{y^2 s_L c_L}{x} + \dfrac{\left(z^2 - w^2\right) s_L c_L + wz \cos(2\theta_L)}{w} e^{2i\xi} \\ \times & \times & \dfrac{y^2 s_L^2}{x} + \dfrac{(w c_L + z s_L)^2}{w} e^{2i\xi} \end{pmatrix} \, . \tag{4.12}$$

Since the matrix above is symmetric we mark with an "$\times$" the repeated elements. Note that for 5_1^μ and 5_1^τ the permutations $\mathbf{P}_{12}$ and $\mathbf{P}_{12}\mathbf{P}_{23}$ of Eq. (4.6) have to be applied on the left and right. The above matrix must be matched with the one defined in terms of the physical low-energy parameters according to Eqs. (3.13)-(3.15) and (2.36), for which the matrix elements are

$$\text{NO} : M_{ij} = \left[\mathbf{U}'^{*} \text{diag}\left(0, \sqrt{\Delta m_{21}^2}, \sqrt{\Delta m_{31}^2}\right) \mathbf{U}'^{\dagger} \right]_{ij} \, , \tag{4.13}$$

$$\text{IO} : M_{ij} = \left[\mathbf{U}'^{*} \text{diag}\left(\sqrt{\Delta m_{31}^2}, \sqrt{\Delta m_{21}^2 + \Delta m_{31}^2}, 0\right) \mathbf{U}'^{\dagger} \right]_{ij} \, , \tag{4.14}$$

for both NO and IO neutrino masses [see Eqs. (2.38) and (2.39)]. The lepton mixing matrix $\mathbf{U}'$ is parameterised as in Eq. (2.36), with only one physical Majorana phase α since, in our framework, one

[1] Spontaneous CP violation can also be successfully communicated to the lepton sector for the texture combinations $\left(4_3^\ell, \text{T}_{124}\right)$ and $\left(4_3^\ell, \text{T}_{456}\right)$. This is not the case for the pairs $\left(4_3^\ell, \text{T}_{136,\text{I}}\right)$ and $\left(4_3^\ell, \text{T}_{146,\text{I}}\right)$ for which $\mathbf{M}_D$ has one texture zero per row (see Table 3.4) and the complex phase ξ can be rephased away.

neutrino is massless (see Section 3.2.1). It is clear from Eq. (4.12) that there are six relevant effective parameters (x, y, z, w, ξ and θ_L) that determine neutrino masses and mixings. These are to be compared with seven low-energy physical parameters which define M_{ij}, namely three mixing angles θ_{ij}, two neutrino masses and two CPV phases (the Dirac and Majorana phases δ and α, respectively). Thus, there is a relation among the elements of the effective neutrino mass matrix, which results in a correlation between two low-energy parameters. It can be shown that, for the 5_1^e case, the said relation is

$$5_1^e : \arg\left[M_{11}^{*2} M_{13}^2 \frac{\mathrm{D}_{12}}{\mathrm{D}_{23}}\right] = 0 \,, \; \mathrm{D}_{ij} = M_{ii} M_{jj} - M_{ij}^2 \,, \tag{4.15}$$

while the corresponding ones for the 5_1^μ and 5_1^τ cases can be obtained by performing the index replacements $(11 \to 12, 13 \to 23)$ and $(11 \to 13, 13 \to 33)$, respectively. For a given set of θ_{ij} and $\Delta m^2_{21,31}$ values, the above equations establish how the two CP-phases δ and α are correlated. Moreover, we notice that all parameters in Eq. (4.12) can be expressed in terms of low-energy neutrino observables. Indeed, for 5_1^e we have

$$\begin{aligned}
5_1^e : \quad & \tan\theta_L = \left|\frac{M_{13}}{M_{12}}\right| \,, \quad x = |M_{11}| \,, \quad \xi = \arg\left[M_{12}^* \sqrt{\mathrm{D}_{12}}\right] \,, \\
& |y|^2 = |D_{23}| x^2 \left(\frac{\sqrt{|D_{13}|} c_L^2 \pm \sqrt{|D_{12}|} s_L^2}{|D_{13}| c_L^2 - |D_{12}| s_L^2}\right)^2 \,, \\
& w = \frac{\sqrt{|D_{13}|} c_L^2 \mp \sqrt{|D_{12}|} s_L^2}{x} \,, \\
& z = \frac{(|D_{13}| - |D_{12}|)\sin(2\theta_L) \mp 2\sqrt{|D_{13} D_{12}|}\cos(2\theta_L)}{4x} \,.
\end{aligned} \tag{4.16}$$

The equivalent expressions for 5_1^μ and 5_1^τ can be obtained performing the replacements $(11 \to 22, 13 \leftrightarrow 23)$ and $(11 \to 33, 13 \to 23, 12 \to 13, 23 \to 12)$, respectively.

In order to establish numerically how δ and α are related, we vary the mixing angles θ_{ij} and the neutrino mass-squared differences $\Delta m^2_{21,31}$ within their experimental 1σ and 3σ ranges (see Table 2.2), while changing δ from 0 to 2π. Then, for both NO and IO cases, we compute M_{ij} through Eqs. (4.13) and (4.14), respectively. The Majorana phase α is obtained by solving Eq. (4.15) for $5_1^{e,\mu,\tau}$, leading to the results presented in Fig. 4.1, where in the left (right) column we show the allowed regions in the (δ, α) plane for the $\mathrm{NO}_{e,\mu,\tau}$ ($\mathrm{IO}_{e,\mu,\tau}$) corresponding to $5_1^{e,\mu,\tau}$ with a NO (IO) neutrino mass spectrum. The blue (magenta) regions were obtained taking the 1σ (3σ) intervals for θ_{ij} and $\Delta m^2_{21,31}$, while the vertical dark (light) grey band marks the current experimentally allowed region for the Dirac CP phase δ at 1σ (3σ). The results show that there is a strong correlation between α and δ. For both NO and IO mass ordering, the plots exhibit an approximate symmetry under the shift $\delta \to \delta + \pi$, which is due to the fact that Eq. (4.15) is nearly invariant under that transformation at zeroth order in the smallest mixing angle θ_{13}. Note that the absence of Dirac-type CP violation ($\delta = 0, \pi$) implies $\alpha = k\pi \, (k \in \mathbb{Z})$. This can be confirmed analytically by evaluating the Dirac and Majorana CP weak basis invariants, $\mathcal{J}^{\mathrm{CP}}_{\mathrm{Dirac}}$ and $\mathcal{J}^{\mathrm{CP}}_{\mathrm{Maj}}$ [135], which are both proportional to $\sin(2\xi)$. Notice also that a future measurement of δ in the intervals $[45°, 135°]$ and $[135°, 225°]$ would exclude the NO_μ and NO_τ cases since, in these ranges, Eq. (4.15) has no solution.

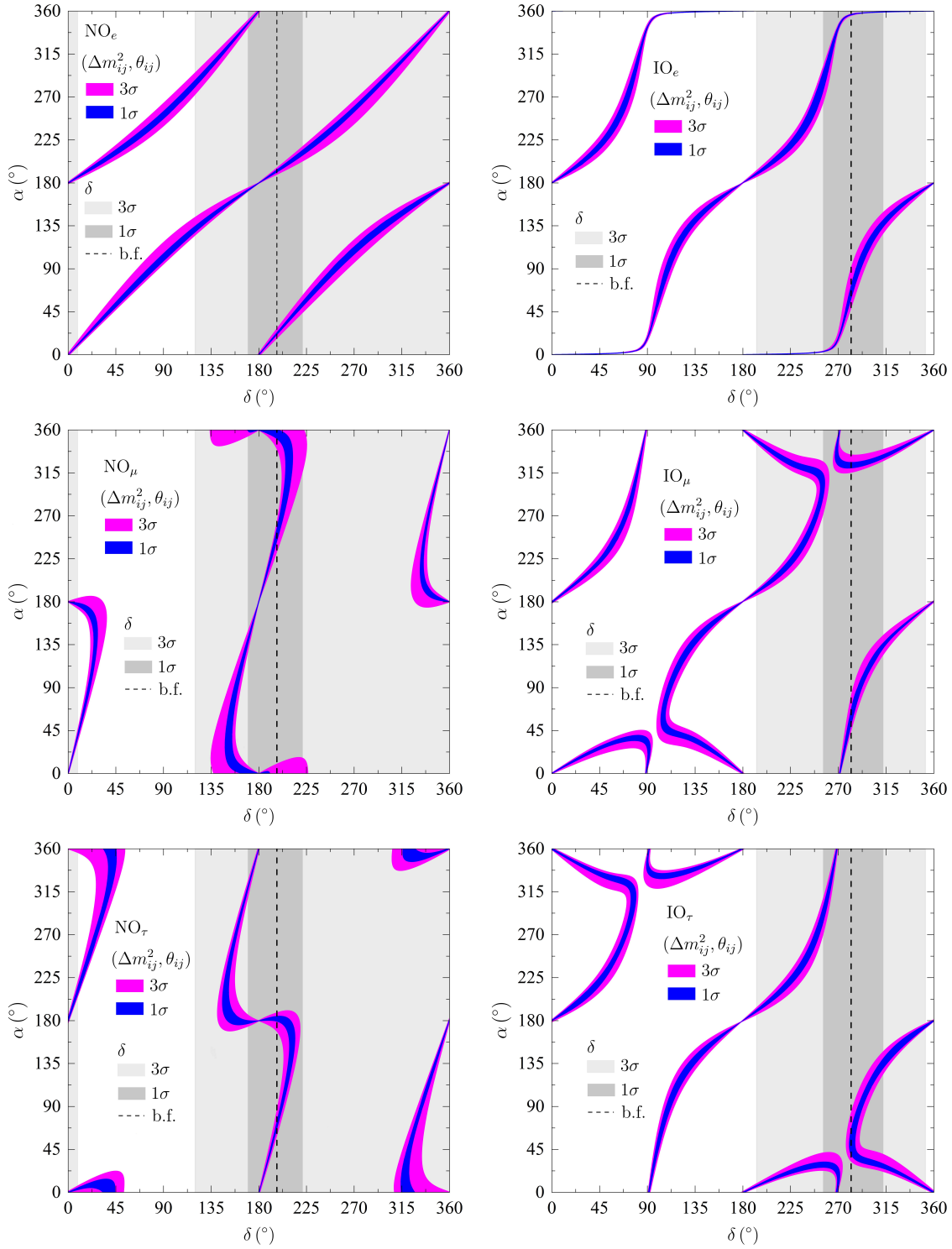

Figure 4.1: Predictions for the Majorana phase α as function of the Dirac CP phase δ varying the neutrino mixing angles θ_{ij} and the neutrino mass-squared differences Δm^2_{21} and Δm^2_{31} in the 1σ (blue) and 3σ (magenta) allowed ranges given in Table 2.2. The dark (light) grey vertical band marks the 1σ (3σ) range for δ shown in the same table, while the vertical dashed line is at the δ best-fit value. The left (right) column corresponds to the cases with NO (IO) neutrino mass spectrum and a charged lepton mass matrix of the 5^e_1 (top), 5^μ_1 (middle) and 5^τ_1 (bottom) type. Hereafter, these different possibilities will be labelled as NO$_{e,\mu,\tau}$ and IO$_{e,\mu,\tau}$.

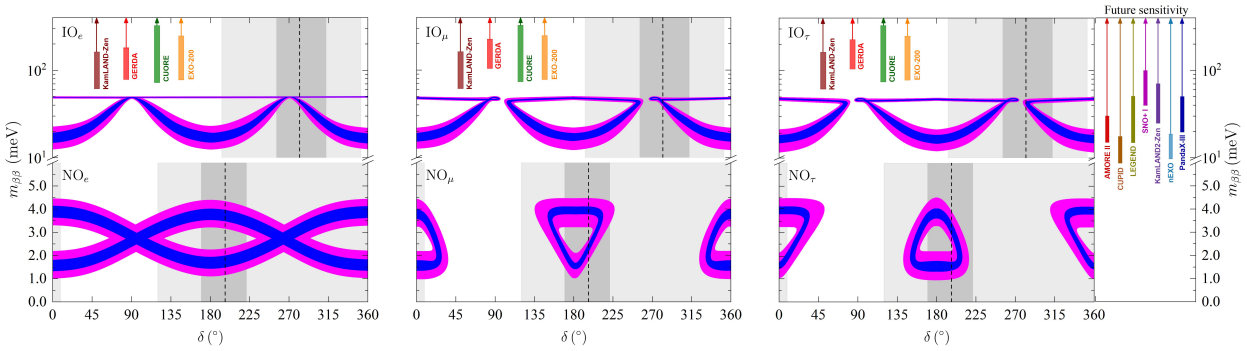

Figure 4.2: Effective neutrino mass parameter $m_{\beta\beta}$ as function of the Dirac CP-violating phase for the 5^e_1 (left), 5^μ_1 (centre) and 5^τ_1 (right) cases (the colour codes are the same as in Fig. 4.1). In each panel we show the NO and IO results in the lower and upper fraction of the vertical scale, respectively. We also show the upper bounds on $m_{\beta\beta}$ reported by the KamLAND-Zen [110], GERDA [111], CUORE [112] and EXO-200 [113] collaborations (the height of the corresponding rectangles represent the uncertainty in the upper bounds). On the right the sensitivity of several future experiments is shown (see Table 2.3).

The fact that the Majorana and Dirac CP-violating phases are related brings up an interesting connection between neutrinoless double beta decay ($\beta\beta_{0\nu}$) and neutrino oscillations. With one massless neutrino, the $\beta\beta_{0\nu}$ widths are proportional to the effective neutrino mass parameter $m_{\beta\beta}$ that, in the most general case, should only be sensitive to Majorana phases. Namely, for the NO and IO cases [136] one has [see Eqs. (2.41) and (2.42)]

$$\text{NO:}\;\; m_{\beta\beta} = \left| \sqrt{\Delta m^2_{21}}\, c^2_{13} s^2_{12}\, e^{-2i\alpha} + \sqrt{\Delta m^2_{31}}\, s^2_{13} \right| , \tag{4.17}$$

$$\text{IO:}\;\; m_{\beta\beta} = c^2_{13} \left| \sqrt{|\Delta m^2_{31}|}\, c^2_{12} + \sqrt{\Delta m^2_{21} + |\Delta m^2_{31}|}\, s^2_{12}\, e^{-2i\alpha} \right| . \tag{4.18}$$

Given that α is related to δ through Eqs. (4.15), a dependence of $m_{\beta\beta}$ on δ can be established, as shown in Fig. 4.2 for the same cases treated in Fig. 4.1. We also show the present upper limits and future sensitivities on $m_{\beta\beta}$ which are reported in Table 2.3 (the height of the bars reflects the uncertainties in the nuclear matrix elements relevant for the computation of the decay rates). Our results show that, although $m_{\beta\beta}$ is always below the current bounds (even taking the less conservative limits), several future experiments will be able to probe the whole $m_{\beta\beta}$ for IO neutrino masses. In particular, for the current best-fit values given in Table 2.2, we have $m_{\beta\beta} \simeq 40$ meV, which is on the upper IO region. As usual, future experiments with sensitivities of (1.0 - 4.5) meV will be needed to probe the NO regime (see e.g. Refs. [137] and [138] for reviews on future prospects of $\beta\beta_{0\nu}$ experiments).

We will now study the properties of the sterile neutrino sector, particularly its spectrum and mixing with active light neutrinos (heavy-light mixing). Although for our phenomenological analysis a full numerical computation will be carried out, we first provide an analytical insight following the discussion in Section 3.1 – see Eqs. (3.16)-(3.20). According to the definition of the effective heavy neutrino mass matrix $\mathbf{M}_{\text{heavy}}$ given in Eq. (3.9), and taking into account $\mathbf{M}_R$ and $\mathbf{M}_s$ from Eq. (4.9), we have for the

4×4 unitary matrix $\mathbf{U}_s$:

$$\mathbf{U}_s = \begin{pmatrix} -ic_1 e^{-i\xi/2} & s_1 e^{-i\xi/2} & 0 & 0 \\ 0 & 0 & -ic_2 e^{i\xi/2} & s_2 e^{i\xi/2} \\ 0 & 0 & is_2 e^{-i\xi/2} & c_2 e^{-i\xi/2} \\ is_1 e^{i\xi/2} & c_1 e^{i\xi/2} & 0 & 0 \end{pmatrix} , \tag{4.19}$$

where $c_{1,2} \equiv \cos\varphi_{1,2}$, $s_{1,2} \equiv \sin\varphi_{1,2}$ and

$$\tan(2\varphi_1) = \frac{2M}{\mu_s} , \quad \tan(2\varphi_2) = \frac{2qM}{p\mu_s} . \tag{4.20}$$

In the ISS approximation, $\varphi_1 \simeq \varphi_2 \simeq \pi/4$ leading to $c_1 \simeq s_1 \simeq c_2 \simeq s_2 \simeq 1/\sqrt{2}$, which characterises the two pairs of pseudo-Dirac neutrinos with masses [2]

$$\tilde{m}_{4,5} \simeq M \left[\sqrt{1 + \left(\frac{\mu_s}{2M}\right)^2} \mp \frac{\mu_s}{2M} \right] , \quad \tilde{m}_{6,7} \simeq qM \left[\sqrt{1 + \left(\frac{p\mu_s}{2qM}\right)^2} \mp \frac{p\mu_s}{2qM} \right] , \tag{4.21}$$

and mass differences $\tilde{m}_5 - \tilde{m}_4 = \mu_s$, $\tilde{m}_7 - \tilde{m}_6 = p\mu_s$. As expected, the degree of degeneracy between the masses is controlled by the small LNV parameter μ_s.

From Eqs. (3.19), (4.5) and (4.19), we obtain for the heavy-light neutrino mixing defined in Eq. (3.20), where for $\alpha = e, \mu, \tau$ and $j = 4, 5, 6, 7$, $\mathbf{B}_{\alpha j}$ is given by the matrix,

$$\begin{pmatrix} i\frac{m_{D_4}}{M} s_1 e^{i\xi/2} & \frac{m_{D_4}}{M} c_1 e^{i\xi/2} & 0 & 0 \\ i\frac{m_{D_1}}{M} s_1 c_L e^{i\xi/2} & \frac{m_{D_1}}{M} c_1 c_L e^{i\xi/2} & i\frac{(m_{D_3} c_L - m_{D_2} s_L)}{qM} s_2 e^{-i\xi/2} & \frac{(m_{D_3} c_L - m_{D_2} s_L)}{qM} c_2 e^{-i\xi/2} \\ i\frac{m_{D_1}}{M} s_1 s_L e^{i\xi/2} & \frac{m_{D_1}}{M} c_1 s_L e^{i\xi/2} & i\frac{(m_{D_3} s_L + m_{D_2} c_L)}{qM} s_2 e^{-i\xi/2} & \frac{(m_{D_3} s_L + m_{D_2} c_L)}{qM} c_2 e^{-i\xi/2} \end{pmatrix} , \tag{4.22}$$

for the 5_1^e case. The corresponding results for 5_1^μ and 5_1^τ are obtained applying on the left of the above matrix the permutation $\mathbf{P}_{12}$ and $\mathbf{P}_{12}\mathbf{P}_{23}$ of Eq. (4.6), respectively. Notice that each neutrino in a quasi-Dirac pair couples similarly to each lepton flavour α, i.e. $\mathbf{B}_{\alpha 4} \simeq \mathbf{B}_{\alpha 5}$ and $\mathbf{B}_{\alpha 6} \simeq \mathbf{B}_{\alpha 7}$. Since we are working in the charged-lepton mass basis, the above matrix provides an approximation to the mixing among the charged lepton e_α and the sterile neutrinos ν_{4-7}. It turns out that, due to the Abelian symmetries imposed to realise the maximally-restricted textures, the CC flavour mixings for distinct lepton flavours are related by low-energy neutrino parameters. Indeed, for the 5_1^e case,

$$\frac{\mathbf{B}_{e4}}{\mathbf{B}_{\mu 4}} \simeq \frac{\mathbf{B}_{e5}}{\mathbf{B}_{\mu 5}} \simeq \frac{x}{yc_L} , \quad \frac{\mathbf{B}_{\tau 4}}{\mathbf{B}_{\mu 4}} \simeq \frac{\mathbf{B}_{\tau 5}}{\mathbf{B}_{\mu 5}} \simeq \tan\theta_L , \quad \frac{\mathbf{B}_{\mu 6}}{\mathbf{B}_{\tau 6}} \simeq \frac{\mathbf{B}_{\mu 7}}{\mathbf{B}_{\tau 7}} \simeq \frac{z - w\tan\theta_L}{w + z\tan\theta_L} , \quad \mathbf{B}_{e6} \simeq \mathbf{B}_{e7} \simeq 0 , \tag{4.23}$$

where all parameters involved depend on the neutrino observables as shown in Eq. (4.16). The corresponding relations for the 5_1^μ and 5_1^τ textures are obtained by performing the replacements $(e \leftrightarrow \mu)$ and $(e \leftrightarrow \tau)$, respectively. In Table 4.1 we show the numerical values of some heavy-light mixing ratios using the best-fit values for the low-energy neutrino parameters given in Table 2.2.

[2] The sterile neutrinos are labelled from 4 to 7 in increasing order of their mass. Thus, in the following equations the $-$ $(+)$ sign refers to the lightest (heaviest) neutrino mass, labelled with indices 4 and 6 (5 and 7).

	NO_e	NO_μ	NO_τ	IO_e	IO_μ	IO_τ
$\mathbf{B}_{e4}/\mathbf{B}_{\mu4} \simeq \mathbf{B}_{e5}/\mathbf{B}_{\mu5}$	0.21	0.17	0.17	2.73	0.21	0.41
$\mathbf{B}_{\tau4}/\mathbf{B}_{\mu4} \simeq \mathbf{B}_{\tau5}/\mathbf{B}_{\mu5}$	0.27	0.88	0.87	0.51	1.09	1.24
$\mathbf{B}_{\tau4}/\mathbf{B}_{e4} \simeq \mathbf{B}_{\tau5}/\mathbf{B}_{e5}$	1.27	5.07	5.24	0.19	5.33	5.02
$\mathbf{B}_{e6}/\mathbf{B}_{\mu6} \simeq \mathbf{B}_{e7}/\mathbf{B}_{\mu7}$	0	–	0.36	0	–	4.96
$\mathbf{B}_{\tau6}/\mathbf{B}_{\mu6} \simeq \mathbf{B}_{\tau7}/\mathbf{B}_{\mu7}$	0.61	–	0	1.14	–	0
$\mathbf{B}_{\tau6}/\mathbf{B}_{e6} \simeq \mathbf{B}_{\tau7}/\mathbf{B}_{e7}$	–	1.64	0	–	0.23	0

Table 4.1: Predictions for ratios of heavy-light mixing parameters $\mathbf{B}_{\alpha j}$ computed using Eq. (4.23). The results are shown for the $\text{NO}_{e,\mu,\tau}$ and $\text{IO}_{e,\mu,\tau}$ cases.

4.2 Radiative corrections to neutrino masses

The analysis presented in the previous section was based on the assumption that the (tree-level) ISS approximation for the neutrino mass matrix given in Eq. (3.12) is valid, i.e., the parameters in Eq. (4.9) are such that $\mu_s, m_{D_i} \ll M$. However, the presence of new fermions and scalars may induce relevant corrections to the light-neutrino masses that should not be overlooked. This matter becomes even more important when considering the high precision achieved in the determination of the oscillation parameters, which is currently at the level of a few per cent for some of those observables (see Table 2.2). The one-loop radiative corrections to neutrino masses have been computed in several works [139–142]. Here we revisit the calculation of the one-loop corrections to the light neutrino mass matrix, and adapt it to our case (the one-loop neutrino self-energy diagrams are succinctly presented in Fig. 4.3). We compute the 3×3 one-loop correction matrix $\delta\boldsymbol{\mathcal{M}}$ given by [139, 140]

$$\begin{aligned}\delta\boldsymbol{\mathcal{M}}_{ij} = \boldsymbol{\Sigma}_{ij}(\not{p})\big|_{\not{p}=0} = (\delta\boldsymbol{\mathcal{M}}_{W^\pm})_{ij} + (\delta\boldsymbol{\mathcal{M}}_{G^\pm})_{ij} + \sum_{a=1}^{n_\pm-1} (\delta\boldsymbol{\mathcal{M}}_{S_a^\pm})_{ij} \\ + (\delta\boldsymbol{\mathcal{M}}_{Z})_{ij} + (\delta\boldsymbol{\mathcal{M}}_{G^0})_{ij} + \sum_{a=1}^{n_0-1} (\delta\boldsymbol{\mathcal{M}}_{S_a^0})_{ij}\,, \quad i,j = 1,2,3\,,\end{aligned} \tag{4.24}$$

where $\boldsymbol{\Sigma}(\not{p})$ are the (active) neutrino self-energies, evaluated at $\not{p} = 0$ since the tree-level light neutrino masses are extremely small. The number of neutral (charged) scalar mass eigenstates S_a^0 ($S_a^\pm$) is denoted by $n_0 - 1$ and $(n_\pm - 1)$, respectively. First, note that the $W^\pm$-boson contribution vanishes since the self-energies are evaluated at $\not{p} = 0$. Furthermore, by using the unitarity of the full $n_f \times n_f$ matrix $\boldsymbol{\mathcal{U}}$ defined in Eq. (3.6), it can be shown that the $G^\pm$ and $S_a^\pm$ contributions to $\delta\boldsymbol{\mathcal{M}}$ also vanish [141]. Thus, only $\delta\boldsymbol{\mathcal{M}}_Z$, $\delta\boldsymbol{\mathcal{M}}_{G^0}$ and $\delta\boldsymbol{\mathcal{M}}_{S_a^0}$ will be relevant. Performing the computation in the basis where the tree-level neutrino mass matrix $\boldsymbol{\mathcal{M}}$ given in Eq. (3.6) is diagonal, we obtain

$$(\delta\boldsymbol{\mathcal{M}}_Z)_{ij} = -\frac{\alpha_W}{4\pi c_W^2} \sum_{k=1}^{n_f} m_k \boldsymbol{\mathcal{C}}_{ik}^* \boldsymbol{\mathcal{C}}_{kj}\; f\left(\frac{m_k^2}{M_Z^2}\right)\,, \tag{4.25}$$

$$(\delta\boldsymbol{\mathcal{M}}_{G^0})_{ij} = \frac{\alpha_W}{16\pi} \sum_{k=1}^{n_f} \frac{m_k}{M_W^2} \left(m_i \boldsymbol{\mathcal{C}}_{ik} + m_k \boldsymbol{\mathcal{C}}_{ik}^*\right)\left(m_j \boldsymbol{\mathcal{C}}_{kj}^* + m_k \boldsymbol{\mathcal{C}}_{kj}\right)\; f\left(\frac{m_k^2}{M_Z^2}\right)\,, \tag{4.26}$$

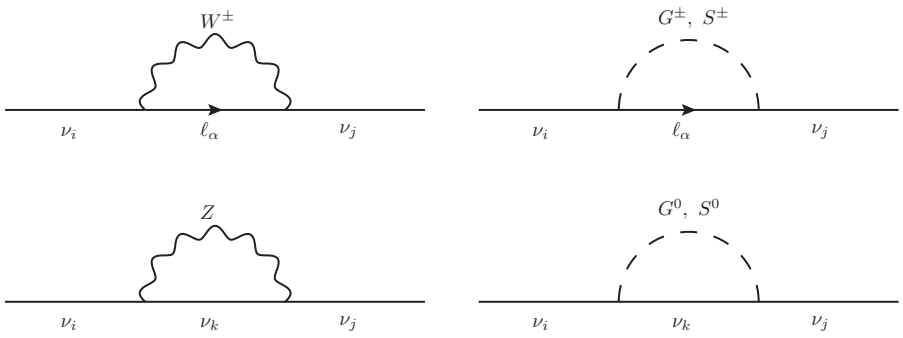

Figure 4.3: Self-energy Feynman diagrams contributing to the radiative corrections to the neutrino masses.

$$\left(\delta\boldsymbol{\mathcal{M}}_{S_a^0}\right)_{ij} = -\frac{1}{4\pi^2}\sum_{k=1}^{n_f} m_k \left(\boldsymbol{\Delta}_\nu^a\right)_{ik}^* \left(\boldsymbol{\Delta}_\nu^a\right)_{kj}^* \ f\left(\frac{m_k^2}{m_{S_a^0}^2}\right). \tag{4.27}$$

The couplings $\boldsymbol{\mathcal{C}}_{ij}$ are defined in Eq. (3.20), m_k are the tree-level neutrino masses, and $m_{S_a^0}$ are the neutral scalar masses. The Yukawa couplings matrices $\boldsymbol{\Delta}_\nu^a$ appear in the interaction terms between neutrinos and neutral scalars S_a^0 – see Eq. (B.6) of Appendix B. The loop function in the above expressions is [see Eq. (D.2) of Appendix D.1]

$$f(x) = -\frac{x\ln x}{1-x} - 1. \tag{4.28}$$

In our framework, the neutral scalar degrees of freedom originate from the two Higgs doublets $\Phi_{1,2}$ and the two scalar singlets $S_{1,2}$ (see Table 3.5), which results in a total of seven scalar mass eigenstates (S_{1-7}) (see Appendix A for more details on the scalar sector). In the exact alignment limit with no mixing among scalar doublets and singlets, and following the same argument as before regarding the unitarity of $\boldsymbol{\mathcal{U}}$ [141], it can be shown that the $S_{3,4}^0$ and $S_{6,7}^0$ contributions, stemming from the neutral singlets d.o.f., to $\delta\boldsymbol{\mathcal{M}}$ vanish. Hence, only the (SM Higgs boson) $S_1^0 = H^0$, $S_2^0 = R$ and $S_5^0 = I$ will be relevant, being their contributions given by

$$\left(\delta\boldsymbol{\mathcal{M}}_{H^0}\right)_{ij} = -\frac{\alpha_W}{16\pi}\sum_{k=1}^{n_f}\frac{m_k}{M_W^2}\left(m_i\boldsymbol{\mathcal{C}}_{ik} + m_k\boldsymbol{\mathcal{C}}_{ik}^*\right)\left(m_j\boldsymbol{\mathcal{C}}_{kj}^* + m_k\boldsymbol{\mathcal{C}}_{kj}\right)\ f\left(\frac{m_k^2}{m_{H^0}^2}\right), \tag{4.29}$$

$$\left(\delta\boldsymbol{\mathcal{M}}_{R}\right)_{ij} = -\frac{\alpha_W}{16\pi}\sum_{k=1}^{n_f}\frac{m_k}{M_W^2}\left[\left(\mathbf{N}_\nu^\dagger\right)_{ik} + \left(\mathbf{N}_\nu^*\right)_{ik}\right]\left[\left(\mathbf{N}_\nu^\dagger\right)_{kj} + \left(\mathbf{N}_\nu^*\right)_{kj}\right]\ f\left(\frac{m_k^2}{m_R^2}\right), \tag{4.30}$$

$$\left(\delta\boldsymbol{\mathcal{M}}_{I}\right)_{ij} = \frac{\alpha_W}{16\pi}\sum_{k=1}^{n_f}\frac{m_k}{M_W^2}\left[\left(\mathbf{N}_\nu^\dagger\right)_{ik} + \left(\mathbf{N}_\nu^*\right)_{ik}\right]\left[\left(\mathbf{N}_\nu^\dagger\right)_{kj} + \left(\mathbf{N}_\nu^*\right)_{kj}\right]\ f\left(\frac{m_k^2}{m_I^2}\right), \tag{4.31}$$

where the matrix $\mathbf{N}_\nu$ is defined in Eq. (B.9). Notice that, assuming $m_R = m_I$, the R and I contributions cancel each other. This is what we will assume in our analysis (we refer the reader to Ref. [143] for a model where these neutral scalar contributions are taken into account). As for divergences, those coming from the G^0 and H^0 loops cancel each other, likewise for the R and I scalars. The Z-boson contribution is finite by itself due to the first relation in Eq. (3.22).

We now wish to evaluate how the results of the previous section are affected when performing a

numerical analysis to compute neutrino mass and mixing observables, including the loop corrections discussed above. In particular, we are interested in

- Comparing the tree-level light neutrino parameters obtained using the seesaw-approximated $\mathbf{M}_{\rm eff}$ of Eq. (3.12) with those stemming from the full neutrino mass matrix $\boldsymbol{\mathcal{M}}$ in Eq. (3.3). This will not only provide an insight about how the results are affected by neglecting higher-order terms in the seesaw expansion, but will also set limits on the parameters, above which the approximation holds up to a certain precision. As a reference observable we choose the neutrino mass-squared difference Δm^2_{31}, which turns out to be the most sensitive one to such corrections. To quantify the effect of considering the ISS approximation at lowest order, we define the parameter

$$\Delta_{\rm ISS} \equiv \frac{|\Delta m^2_{31} - \Delta \tilde{m}^2_{31}|}{\Delta \tilde{m}^2_{31}}\,, \quad \Delta \tilde{m}^2_{31} = \tilde{m}^2_3 - \tilde{m}^2_1\,, \tag{4.32}$$

  where the light-neutrino masses m_i and $\tilde{m}_i$ are determined using Eqs. (3.6) and (3.13), respectively. For instance, $\Delta_{\rm ISS} = 0.1$ indicates that the value of Δm^2_{31} determined from $\boldsymbol{\mathcal{M}}$ differs from that computed with $\mathbf{M}_{\rm eff}$ by 10%.

- Evaluating the impact of the one-loop $\delta\boldsymbol{\mathcal{M}}$ on the determination of low-energy neutrino parameters. For that, we will consider the neutrino mass squared differences Δm^2_{21} and Δm^2_{31}, since for the mixing angles and CP phases the corrections are negligible when compared with the current experimental precision. Likewise the previous case, we define the parameter

$$\Delta^{ij}_{\rm 1L} \equiv \frac{|\Delta \widehat{m}^2_{ij} - \Delta m^2_{ij}|}{\Delta m^2_{ij}}\,, \quad \Delta \widehat{m}^2_{ij} = \widehat{m}^2_i - \widehat{m}^2_j\,, \tag{4.33}$$

  where $\widehat{m}_i$ are the one-loop corrected neutrino masses and Δm^2_{ij} are the tree-level neutrino mass-squared differences computed with the full $\boldsymbol{\mathcal{M}}$. Notice that, since we evaluate $\delta\boldsymbol{\mathcal{M}}$ in the basis where $\boldsymbol{\mathcal{M}}$ is diagonal, the light neutrino masses $\widehat{m}_i$ are determined diagonalising the matrix $\mathbf{M}_{\rm light} = {\rm diag}(m_1, m_2, m_3) + \delta\boldsymbol{\mathcal{M}}_{ij}$, where $\delta\boldsymbol{\mathcal{M}}_{ij}$ is given by Eqs. (4.24)-(4.29) with $i, j = 1, 2, 3$ and $n_f = 7$ (total number of neutrino mass eigenstates).

For numerical computations in the $5^{e,\mu\tau}_1$ cases discussed in Sections 3.2.2 and 4.1, we consider a benchmark scenario based on the following assumptions. We choose $p = 1$ and $q = 10$ in Eq. (4.9), implying $m_{6,7} \simeq 10\, m_{4,5}$ and $m_5 - m_4 \simeq m_7 - m_6 \simeq \mu_s$. Regarding the scalar sector, we take $\tan\beta = 1$ [see Eq. (4.8)] and consider all physical neutral and charged scalar masses to be 1 TeV, except for the SM Higgs boson with mass $m_{H^0} = 125$ GeV. Under these premises we span the parameter space in the following way:

- The low-energy neutrino parameters are fixed to their best-fit values given in Table 2.2, and the effective neutrino mass matrix elements M_{ij} (defined in the ISS approximation) are computed according to Eqs. (4.13) and (4.14), for both NO and IO neutrino mass spectra. Relations (4.15) are then solved to find the predicted value for the Majorana phase α, and the parameters in Eq. (4.16) are determined. Notice that, although the values of x, y, z and w are set by low-energy

neutrino parameters, the scales m_{D_i}, M and μ_s are not uniquely defined since $\mathbf{M}_{\rm eff}$ in Eq. (4.11) is invariant under the rescalings

$$M \to aM \ , \ \mu_s \to b\mu_s \ , \ m_{D_i} \to \frac{a}{\sqrt{b}}\, m_{D_i} \ . \tag{4.34}$$

Choosing the initial values $M = 100$ GeV and $\mu_s = 10$ eV, we determine m_{D_i} as shown in Eq. (4.11). In order to probe a wide range of scales, we vary M and μ_s in the intervals $[1, 10^4]$ GeV and $[1, 10^{11}]$ eV. For an arbitrary pair (M, μ_s), we set the rescaling parameters with respect to the initial values, namely $a = M/100$ and $b = \mu_s/10$. The corresponding m_{D_i} are obtained using Eq. (4.34). This procedure leaves invariant the effective neutrino mass matrix (in the ISS approximation) and guarantees that the low-energy parameters are always those corresponding to the experimental best-fit values. Notice that such procedure may lead to very large Dirac masses m_{D_i}. Thus, in order to ensure perturbativity of the Yukawa couplings b_i in Eq. (4.7), we require $y_{\rm max} = \max\{m_{D_{1,2}}/v_1, m_{D_{3,4}}/v_2\} \leq 5$. It is important to stress that rescaling M, μ_s and m_{D_i} is the only way to probe the parameter space of our model since ratios among different m_{D_i} are determined by low-energy parameters which are fixed.

- For each set of (M, μ_s, m_{D_i}), the full 7×7 neutrino mass matrix $\boldsymbol{\mathcal{M}}$ is defined using Eqs. (3.3) and (4.9), and then diagonalised as indicated in Eq. (3.6) to determine $\boldsymbol{\mathcal{U}}$ and m_{1-7}. The active neutrino mixing is characterised by the 3×3 (non-unitary) matrix $\mathbf{U}$ of Eq. (3.17), which is the upper-left 3×3 block of $\boldsymbol{\mathcal{U}}$, in the physical charged-lepton basis. The non-unitarity effects are parameterised by the matrix $\boldsymbol{\eta}$ of Eq. (3.17). Finally, we compute the one-loop corrections to the light neutrino masses as explained above.

We remark that the CC mixing between the charged lepton with flavour $\alpha = e, \mu, \tau$ and the heavy sterile neutrino ν_j ($j = 4-7$) is set by $\mathbf{B}_{\alpha j}$ as defined in Eq. (3.20)–see also Eq. (B.1). In practice, $\mathbf{B}_{\alpha j}$ is the (α, j) element of $\boldsymbol{\mathcal{U}}$ computed above and defined in the charged-lepton mass basis. Notice also that we will be able to cover wide ranges of $\mathbf{B}_{\alpha j}$ since these elements scale as m_D/M. Throughout the remaining of this work, we will use as reference parameters the average mass of the lightest sterile neutrino pair m_{45}, a degeneracy parameter r_N and the mixing of the electron with the lightest sterile neutrino V_{eN}, defined as

$$m_{45} = \frac{m_4 + m_5}{2} \simeq M \ , \quad r_N = \frac{m_5 - m_4}{m_{45}} \simeq \frac{\mu_s}{m_{45}} \ , \quad V_{eN} = |\mathbf{B}_{e4}| \simeq \frac{m_{D_4}}{\sqrt{2}\, m_{45}} \, . \tag{4.35}$$

In Fig. 4.4 we show the contour-level plots for $\Delta^{21}_{\rm 1L}$ (left panels) and $\Delta^{32}_{\rm 1L}$ (right panels) defined in Eq. (4.33) for the NO$_e$ (upper panels) and IO$_e$ (lower panels) cases. The contours of V^2_{eN}, r_N and $\Delta_{\rm ISS}$ are also shown by solid, dash-dotted and dotted lines, respectively. Within the grey shaded region $b_i^{\rm max} > 5$. From the inspection of these plots we conclude the following:

- The validity of the (tree-level) inverse-seesaw approximation is verified at less than the percent level for $\mu_s \gtrsim 10 - 20$ eV (region above the $\Delta_{\rm ISS} = 1\%$ horizontal line). The reason why $\Delta_{\rm ISS}$ does

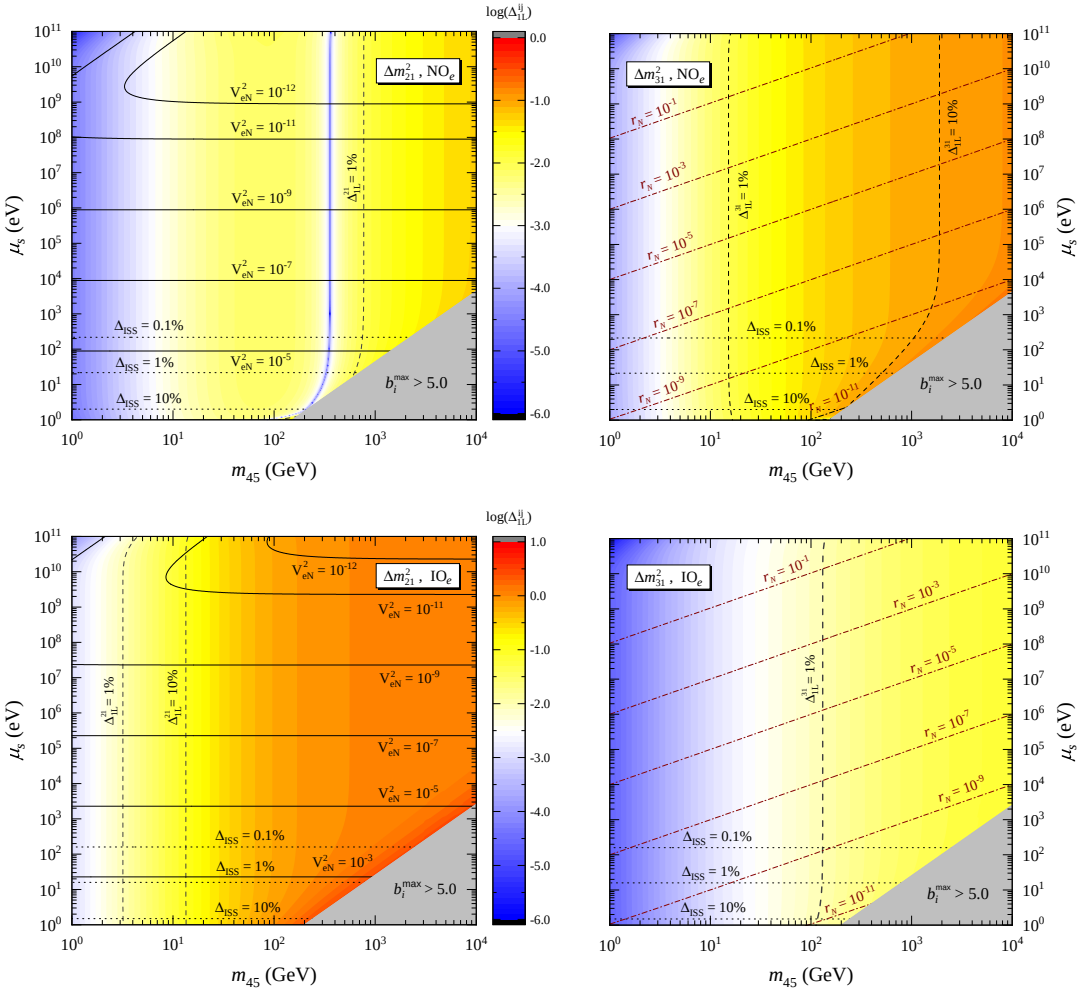

Figure 4.4: Impact of one-loop corrections on Δm^2_{21} (left panels) and Δm^2_{31} (right panels) for the NO$_e$ (upper panels) and IO$_e$ (lower panels) cases. The coloured contour levels are for the $\Delta^{ij}_{1\mathrm{L}}$ parameter defined in Eq. (4.33). For reference, we show the dashed contours with $\Delta^{ij}_{1\mathrm{L}} = 1\%, 10\%$. The solid, dash-dotted and dotted lines correspond to V_{eN}, r_N and Δ_{ISS} contours, respectively. Within the grey shaded region on the lower-right corner of each panel the largest Yukawa coupling of $\mathbf{Y}^{1,2}_D$ [see Eq. (4.7)] obeys $b^{\max}_i > 5$.

not depend on m_{45} for a given μ_s, can be understood taking into account that the next-to-leading-order approximation of the inverse seesaw scales as $\mu_s m^4_D/M^4$ and, consequently, $\Delta_{\mathrm{ISS}} \sim m^2_D/M^2 \simeq m^2_D/m^2_{45}$. Thus, if μ_s is kept constant [$b = 1$ in Eq. (4.34)], m_{D_i} scales as m_{45} leaving Δ_{ISS} invariant. Moreover, for a given m_{45}, a rescaling of $\mu_s \to b\mu_s$ leads to a rescaling of $\Delta_{\mathrm{ISS}} \to \Delta_{\mathrm{ISS}}/b$, as can be seen in Fig. 4.4.

- The chosen intervals for μ_s and M allows us to swipe a wide range for the heavy-light mixing parameter, namely V^2_{eN} lies between 10^{-13} (or even less) and 10^{-3} in the parameter-space region where the inverse seesaw approximation holds up to 1%. The V^2_{eN} contours are approximate horizontal lines since, as shown in Eq. (4.22), heavy-light mixing scales as m_{D_i}/m_{45} and, consequently, V^2_{eN} remains invariant for constant μ_s due to the same rescaling of m_{D_i} and m_{45}. Notice that this feature fails for $\mu_s \sim m_{45}$ (upper-left corner of the left panels in Fig. 4.4) since in this case the leading-order ISS approximation for V_{eN} is no longer valid. For the degeneracy parameter r_N, the

contours follow the linear relation $r_N \simeq \mu_s/m_{45}$ already shown in Eq. (4.35) (dash-dotted lines in the right panels of Fig. 4.4).

- The nearly-vertical levels of $\Delta^{ij}_{1\mathrm{L}}$ indicate that radiative corrections to neutrino masses depend mainly on m_{45}. For NO_e, the one-loop corrected Δm^2_{21} deviates from the tree-level result by less than 1% for $m_{45} \lesssim 700$ GeV, while for Δm^2_{31} that threshold is at $m_{45} \lesssim 20$ GeV. Instead, the corresponding upper limits on m_{45} for IO_e are at 3 GeV and 100 GeV, respectively. Notice that, being the one-loop corrections typically larger than the experimental uncertainty (see Table 2.2) for m_{45} above those values, this does not mean that the symmetry realisation presented in Section 3.2.2 is no longer valid. It just signals the fact that the tree-level relations (4.16) start failing. The take-home message to learn from this analysis is that the scale invariance of the tree-level inverse-seesaw approximation holds up to a certain level depending on the sterile neutrino mass.

4.3 Charged lepton flavour violation

Lepton flavour violating processes are in the front line of experimental searches for physics beyond the SM [144]. The ISS model, being a paradigm for low-scale neutrino mass generation, provides a natural scenario for the observation of flavour transitions beyond neutrino oscillations. The charged and neutral current interactions with heavy sterile neutrinos induce new phenomena which are strongly suppressed in the SM extended with light neutrinos only. Nevertheless, the predictive power of the general ISS is limited by the arbitrariness of its parameter values. In the present framework, the symmetries discussed in Section 3.2.2 provide the ground for a testable scenario in the light of present and future experimental probes on LFV processes. Thus, we now study LFV in the context of the scenarios set in the previous sections. Our attention will be focused on the cLFV processes listed in Table 4.2, where the present experimental upper limits and future sensitivities for the BRs and CRs are shown. We have revisited the computation of the rates taking into account the field content in our framework. The details are shown in Appendices B-D.

As stated in Section 4.1, we focus our study on the case of the charged lepton matrix texture 5^{ℓ}_1. To justify this choice, let us look at the cLFV decay $\ell^-_\alpha \to \ell^-_\beta \ell^+_\gamma \ell^-_\delta$, which is mediated at tree level by the neutral scalars R and I coming from the two Higgs doublets (in the alignment limit). The corresponding BR for this process reads [72]

$$\begin{aligned}\frac{\mathrm{BR}(\ell^-_\alpha \to \ell^-_\beta \ell^+_\gamma \ell^-_\delta)}{\mathrm{BR}\,(\ell_\alpha \to \ell_\beta \nu_\alpha \overline{\nu_\beta})} = \frac{1}{16(1+\delta_{\beta\delta})}\Big\{ \Big[\Big|g^{\alpha\beta,\gamma\delta}_{LL}\Big|^2 + \Big|g^{\alpha\beta,\gamma\delta}_{LR}\Big|^2 + (\beta \leftrightarrow \delta)\Big] \\ - \mathrm{Re}\left[g^{\alpha\beta,\gamma\delta}_{LL} g^{\alpha\delta,\gamma\beta *}_{LL}\right] + (L \leftrightarrow R)\Big\},\end{aligned} \tag{4.36}$$

where

$$\begin{aligned} g^{\alpha\beta,\gamma\delta}_{LL} &= (\mathbf{N}^\dagger_e)_{\beta\alpha}(\mathbf{N}^\dagger_e)_{\delta\gamma}\Big(\frac{1}{m^2_R} - \frac{1}{m^2_I}\Big), \quad g^{\alpha\beta,\gamma\delta}_{RR} = (\mathbf{N}_e)_{\beta\alpha}(\mathbf{N}_e)_{\delta\gamma}\Big(\frac{1}{m^2_R} - \frac{1}{m^2_I}\Big), \\ g^{\alpha\beta,\gamma\delta}_{LR} &= (\mathbf{N}^\dagger_e)_{\beta\alpha}(\mathbf{N}_e)_{\delta\gamma}\Big(\frac{1}{m^2_R} + \frac{1}{m^2_I}\Big), \quad g^{\alpha\beta,\gamma\delta}_{RL} = (\mathbf{N}_e)_{\beta\alpha}(\mathbf{N}^\dagger_e)_{\delta\gamma}\Big(\frac{1}{m^2_R} + \frac{1}{m^2_I}\Big), \end{aligned} \tag{4.37}$$

being $m_{R,I}$ the neutral scalar masses. The matrix $\mathbf{N}_e$ dictates the interactions between charged leptons

cLFV process	Present limit (90% CL)	Future sensitivity
$\mathrm{BR}(\mu \to e\gamma)$	4.2×10^{-13} (MEG [34])	6×10^{-14} (MEG II [35])
$\mathrm{BR}(\tau \to e\gamma)$	3.3×10^{-8} (BaBar [145])	3×10^{-9} (Belle II [146])
$\mathrm{BR}(\tau \to \mu\gamma)$	4.4×10^{-8} (BaBar [145])	10^{-9} (Belle II [146])
$\mathrm{BR}(\mu^- \to e^- e^+ e^-)$	1.0×10^{-12} (SINDRUM [36])	10^{-16} (Mu3e [147])
$\mathrm{BR}(\tau^- \to e^- e^+ e^-)$	2.7×10^{-8} (Belle [148])	5×10^{-10} (Belle II [146])
$\mathrm{BR}(\tau^- \to e^- \mu^+ \mu^-)$	2.7×10^{-8} (Belle [148])	5×10^{-10} (Belle II [146])
$\mathrm{BR}(\tau^- \to e^+ \mu^- \mu^-)$	1.7×10^{-8} (Belle [148])	3×10^{-10} (Belle II [146])
$\mathrm{BR}(\tau^- \to \mu^- e^+ e^-)$	1.8×10^{-8} (Belle [148])	3×10^{-10} (Belle II [146])
$\mathrm{BR}(\tau^- \to \mu^+ e^- e^-)$	1.5×10^{-8} (Belle [148])	3×10^{-10} (Belle II [146])
$\mathrm{BR}(\tau^- \to \mu^- \mu^+ \mu^-)$	2.1×10^{-8} (Belle [148])	4×10^{-10} (Belle II [146])
$\mathrm{CR}(\mu - e, \mathrm{Al})$	–	3×10^{-17} (Mu2e [149])
		$10^{-15} - 10^{-17}$ (COMET I-II [150])
$\mathrm{CR}(\mu - e, \mathrm{Ti})$	4.3×10^{-12} (SINDRUM II [37])	10^{-18} (PRISM/PRIME [151])
$\mathrm{CR}(\mu - e, \mathrm{Au})$	7×10^{-13} (SINDRUM II [39])	–
$\mathrm{CR}(\mu - e, \mathrm{Pb})$	4.6×10^{-11} (SINDRUM II [38])	–
cLFV process	Present limit (95% CL)	Future sensitivity
$\mathrm{BR}(Z \to e^\mp \mu^\pm)$	7.3×10^{-7} (CMS [152])	$10^{-8} - 10^{-10}$ (FCC-ee [153])
$\mathrm{BR}(Z \to e^\mp \tau^\pm)$	9.8×10^{-6} (OPAL [154])	10^{-9} (FCC-ee [153])
$\mathrm{BR}(Z \to \mu^\mp \tau^\pm)$	1.2×10^{-5} (DELPHI [155])	10^{-9} (FCC-ee [153])

Table 4.2: Current experimental bounds and future sensitivities for the branching ratios (BRs) and capture rates (CRs) of cLFV processes.

and the neutral scalars as shown in Eq. (B.13). For the 5_1^ℓ case, the structure of $\mathbf{N}_e$ is

$$5_1^e : \mathbf{N}_e \sim \begin{pmatrix} \times & 0 & 0 \\ 0 & \times & \times \\ 0 & \times & \times \end{pmatrix}, \; 5_1^\mu : \mathbf{N}_e \sim \begin{pmatrix} \times & 0 & \times \\ 0 & \times & 0 \\ \times & 0 & \times \end{pmatrix}, \; 5_1^\tau : \mathbf{N}_e \sim \begin{pmatrix} \times & \times & 0 \\ \times & \times & 0 \\ 0 & 0 & \times \end{pmatrix}. \tag{4.38}$$

The presence of zeros in $\mathbf{N}_e$ imposed by the flavour symmetry leads to a natural suppression of the above BRs. In fact, considering the most constraining three-body decay $\mu \to 3e$ (see Table 4.2), the tree-level contribution vanishes for the textures $5_1^{e,\mu}$ (decoupled electron or muon) irrespective of $m_{R,I}$. Although this does not hold for 5_1^τ, in this case the BRs are strongly suppressed by the tiny couplings in the $\mu - e$ sector. The same conclusion cannot be drawn for the texture 4_3^ℓ since the flavour symmetry does not yield the charged-lepton decoupling feature. To suppress the decay rates in this case, not only very large $m_{R,I}$ masses are required but also they must be extremely fine tuned [72], as can be readily seen from Eq. (4.37). Similarly, the analysis of the one-loop contribution of the neutral scalars R and I to the decay $\ell_\alpha \to \ell_\beta \gamma$ reveals that in the 4_3^ℓ case requires fine-tuned scalar masses. On the other hand, for $5_1^{e,\mu}$ the scalar contribution to the $\mu \to e\gamma$ amplitude vanishes.

We now analyse the constraints imposed on the parameter space taking into account the present limits and future sensitivities for the processes indicated in Table 4.2. We focus on $\mu \to e\gamma$, $\mu \to 3e$ and $\mu - e$ conversion in Au, Ti and Al, since these are either the most constraining at present or the ones for which the projected sensitivity is higher. Later on, we will comment on other LFV three-

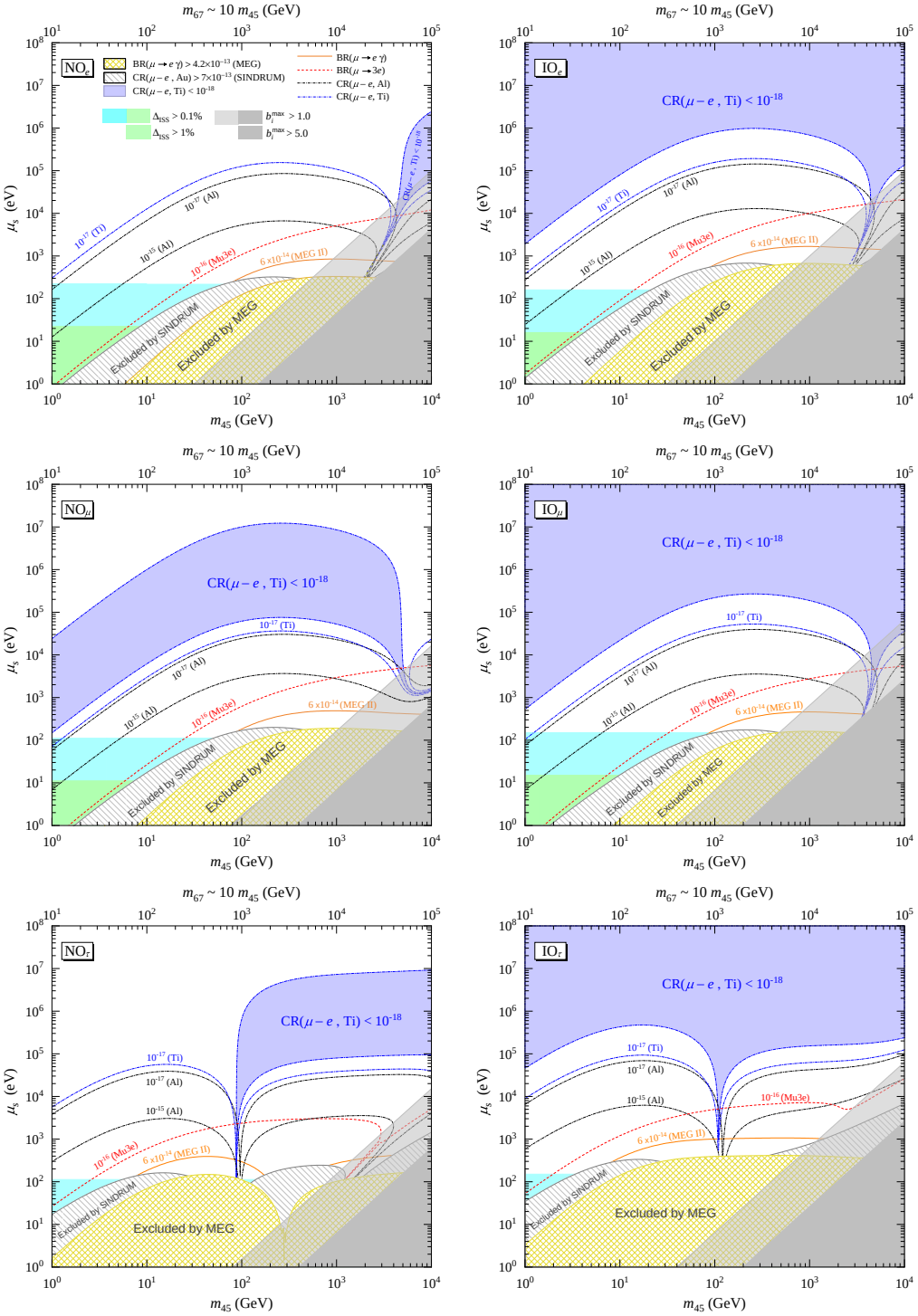

Figure 4.5: Constraints on the (m_{45}, μ_s) parameter space imposed by the MEG bound on BR$(\mu \to e\gamma)$ (yellow crosshatched region) and the SINDRUM II limit on CR$(\mu - e, \text{Au})$ (grey hatched region). The contours corresponding to the future sensitivities of the MEG II (solid orange) and Mu3e (red dashed) experiments are also given. The black and blue dash-dotted lines show the contours of CR$(\mu - e, \text{Al})$ and CR$(\mu - e, \text{Ti})$, respectively, for values within the sensitivity of future experiments (see Table 4.2). In the blue shaded region CR$(\mu - e, \text{Ti}) < 10^{-18}$. Limits on $b_i^{\rm max}$ and $\Delta_{\rm ISS}$ are also shown (grey, green and cyan shaded regions). The results are shown for all cases found to be realisable through Abelian symmetries, i.e. for the $5_1^{e,\mu,\tau}$ cases with NO (left panels) and IO (right panels) neutrino mass spectra.

body and Z decays. The (m_{45}, μ_s) parameter space is covered by means of a full numerical analysis as described in the previous section, using the results given in Appendices B-D. For simplicity, we work in the alignment limit for the two Higgs doublets and in the decoupling limit for the two neutral scalar singlets, as explained in Appendix A. The interaction terms between fermions and scalar eigenstates are those given in Section B.2. Since the analysis of textures and symmetries for the quark sector is out of the scope of this work, the up-quark and down-quark mass matrices are taken to be diagonal, i.e., $\mathbf{M}_u = \text{diag}(m_u, m_c, m_t)$ and $\mathbf{M}_d = \text{diag}(m_d, m_s, m_b)$ [89]. Consequently, the CKM matrix $\mathbf{V}$ is the identity matrix, and the flavour-changing matrices $\mathbf{N}_d$ and $\mathbf{N}_u$, defined in Eqs. (B.10) and (B.11), vanish.

The results of our numerical analysis are shown in Fig. 4.5 for the six cases $\text{NO}_{e,\mu,\tau}$ (left panels) and $\text{IO}_{e,\mu,\tau}$ (right panels). The colour codes in the legend of the upper-left panel apply to the whole figure. By inspecting these results we conclude the following:

- The validity of the inverse-seesaw approximation up to 1% level, i.e. $\Delta_{\text{ISS}} < 1\%$, imposes lower bounds on the LNV parameter $\mu_s > 10 - 20$ eV (cyan shaded regions), which correspond to upper bounds on the mixing $V_{eN}^2 \lesssim 10^{-4} - 10^{-3}$ (see Fig. 4.4). The light (dark) grey regions show that a considerable fraction of the parameter space is excluded if one takes into account $b_i^{\max} < 1\,(5)$ as a perturbativity requirement.

- The MEG and SINDRUM II limits on $\text{BR}(\mu \to e\gamma)$ and $\text{CR}(\mu - e, \text{Au})$ exclude $m_{45} \gtrsim 1 - 10$ GeV for $\Delta_{\text{ISS}} \gtrsim 1\%$. Moreover, the improvement on $\text{BR}(\mu \to e\gamma)$ foreseen by MEG II (solid orange contour) would have a marginal impact in covering the parameter space in our framework. On the other hand, reaching a sensitivity of $\text{BR}(\mu \to 3e)$ at the 10^{-16} level would be more relevant in constraining the parameter space, especially for heavier sterile neutrinos, i.e., for larger m_{45}.

- The COMET and PRISM/PRIME projected sensitivities for $\text{CR}(\mu - e, \text{Al})$ and $\text{CR}(\mu - e, \text{Ti})$, represented by black and blue dash-dotted contours, respectively, cover a considerable part of the parameter space, leaving unprobed the regions in shaded blue where $\text{CR}(\mu - e, \text{Ti}) < 10^{-18}$. In the best-case scenario (NO_e), probing $\text{CR}(\mu - e, \text{Ti})$ down to 10^{-18} would cover the whole parameter space, as can be seen in the upper left panel.

The above results provide a general idea regarding how present experimental data constrain the minimal ISS with Abelian symmetries, and how future experiments would further probe its parameter space. However, it is interesting to investigate possible relations among different processes and, in particular, to ask whether the observation of a particular cLFV decay would allow us to draw conclusions regarding others. Notice that, in general, this is only possible when there is some relation among the LFV parameters and/or masses, as it is our case (see Table 4.1). With this purpose, we compare $\text{BR}(\mu \to e\gamma)$ with $\text{BR}(\tau \to \ell_\alpha \gamma)$, and $\text{CR}(\mu - e, \text{Ti})$ with $\text{BR}(\mu \to 3e)$. The results are shown in Figs. 4.6 and 4.7 for NO and IO, respectively, where all points respect the present limits shown in Table 4.2. The colour of each point is linked to the corresponding value of m_{45} following the colour map shown in the middle of the figure. Some important conclusions stand out from the observation of these results. Namely, it is clear that any future observation of a radiative (or three-body) τ decay with a BR down to 10^{-9} would exclude all scenarios presented in this work. In fact, for both $\tau \to \mu\gamma$ and $\tau \to e\gamma$ the BRs are 10^{-11} at most,

well below the Belle II sensitivity (left panels). In general, the spreading of the scatter points is due to variations in heavy-light mixing and heavy neutrino masses. However, in some cases, we observe a linear relation between $\mathrm{BR}(\tau \to \mu\gamma)$ or $\mathrm{BR}(\tau \to e\gamma)$ and $\mathrm{BR}(\mu \to e\gamma)$. For instance, using Eqs. (C.2) and (C.3) together with the approximate results of Table 4.1, it can be shown that for NO_e the relation

$$\frac{\mathrm{BR}(\tau \to e\gamma)}{\mathrm{BR}(\mu \to e\gamma)} \simeq \left|\frac{\mathbf{B}_{\tau 4}}{\mathbf{B}_{\mu 4}}\right|^2 \mathrm{BR}(\tau \to \nu_\tau e \bar{\nu}_e) \simeq 0.013 \tag{4.39}$$

holds for the whole range of m_{45}, in perfect agreement with the numerical results shown in the inner plot of the upper-left panel in Fig. 4.6. From the comparison of $\mathrm{CR}(\mu - e, \mathrm{Ti})$ with $\mathrm{BR}(\mu \to 3e)$ (right panels of Figs. 4.6 and 4.7) we see that in all cases $\mathrm{BR}(\mu \to 3e)$ is at most 10^{-13}. Notice also that, for $m_{45} \lesssim 100$ GeV, there is an approximate linear relation between $\mathrm{CR}(\mu - e, \mathrm{Ti})$ with $\mathrm{BR}(\mu \to 3e)$, which is no longer valid for higher masses due to cancellations among the various contributions to $\mu - e$ conversion amplitudes. We have also investigated whether our framework could lead to observable signals in LVF Z decays by computing $\mathrm{BR}(Z \to \ell_\alpha \ell_\beta)$ with $\alpha \neq \beta = e, \mu, \tau$. We have concluded that, after imposing the present constraints on $\mu \to e\gamma$ and $\mu - e$ conversion in nuclei, the $Z \to \ell_\alpha \ell_\beta$ rates are well below the future sensitivities given in Table 4.2.

4.4 Constraints on heavy sterile neutrinos and future prospects

In the previous section we have analysed the constraints imposed by LFV experimental searches on the minimal inverse seesaw model with Abelian flavour symmetries, adopting as reference parameters the LNV parameter μ_s and the average sterile neutrino mass m_{45}. Although this provides a clear understanding on how constrained the original scales in the Lagrangian are, it is convenient to look at the problem from a perspective where μ_s is replaced by the active-sterile mixing parameters $\mathbf{B}_{\alpha j}$. Notice that, in our framework, we only need to consider one of these quantities since, as seen in Section 4.1 and summarised in Table 4.1, they are all correlated. From now on, we will take as constrained parameters m_{45} and V_{eN}^2 defined in Eq. (4.35). For each of the scenarios analysed in this work, the correspondence between the (m_{45}, μ_s) and (m_{45}, V_{eN}^2) parameter spaces is established by figures like Fig. 4.4 (left panels). Following this approach, we will be able to compare the constraining power of the cLFV processes discussed in the previous section with other experimental searches which are usually translated into constraints on mass and mixing parameters (see e.g. Refs. [45, 51, 53, 156–159]). We are not interested in carrying out an exhaustive analysis of all sensitivity studies performed so far. Instead, we will consider the following searches:

- **Beam-dump experiments:** In a beam-dump experiment a primary beam strikes a high-density target and produces a large number of secondary heavy mesons which, in the presence of active-sterile mixing, can decay to final states with sterile neutrinos. Part of them fly towards a detector, decaying inside its volume. The NA3 experiment used a 300 GeV π^- beam incident on 2 meter long beam dump to, among other purposes, look for the decays of heavy neutrinos N into $\ell\ell\nu$ and

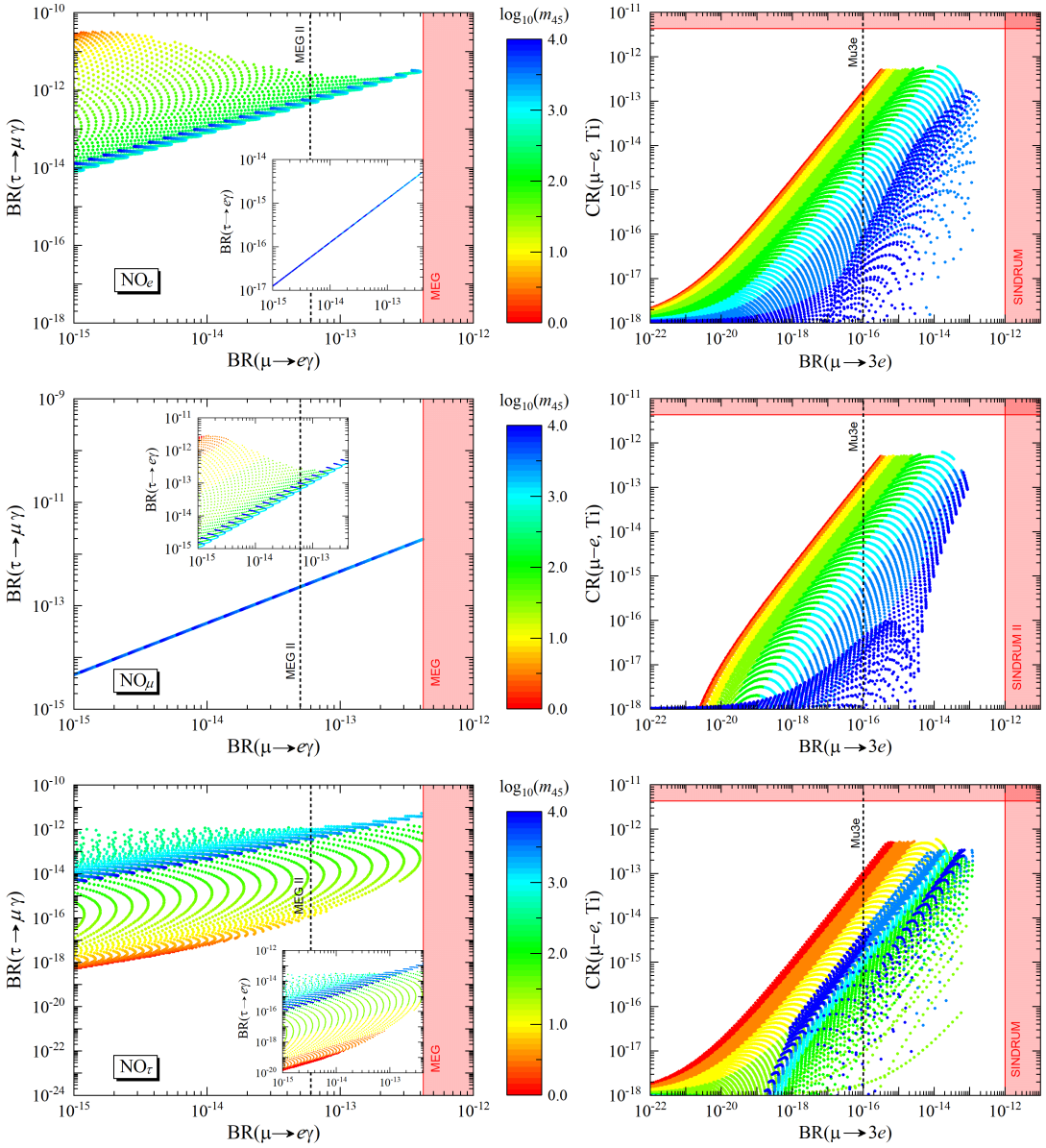

Figure 4.6: [Left] BR($\tau \to \mu\gamma$) and BR($\tau \to e\gamma$) (inner plots) vs. BR($\mu \to e\gamma$) for NO$_{e,\mu,\tau}$ from top to bottom. The MEG bound BR($\tau \to e\gamma$) $< 4.2 \times 10^{-13}$ sets the vertical red exclusion band, while the vertical dashed line corresponds to the MEG II projected sensitivity. [Right] CR($\mu-e$, Ti) vs. BR($\mu \to 3e$) for the same NO case as in the left panel. The vertical and horizontal red exclusion bands result from the SINDRUM and SINDRUM II limits on BR($\mu \to 3e$) and CR($\mu - e$, Ti), respectively (see Table 4.2). The vertical dashed line corresponds to the Mu3e projected sensitivity for $\mu \to 3e$. In all panels, the scatter points obey all constraints shown in Table 4.2, being their colour linked to the value of m_{45} according to the colourmap shown in the middle.

$\pi^+\ell^-$ ($\ell = e, \mu$) final states. In such experiment, heavy neutrinos may originate from the rare π and K meson decays, or in semi-leptonic decays of charm D and F or beauty B mesons. At NA3 the limit $V_{eN}^2 \lesssim 10^{-4}$ has been set within a heavy neutrino mass region $1 - 2$ GeV. The CHARM experiment [160] has conducted similar $N \to \ell\ell\nu$ searches using a prompt neutrino beam produced by dumping 400 GeV protons on a copper beam dump, setting $V_{eN}^2 \lesssim 10^{-7}$ for $1 - 2$ GeV heavy neutrinos. We will consider the NA3 and CHARM exclusion regions reported in Figs. 8a and 2 of Refs. [161] and [160], respectively.

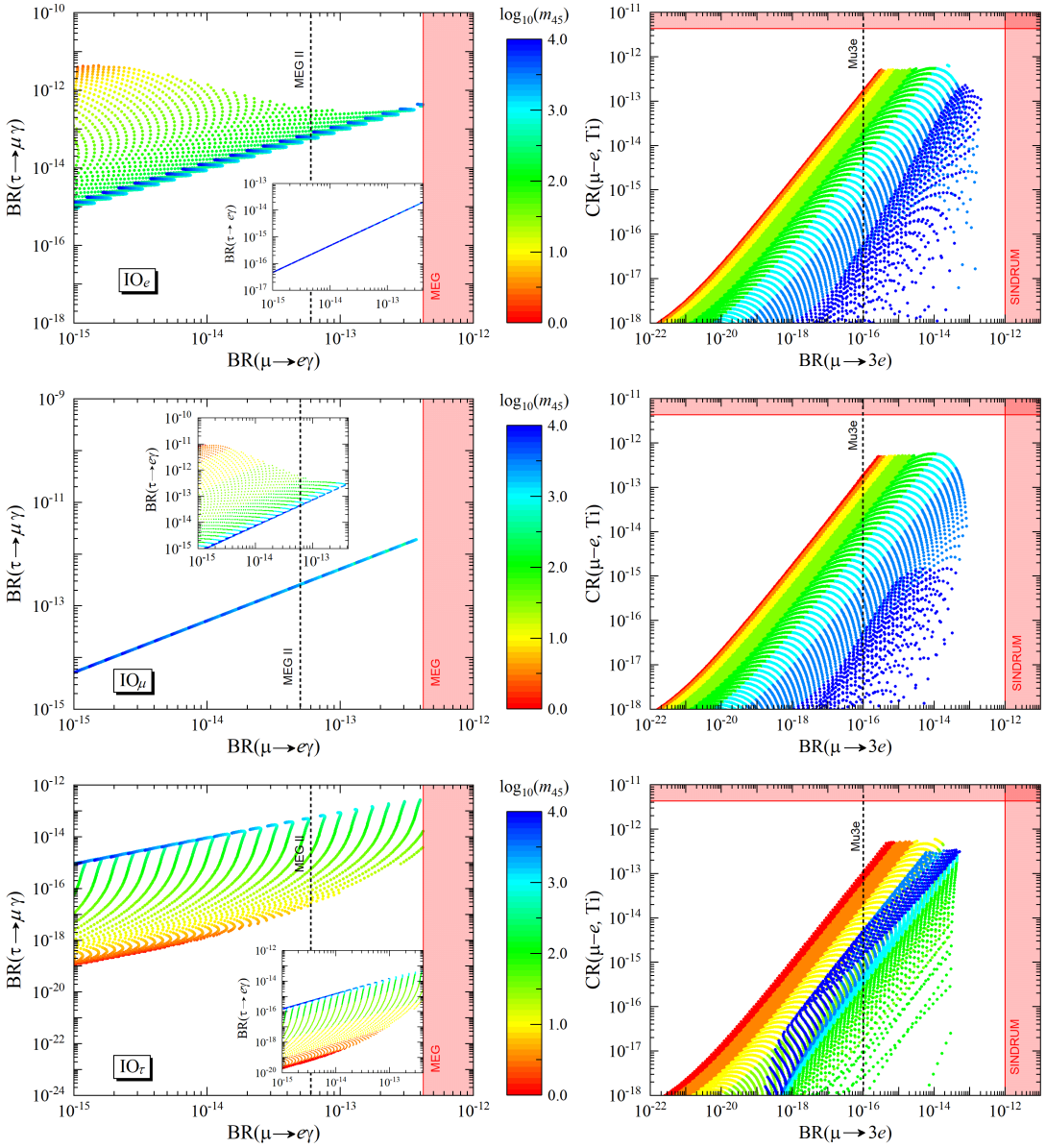

Figure 4.7: The same as in Fig. 4.6 for IO_e, IO_μ and IO_τ.

Future: The beam-dump experiment SHIP will use 400 GeV protons extracted from the CERN Super Proton Synchrotron (SPS) accelerator, dumped on a high-density target. The experiment will search for heavy neutrinos with mass up to ~ 6 GeV produced in the decays of D and B mesons. As for active-sterile mixing, SHIP will be able to probe it down to $V_{eN}^2 \sim 10^{-10}$ for 1.6 GeV heavy neutrinos. In this work, we will consider the SHIP exclusion region given in Fig. 3 of Ref. [162]. Although designed to measure active neutrino oscillation parameters with high precision [163], the DUNE experiment will also be able to search for heavy sterile neutrinos [164]. This will be achieved by striking a target with a very high-energy proton beam (up to 120 GeV), leading to the production of mainly pions and kaons which may produce sterile neutrinos in their decays. For illustration, we will consider the results presented in Fig. 2 of Ref. [164].

- **High-energy colliders:** At the Large Electron-Positron (LEP) collider, the L3 and DELPHI collaborations have looked for heavy neutrinos N produced via on-shell Z boson decays $e^+e^- \to Z \to N\nu$. Several N decay modes were considered, namely $N \to Z^*\nu\,(Z^* \to \ell\ell, \nu\nu, jj)$ and $N \to W^*\ell\,(W^* \to \ell\nu_\ell, jj')$. The L3 results were able to probe V_{eN}^2 down to 10^{-4} for ~ 20 GeV heavy neutrinos, while the DELPHI collaboration conducted similar searches excluding $V_{eN}^2 \gtrsim 3 \times 10^{-5}$ for masses in the range $3 - 50$ GeV. We will consider the L3 and DELPHI exclusion regions given in Figs. 6 and 10 of Refs. [165] and [166], respectively.

  At the LHC, the ATLAS and CMS collaborations are also looking for heavy neutrino signals. Both collaborations search for N production in $W^\pm \to \ell^\pm N$ followed by subsequent decays $N \to W^{\pm *}\ell^\mp\,(W^{\pm *} \to \ell^\pm\nu_\ell)$ with $\ell = e, \mu$. ATLAS has explored event signatures consisting of three charged leptons (electrons and muons) with same-sign dileptons of the same flavour (LNV mode). CMS has extended the search to include events with lepton number conservation, thus being sensitive to displaced decays. Overall, the ATLAS and CMS analyses on trilepton signatures excluded $V_{eN}^2 \gtrsim 10^{-4} - 10^{-5}$ for heavy neutrino masses in the $5 - 50$ GeV range. Both collaborations have also searched for the decays of heavy neutrinos produced in $pp \to W^{\pm *} \to \ell^\pm N$ into same-sign dileptons and jets $N \to W^\pm \to \ell^\pm\,(W^\pm \to jj')$. For the ATLAS exclusion regions we will consider the results given in Figs. 6 and 8 of Refs. [167] and [168], while for the CMS ones we take the results of Figs. 2 and 4 of Refs. [169] and [170], respectively. In the presence of active-sterile neutrino mixing, new interactions of the SM Higgs boson may arise, opening the $H^0 \to N\nu$ decay channel (if kinematically allowed). The subsequent decays $N \to \ell W^*\,(W^* \to \ell\nu)$ and $N \to \ell Z^*\,(Z^* \to \ell^+\ell^-)$ at the LHC have been studied in Ref. [171] to constrain the mixing-mass parameter space as shown in Fig. 3 of that reference.

Future: Future high-energy colliders will play a crucial role in searching for heavy sterile neutrinos. In particular, during the high-luminosity LHC phase (HL-LHC), ATLAS and CMS will be able to cover masses up to $2 - 3$ TeV. Sensitivity studies have also been performed for a Future Circular Hadron Collider (FCC-hh) at a 100 TeV centre-of-mass energy [52, 172]. For the HL-LHC and FCC-hh cases we will consider the exclusion regions given in Fig. 25 of Ref. [172] corresponding to LHC14 and LHC100 with integrated luminosities $\mathcal{L} = 3$ ab^{-1} and 15 ab^{-1}, respectively. Heavy-neutrino searches performed at a future high-luminosity e^+e^- storage ring collider (FCC-ee) can drastically improve the limits on active-sterile mixing down to 10^{-11} for ~ 60 GeV neutrinos (Fig. 8 of Ref. [173]). In a future e^+e^- linear collider, as the International Linear Collider (ILC), the sensitivity on heavy-light neutrino mixing can reach values down to 10^{-4} for a 500 GeV centre-of-mass energy and an integrated luminosity of $100\,\text{fb}^{-1}$ (Fig. 15 of Ref. [174]). For a Compact Linear Collider (CLIC) operating at 3 TeV and with $\mathcal{L} = 1\,\text{ab}^{-1}$, values of $V_{eN} \sim 10^{-5} - 10^{-4}$ can be probed for a $600\,\text{GeV} - 2.5\,\text{TeV}$ mass range (Fig. 24 of Ref. [174]).

  Detectors placed near LHC interaction points would allow for searches of heavy-sterile neutrinos produced in pp collisions through the reconstruction of displaced vertices in a low-background environment. Several proposals have been been put forward to conduct this kind of analyses, namely

the AL3X [175], CODEX-b [176], FASER2 [177], MATHUSLA [178] and MoEDAL [179] detectors. The sensitivity improvement with respect to that achieved by the main detectors (ATLAS, CMS and LHCb) could be of several orders of magnitude in the low-mass regime. In this work we will consider the FASER2 and MATHUSLA exclusion regions given in Figs. 5 and 37 of Refs. [180] and [178], respectively.

Given that we are dealing with nearly-degenerate sterile neutrinos due to the smallness of μ_s, LNV decay modes are expected to be suppressed as a result of the quasi-Dirac nature of the heavy sterile neutrinos. This is, however, not the case if the average decay width is of the order of the mass splitting, i.e. $\Gamma_N = (\Gamma_{N_1} + \Gamma_{N_2})/2 \simeq \Delta m_N$. This issue is especially relevant when looking for the same-sign dilepton signatures discussed above. In order to provide an insight regarding whether LNV decays are suppressed or not, we will use the same-sign to opposite-sign ratio [51, 181]

$$R_{ll} = \frac{\Delta m_N^2}{2\Gamma_N^2 + \Delta m_N^2}\,, \tag{4.40}$$

such that $R_{ll} \geq 1/3$ can be adopted as a criterion to identify the regions of the parameter space where LNV decays are unsuppressed [182]. To compute $\Gamma_N = (\Gamma_4 + \Gamma_5)/2$ in terms of the sterile neutrino masses and mixings we use the results of Ref. [156].

- **Electroweak precision data (EWPD):** As already mentioned, in the presence of sterile neutrinos, the active neutrino mixing matrix $\mathbf{U}$ relevant for neutrino oscillations [cf. Eq. (3.17)] is no longer unitary. Deviations from unitarity are constrained by neutrino oscillation data, electroweak precision tests and lepton flavour violating decays [158, 183, 183–188]. In fact, the off-diagonal elements of $\boldsymbol{\eta}_{\alpha\beta}$ defined in Eq. (3.23) are mainly restricted by the LFV decays studied in the previous section. On the other hand, $\boldsymbol{\eta}_{\alpha\alpha}$ are restricted by SM gauge boson decays, namely $W \to \ell_\alpha \nu_\alpha$ and $Z \to \nu\nu$, and universality tests in W and π decays. We will use here the limits for $|\boldsymbol{\eta}_{\alpha\alpha}|$ obtained in Ref. [158], namely:

$$|\boldsymbol{\eta}_{ee}| < 1.25 \times 10^{-3}, \quad |\boldsymbol{\eta}_{\mu\mu}| < 2.2 \times 10^{-4}, \quad |\boldsymbol{\eta}_{\tau\tau}| < 2.8 \times 10^{-3}\,. \tag{4.41}$$

Notice that, in our framework, the $\boldsymbol{\eta}_{\alpha\beta}$ are not independent since the $\mathbf{B}_{\alpha i}$ are related to each other as a result of the Abelian flavour symmetries. These relations are written in terms of low-energy neutrino observables as shown in Eq. (4.22), implying that $\boldsymbol{\eta}_{\alpha\beta}$ can be expressed by a single mixing parameter which, for convenience of our analysis, we choose to be $V_{eN}^2 = |\mathbf{B}_{e4}|^2$. In this case, we have

$$|\boldsymbol{\eta}_{\alpha\alpha}| = \frac{1}{2}\sum_{i=4}^{7} |\mathbf{B}_{\alpha i}|^2 \simeq V_{eN}^2 (x_{\alpha 4} + x_{\alpha 6})\,,\; x_{\alpha j} = \left|\frac{\mathbf{B}_{\alpha j}}{\mathbf{B}_{e4}}\right|^2\,, \tag{4.42}$$

where we have used Eq. (3.23) and the fact that $|\mathbf{B}_{\alpha 4}| \simeq |\mathbf{B}_{\alpha 5}|$ and $|\mathbf{B}_{\alpha 6}| \simeq |\mathbf{B}_{\alpha 7}|$. It is then possible to use the above equations together with Table 4.1 to compute the $x_{\alpha i}$ factors and extract upper bounds on V_{eN}^2 from the limits given in Eq. (4.41) for $|\boldsymbol{\eta}_{\alpha\alpha}|$ (see Table 4.3).

	$\lvert\boldsymbol{\eta}_{ee}\rvert$	$\lvert\boldsymbol{\eta}_{\mu\mu}\rvert$	$\lvert\boldsymbol{\eta}_{\tau\tau}\rvert$
NO_e [IO_e]	1.25×10^{-3} [1.25×10^{-3}]	3.90×10^{-6} [3.42×10^{-4}]	1.97×10^{-4} [4.01×10^{-3}]
NO_μ [IO_μ]	2.27×10^{-4} [2.44×10^{-5}]	6.58×10^{-6} [9.29×10^{-6}]	7.43×10^{-5} [9.05×10^{-5}]
NO_τ [IO_τ]	3.86×10^{-4} [7.64×10^{-5}]	4.17×10^{-6} [3.35×10^{-5}]	1.02×10^{-4} [3.09×10^{-4}]

Table 4.3: Upper bounds on V_{eN}^2 imposed by EWPD (see text for details) for $\text{NO}_{e,\mu,\tau}$ and $\text{IO}_{e,\mu,\tau}$.

- **Neutrinoless double beta decay:** In the presence of sterile neutrinos, the effective neutrino mass parameter $m_{\beta\beta}$, relevant for neutrinoless double beta decay, is [189]

$$m_{\beta\beta} \simeq \sum_{i=1}^{n_f} \mathbf{B}_{ei}^2 \; p^2 \frac{m_i}{p^2 - m_i^2} \simeq \sum_{i=1}^{3} \mathbf{B}_{ei}^2 m_i + \sum_{i=4}^{7} p^2 \mathbf{B}_{ei}^2 \; \frac{m_i}{p^2 - m_i^2} \,, \tag{4.43}$$

  where $p^2 \simeq -(100\text{ MeV})^2$ is the virtual momentum of the neutrinos and m_i are the physical neutrino masses. The first and second sums run over the number of light and heavy neutrinos which, in the present case, is three and four, respectively. For the 1 GeV–10 TeV mass range studied in this work, the contributions of the second term in Eq. (4.43) are negligible and, thus, the results in Fig. 4.2 remain valid (for neutrinoless double beta decay studies in the presence of sterile neutrinos see e.g. Refs. [54, 190–195]).

In the left panels of Figs. 4.8 and 4.9 we present a summary of all the current constraints discussed above, together with those stemming from $\mu \to e\gamma$ (MEG) and $\mu - e$ conversion in Au (SINDRUM) searches (see Fig. 4.6), now shown in the (m_{45}, V_{eN}^2) plane. For the EWPD exclusion regions we consider the most restrictive V_{eN}^2 limits given in Table 4.3, i.e. those extracted from $\lvert\boldsymbol{\eta}_{\mu\mu}\rvert$ (third column). On the right of the same figures, the projected sensitivities of the several experiments enumerated above are shown, including the cLFV ones already presented in Fig. 4.6 in the (m_{45}, μ_s) plane. For all cases, the overlap of the current exclusion regions (left panels) is shown in light yellow. By looking at these two figures one can conclude that:

- For $m_{45} \gtrsim 2$ GeV, the strongest constraints are typically those imposed by the SINDRUM and MEG limits on $\text{BR}(\mu \to e\gamma)$ and $\text{CR}(\mu - e, \text{Au})$, respectively, and by EWPD (left panels). One exception is the IO_e case where, for $2\,\text{GeV} \lesssim m_{45} \lesssim 50$ GeV, the DELPHI, ATLAS and CMS limits are stronger. In all situations, the CHARM exclusion region is more constraining when $m_{45} = 1 - 2$ GeV. Notice that the EWPD exclusion regions are not the same for the different NO and IO scenarios since the U(1) flavour symmetries, together with present neutrino data, impose different relations among the $\mathbf{B}_{\alpha j}$. Thus, the limits on $\lvert\boldsymbol{\eta}_{\alpha\alpha}\rvert$ cannot be directly translated into limits of a single $\mathbf{B}_{\alpha j}$ by neglecting the remaining $\mathbf{B}_{\alpha k}$ with different $k \neq j$.

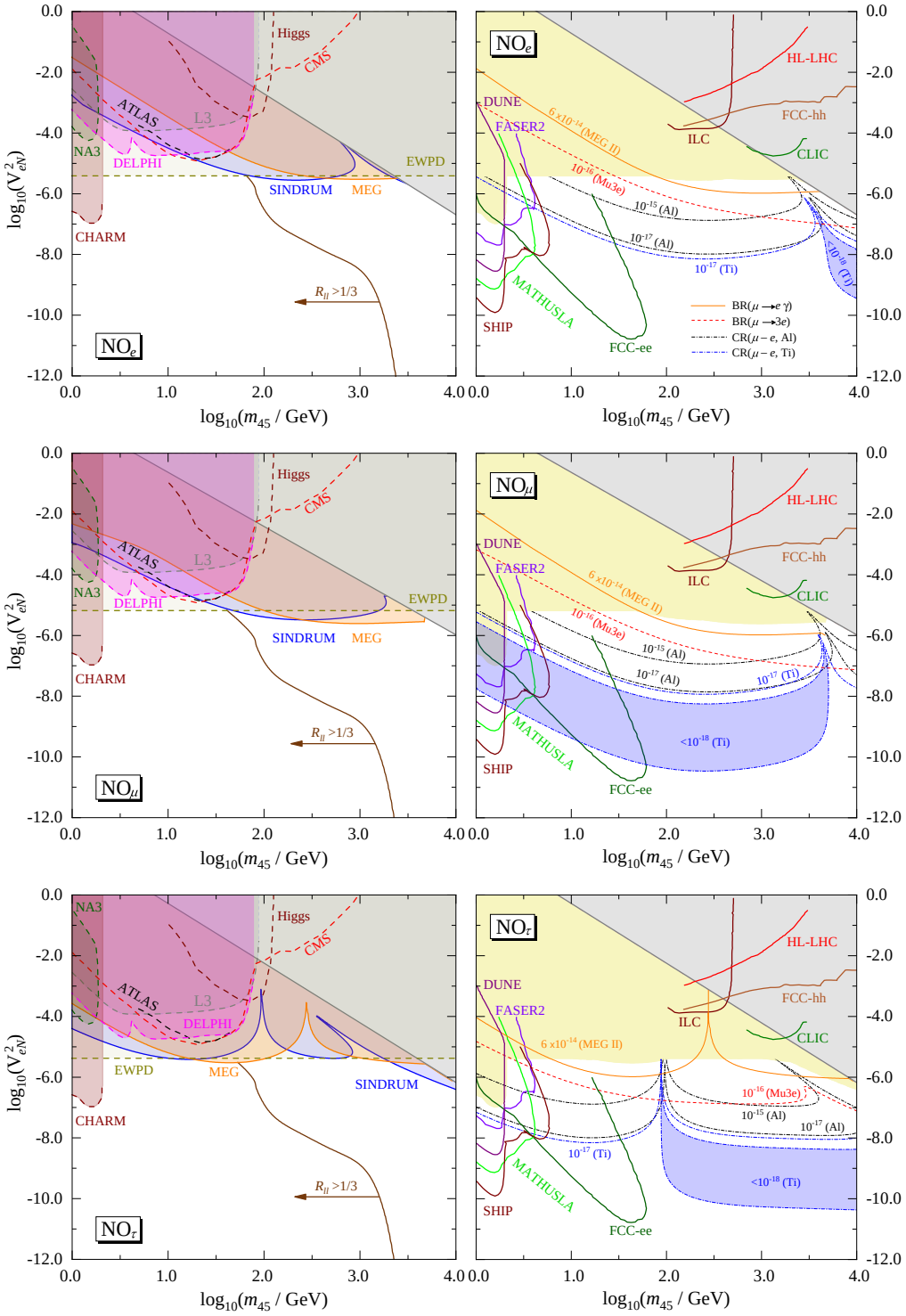

Figure 4.8: [Left] Constraints imposed on the (m_{45}, V^2_{eN}) parameter space by the MEG and SINDRUM limits on BR($\mu \to e\gamma$) and CR($\mu - e$, Au) (see Section 4.3), by the current searches conducted at colliders and beam-dump experiments and by EWPD (see discussion in the main text where the sources of the several exclusion regions are indicated). As in Figs. 4.6 and 4.7, $b_i^{\max} > 5$ within the grey-shaded region. To the left of the solid brown line $R_{ll} > 1/3$. [Right] Projected sensitivities for cLFV searches and other experiments discussed in the main text. The yellow-shaded regions correspond to overlapping the current constraints shown on the left panels. Inside the blue shaded region CR($\mu - e$, Ti $< 10^{-18}$). The top (middle) [bottom] panels correspond to the NO$_e$ (NO$_\mu$) [NO$_\tau$] case.

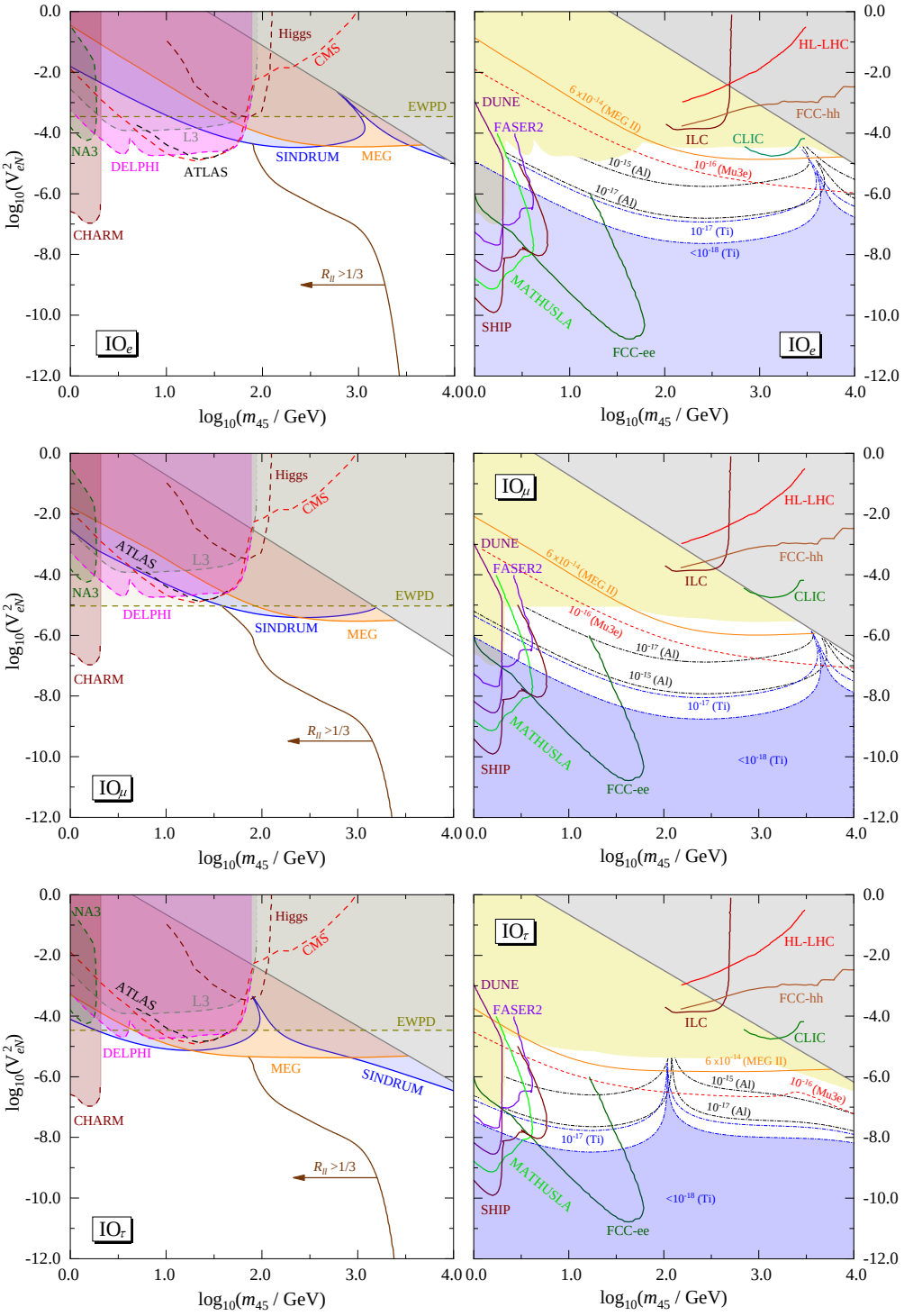

Figure 4.9: The same as in Fig. 4.8 for IO$_e$, IO$_\mu$ and IO$_\tau$.

- Any signal of sterile neutrinos with $V_{eN}^2 \gtrsim 10^{-4}$ at future hadron or linear colliders (HL-LHC, FCC-hh, CLIC and ILC regions) would not be compatible with the limits already imposed by current constraints from LFV searches and EWPD (see right panels). Therefore, in the context of the present work, high-energy collider probes conducted at the FCC-ee and at experiments like SHIP, MATHUSLA, DUNE and FASER2 turn out to be of utmost importance (obviously, taking into account the considered sensitivity studies).

- While for NO_e cLFV indirect searches are fully complementary to the aforementioned direct ones, this is not the case for the remaining NO and IO scenarios. In particular, for inverted neutrino masses, the region with $V_{eN}^2 \lesssim 10^{-9} - 10^{-8}$ cannot be probed by future $\mu - e$ conversion experiments. In this case, such mixing regimes can be covered by displaced-vertex experiments and by a high-luminosity Z factory like the FCC-ee. Notice that $R_{ll} \geq 1/3$ within the sensitivity regions of those searches (see the brown solid lines in the left panels), indicating that LNV sterile neutrino decays are not suppressed by their quasi-Dirac nature. It should also be mentioned that in the absence of a positive $\mu \to e\gamma$ signal, the impact of MEG II data would be mild (compare the yellow regions with the solid orange line in the right panels). Instead, if that decay is observed, ranges for m_{45} and V_{eN}^2 can be set in most of the cases, being the latter relatively narrow. As for $\mu \to 3e$, future probes conducted by the Mu3e collaboration will be able to cover V_{eN}^2 down to $10^{-6} - 10^{-7}$ for wide ranges of sterile neutrino masses.

To conclude this section, we remark that although we have shown the results of our analysis in the (m_{45}, V_{eN}^2) plane, it is relatively easy to infer how the obtained exclusion regions and sensitivity contours would appear choosing a different mixing parameter by taking into account the relations in Table 4.1.

Chapter 5

Conclusions

The success of the Standard Model of particle physics is by now well established. Nonetheless, numerous phenomena remain unexplained within its framework. In particular, neutrino oscillations are an undeniable evidence of physics beyond the SM, since they imply that neutrinos are massive particles and that there is mixing in the lepton sector. In order to account for the origin of the tiny neutrino masses, the mixing patterns between leptons and the hierarchy among their masses, which constitute the so-called *flavour puzzle*, we must work in extensions of the SM.

In Chapter 2, we briefly described the canonical seesaw mechanisms, based on the addition of new particles to the SM in order to explain neutrino observables. We showed that several high and low-scale models can be constructed. The former ones explain the smallness of neutrino masses through very heavy extra particles or unnaturally tiny Dirac Yukawa couplings, as is the case of the Type-I seesaw. The latter models, among which the Type-II seesaw, can generate the neutrino masses through natural $\mathcal{O}(1)$ Yukawa couplings and masses of the new particles of the order of the EW scale.

The work developed in this thesis follows a low-scale seesaw approach, since it opens the possibility for potential detection of direct new physics signals in future experiments. We have thoroughly investigated the minimal inverse-seesaw mechanism with couplings constrained by U(1) flavour symmetries, and with all fermion masses generated via spontaneous symmetry breaking through the vacuum expectation values of scalar fields. In Chapter 3, we presented the low-scale inverse seesaw mechanism. After finding the maximally-restrictive mass matrices compatible with current neutrino data, we identified all possible U(1) symmetry realisations and concluded that at least two Higgs doublets and two complex scalar singlets are required to successfully implement those symmetries.

Having established our model, we proceeded in Chapter 4 to study its most relevant phenomenological implications for the realisable maximally-restrictive texture sets. The presence of scalar singlets in the model opens up the possibility for spontaneous CP violation, which turns out to be successfully communicated to the lepton sector via their couplings to the new sterile fermions. In Section 4.1, we showed that, as a result of SCPV and the Abelian symmetries, the Majorana and Dirac CP phases are related to each other. Furthermore, in Section 4.2, it was shown that, including one-loop corrections to neutrino masses and requiring them to be at the one-percent level, sterile-neutrino mass ranges can be established,

within which the tree-level results are still valid in light of the present experimental precision in the determination of the oscillation parameters. Due to the presence of flavour symmetries, the heavy-light mixings are not independent, and their ratios are entirely determined by the values of the lepton masses, mixing angles and CP-violating phases. This provides a very constrained setup for phenomenological studies in the framework of current and future probes that are sensitive to sterile neutrino states.

In Section 4.3, we then studied several cLFV decays and obtained the exclusion regions set by the experimental limits on the branching ratio $\mathrm{BR}(\mu \to e\gamma)$ and capture rate $\mathrm{CR}(\mu - e, \mathrm{Au})$. These results establish upper bounds on the active-sterile mixing V_{eN}^2 of about $10^{-4} - 10^{-5}$. The prospects to further explore the parameter space were discussed in view of the projected sensitivities of future LFV searches, especially those dedicated to $\mu \to e\gamma$, $\mu \to 3e$ and $\mu - e$ conversion in nuclei. After analysing the constraining power of cLFV processes, we focused our analysis on alternative probes, namely collider and beam-dump experimental searches that are sensitive to the presence of sterile neutrinos. We concluded in Section 4.4 that, in general, the HL-LHC, FCC-hh, ILC and CLIC sensitivity regions are already excluded by current LFV and EWPD constraints for all possible U(1) symmetry realisations.

Searches at a high-luminosity Z factory as the FCC-ee and at experiments like SHIP, MATHUSLA and FASER2 would be highly complementary to the Mu3e, Mu2e, COMET and PRISM/PRIME projects. Although we have not explored all possible future scenarios which could arise from independent results of different searches, it is clear that a single positive signal in any of those experiments would definitely put at test the scenarios studied in this thesis. In this sense, further symmetry-motivated studies based on extensions of the Standard Model and performed in the context of sterile neutrino searches are undoubtedly welcome.

Bibliography

[1] S. Glashow, *Nucl. Phys.* **22**, 579 (1961).

[2] S. Weinberg, *Phys. Rev. Lett.* **19**, 1264 (1967).

[3] A. Salam, *Conf. Proc. C* **680519**, 367 (1968).

[4] G. Aad, *et al.*, *Phys. Rev. Lett.* **114**, 191803 (2015).

[5] B. Pontecorvo, *Sov. Phys. JETP* **6**, 429 (1957).

[6] B. Pontecorvo, *Sov. Phys. JETP* **7**, 172 (1958).

[7] F. Capozzi, *et al.*, *Phys. Rev. D* **95**, 096014 (2017). [Addendum: Phys.Rev.D 101, 116013 (2020)].

[8] P. de Salas, *et al.* (2020).

[9] I. Esteban, M. Gonzalez-Garcia, M. Maltoni, T. Schwetz, A. Zhou, *JHEP* **09**, 178 (2020).

[10] E. Majorana, *Nuovo Cim.* **14**, 171 (1937).

[11] J. Schechter, J. Valle, *Phys. Rev. D* **25**, 2951 (1982).

[12] A. Aguilar-Arevalo, *et al.*, *Phys. Rev. D* **64**, 112007 (2001).

[13] A. Aguilar-Arevalo, *et al.*, *Phys. Rev. Lett.* **121**, 221801 (2018).

[14] K. Abazajian, *et al.* (2012).

[15] J. Kopp, P. A. N. Machado, M. Maltoni, T. Schwetz, *JHEP* **05**, 050 (2013).

[16] M. Dentler, *et al.*, *JHEP* **08**, 010 (2018).

[17] S. Böser, *et al.*, *Prog. Part. Nucl. Phys.* **111**, 103736 (2020).

[18] S. Hagstotz, *et al.* (2020).

[19] P. Minkowski, *Phys. Lett. B* **67**, 421 (1977).

[20] T. Yanagida, *Conf. Proc. C* **7902131**, 95 (1979).

[21] M. Gell-Mann, P. Ramond, R. Slansky, *Conf. Proc. C* **790927**, 315 (1979).

[22] S. Glashow, *NATO Sci. Ser. B* **61**, 687 (1980).

[23] R. N. Mohapatra, G. Senjanovic, *Phys. Rev. Lett.* **44**, 912 (1980).

[24] W. Konetschny, W. Kummer, *Phys. Lett. B* **70**, 433 (1977).

[25] J. Schechter, J. Valle, *Phys. Rev. D* **22**, 2227 (1980).

[26] T. Cheng, L.-F. Li, *Phys. Rev. D* **22**, 2860 (1980).

[27] G. Lazarides, Q. Shafi, C. Wetterich, *Nucl. Phys. B* **181**, 287 (1981).

[28] R. N. Mohapatra, G. Senjanovic, *Phys. Rev. D* **23**, 165 (1981).

[29] R. Foot, H. Lew, X. He, G. C. Joshi, *Z. Phys. C* **44**, 441 (1989).

[30] R. Mohapatra, *Phys. Rev. Lett.* **56**, 561 (1986).

[31] R. Mohapatra, J. Valle, *Phys. Rev. D* **34**, 1642 (1986).

[32] M. Gonzalez-Garcia, J. Valle, *Phys. Lett. B* **216**, 360 (1989).

[33] G. 't Hooft, *NATO Sci. Ser. B* **59**, 135 (1980).

[34] A. Baldini, *et al.*, *Eur. Phys. J. C* **76**, 434 (2016).

[35] A. Baldini, *et al.*, *Eur. Phys. J. C* **78**, 380 (2018).

[36] U. Bellgardt, *et al.*, *Nucl. Phys. B* **299**, 1 (1988).

[37] C. Dohmen, *et al.*, *Phys. Lett. B* **317**, 631 (1993).

[38] W. Honecker, *et al.*, *Phys. Rev. Lett.* **76**, 200 (1996).

[39] W. H. Bertl, *et al.*, *Eur. Phys. J. C* **47**, 337 (2006).

[40] Y. Kuno, *PTEP* **2013**, 022C01 (2013).

[41] H. Natori, *Nucl. Phys. B Proc. Suppl.* **248-250**, 52 (2014).

[42] F. Deppisch, T. Kosmas, J. Valle, *Nucl. Phys. B* **752**, 80 (2006).

[43] A. Abada, M. Lucente, *Nucl. Phys. B* **885**, 651 (2014).

[44] E. Arganda, M. Herrero, X. Marcano, C. Weiland, *Phys. Rev. D* **91**, 015001 (2015).

[45] A. Abada, V. De Romeri, A. Teixeira, *JHEP* **02**, 083 (2016).

[46] A. Abada, V. De Romeri, S. Monteil, J. Orloff, A. Teixeira, *JHEP* **04**, 051 (2015).

[47] V. De Romeri, A. Abada, S. Monteil, J. Orloff, A. M. Teixeira, *PoS* **EPS-HEP2015**, 056 (2015).

[48] E. Arganda, M. Herrero, X. Marcano, C. Weiland, *Phys. Lett. B* **752**, 46 (2016).

[49] A. Abada, A. M. Teixeira, *Front. in Phys.* **6**, 142 (2018).

[50] F. del Aguila, J. Aguilar-Saavedra, *Nucl. Phys. B* **813**, 22 (2009).

[51] F. F. Deppisch, P. Bhupal Dev, A. Pilaftsis, *New J. Phys.* **17**, 075019 (2015).

[52] S. Antusch, E. Cazzato, O. Fischer, *Int. J. Mod. Phys. A* **32**, 1750078 (2017).

[53] A. Caputo, P. Hernandez, J. Lopez-Pavon, J. Salvado, *JHEP* **06**, 112 (2017).

[54] P. D. Bolton, F. F. Deppisch, P. Bhupal Dev, *JHEP* **03**, 170 (2020).

[55] H. Ishimori, *et al.*, *Prog. Theor. Phys. Suppl.* **183**, 1 (2010).

[56] S. Morisi, J. Valle, *Fortsch. Phys.* **61**, 466 (2013).

[57] S. King, *Prog. Part. Nucl. Phys.* **94**, 217 (2017).

[58] Z.-z. Xing, *Phys. Rept.* **854**, 1 (2020).

[59] F. Feruglio, A. Romanino (2019).

[60] W. Grimus, A. S. Joshipura, L. Lavoura, M. Tanimoto, *Eur. Phys. J. C* **36**, 227 (2004).

[61] A. Dighe, N. Sahu (2008).

[62] B. Adhikary, A. Ghosal, P. Roy, *JHEP* **10**, 040 (2009).

[63] S. Dev, S. Gupta, R. R. Gautam, *Phys. Lett. B* **701**, 605 (2011).

[64] R. González Felipe, H. Serôdio, *Nucl. Phys. B* **886**, 75 (2014).

[65] L. M. Cebola, D. Emmanuel-Costa, R. G. Felipe, *Phys. Rev. D* **92**, 025005 (2015).

[66] R. Samanta, A. Ghosal, *Nucl. Phys. B* **911**, 846 (2016).

[67] T. Kobayashi, T. Nomura, H. Okada, *Phys. Rev. D* **98**, 055025 (2018).

[68] M. H. Rahat, P. Ramond, B. Xu, *Phys. Rev. D* **98**, 055030 (2018).

[69] N. Nath, *Mod. Phys. Lett. A* **34**, 1950329 (2019).

[70] D. Barreiros, R. Felipe, F. Joaquim, *Phys. Rev. D* **97**, 115016 (2018).

[71] D. Barreiros, R. Felipe, F. Joaquim, *JHEP* **01**, 223 (2019).

[72] S. Correia, R. Felipe, F. Joaquim, *Phys. Rev. D* **100**, 115008 (2019).

[73] C. I. Low, R. R. Volkas, *Phys. Rev. D* **68**, 033007 (2003).

[74] G. Branco, *et al.*, *Phys. Rept.* **516**, 1 (2012).

[75] C.-N. Yang, R. L. Mills, *Phys. Rev.* **96**, 191 (1954).

[76] F. Englert, R. Brout, *Phys. Rev. Lett.* **13**, 321 (1964).

[77] G. Guralnik, C. Hagen, T. Kibble, *Phys. Rev. Lett.* **13**, 585 (1964).

[78] P. W. Higgs, *Phys. Rev. Lett.* **13**, 508 (1964).

[79] P. W. Higgs, *Phys. Rev.* **145**, 1156 (1966).

[80] Y. Nambu, G. Jona-Lasinio, *Phys. Rev.* **122**, 345 (1961).

[81] Y. Nambu, G. Jona-Lasinio, *Phys. Rev.* **124**, 246 (1961).

[82] J. Goldstone, *Nuovo Cim.* **19**, 154 (1961).

[83] J. Goldstone, A. Salam, S. Weinberg, *Phys. Rev.* **127**, 965 (1962).

[84] M. Gell-Mann, *Phys. Lett.* **8**, 214 (1964).

[85] G. Zweig, *An SU(3) model for strong interaction symmetry and its breaking. Version 2* (1964), pp. 22–101.

[86] G. 't Hooft, *Nucl. Phys. B* **35**, 167 (1971).

[87] G. 't Hooft, M. Veltman, *Nucl. Phys. B* **44**, 189 (1972).

[88] T. Nakano, K. Nishijima, *Prog. Theor. Phys.* **10**, 581 (1953).

[89] P. Zyla, *et al.*, *PTEP* **2020**, 083C01 (2020).

[90] N. Cabibbo, *Phys. Rev. Lett.* **10**, 531 (1963).

[91] M. Kobayashi, T. Maskawa, *Prog. Theor. Phys.* **49**, 652 (1973).

[92] L.-L. Chau, W.-Y. Keung, *Phys. Rev. Lett.* **53**, 1802 (1984).

[93] N. Aghanim, *et al.*, *Astron. Astrophys.* **641**, A1 (2020).

[94] M. Aker, *et al.*, *Phys. Rev. Lett.* **123**, 221802 (2019).

[95] C. W. K. C. Giunti, *Fundamentals of Neutrino Physics and Astrophysics* (2007).

[96] Z. Maki, M. Nakagawa, S. Sakata, *Prog. Theor. Phys.* **28**, 870 (1962).

[97] W. Rodejohann, J. Valle, *Phys. Rev. D* **84**, 073011 (2011).

[98] B. Aharmim, *et al.*, *Phys. Rev. C* **88**, 025501 (2013).

[99] A. Gando, *et al.*, *Phys. Rev. D* **83**, 052002 (2011).

[100] K. Abe, *et al.*, *Phys. Rev. D* **97**, 072001 (2018).

[101] M. Aartsen, *et al.*, *Phys. Rev. Lett.* **120**, 071801 (2018).

[102] M. Aartsen, *et al.*, *Phys. Rev. D* **99**, 032007 (2019).

[103] G. Bak, *et al.*, *Phys. Rev. Lett.* **121**, 201801 (2018).

[104] D. Adey, *et al.*, *Phys. Rev. Lett.* **121**, 241805 (2018).

[105] M. Acero, *et al.*, *Phys. Rev. Lett.* **123**, 151803 (2019).

[106] K. Abe, *et al.*, *Phys. Rev. Lett.* **124**, 161802 (2020).

[107] K. Abe, *et al.*, *Nature* **580**, 339 (2020). [Erratum: Nature 583, E16 (2020)].

[108] P. Adamson, *et al.*, *Phys. Rev. Lett.* **112**, 191801 (2014).

[109] M. Ahn, *et al.*, *Phys. Rev. D* **74**, 072003 (2006).

[110] A. Gando, *et al.*, *Phys. Rev. Lett.* **117**, 082503 (2016). [Addendum: Phys.Rev.Lett. 117, 109903 (2016)].

[111] M. Agostini, *et al.* (2020).

[112] D. Adams, *et al.*, *Phys. Rev. Lett.* **124**, 122501 (2020).

[113] G. Anton, *et al.*, *Phys. Rev. Lett.* **123**, 161802 (2019).

[114] M. H. Lee, *JINST* **15**, C08010 (2020).

[115] G. Wang, *et al.* (2015).

[116] N. Abgrall, *et al.*, *AIP Conf. Proc.* **1894**, 020027 (2017).

[117] S. Andringa, *et al.*, *Adv. High Energy Phys.* **2016**, 6194250 (2016).

[118] J. Albert, *et al.*, *Phys. Rev. C* **97**, 065503 (2018).

[119] X. Chen, *et al.*, *Sci. China Phys. Mech. Astron.* **60**, 061011 (2017).

[120] A. Broncano, M. Gavela, E. E. Jenkins, *Phys. Lett. B* **552**, 177 (2003). [Erratum: Phys.Lett.B 636, 332 (2006)].

[121] M. Gavela, T. Hambye, D. Hernandez, P. Hernandez, *JHEP* **09**, 038 (2009).

[122] A. Abada, C. Biggio, F. Bonnet, M. Gavela, T. Hambye, *JHEP* **12**, 061 (2007).

[123] S. Weinberg, *Phys. Rev. Lett.* **43**, 1566 (1979).

[124] W. Grimus, L. Lavoura, *JHEP* **11**, 042 (2000).

[125] E. Fernandez-Martinez, M. Gavela, J. Lopez-Pavon, O. Yasuda, *Phys. Lett. B* **649**, 427 (2007).

[126] H. Camara, R. Felipe, F. Joaquim, arXiv:2012.04557 [hep-ph] (2020).

[127] A. Ilakovac, A. Pilaftsis, *Nucl. Phys. B* **437**, 491 (1995).

[128] L. M. Cebola, D. Emmanuel-Costa, R. G. Felipe, *Eur. Phys. J. C* **76**, 156 (2016).

[129] R. Gonzalez Felipe, H. Serodio, *J. Phys. G* **44**, 065002 (2017).

[130] P. O. Ludl, W. Grimus, *JHEP* **07**, 090 (2014). [Erratum: JHEP 10, 126 (2014)].

[131] P. Ferreira, J. P. Silva, *Phys. Rev. D* **83**, 065026 (2011).

[132] H. Serôdio, *Phys. Rev. D* **88**, 056015 (2013).

[133] I. P. Ivanov, V. Keus, E. Vdovin, *J. Phys. A* **45**, 215201 (2012).

[134] I. Ivanov, C. Nishi, *JHEP* **11**, 069 (2013).

[135] G. Branco, R. Felipe, F. Joaquim, *Rev. Mod. Phys.* **84**, 515 (2012).

[136] F. Joaquim, *Phys. Rev. D* **68**, 033019 (2003).

[137] A. Barabash, *Front. in Phys.* **6**, 160 (2019).

[138] M. J. Dolinski, A. W. Poon, W. Rodejohann, *Ann. Rev. Nucl. Part. Sci.* **69**, 219 (2019).

[139] A. Pilaftsis, *Z. Phys. C* **55**, 275 (1992).

[140] A. Pilaftsis, *Phys. Rev. D* **65**, 115013 (2002).

[141] W. Grimus, L. Lavoura, *Phys. Lett. B* **546**, 86 (2002).

[142] P. Dev, A. Pilaftsis, *Phys. Rev. D* **86**, 113001 (2012).

[143] E. Aeikens, P. Ferreira, W. Grimus, D. Jurčiukonis, L. Lavoura (2020).

[144] M. Raidal, *et al.*, *Eur. Phys. J. C* **57**, 13 (2008).

[145] B. Aubert, *et al.*, *Phys. Rev. Lett.* **104**, 021802 (2010).

[146] W. Altmannshofer, *et al.*, *PTEP* **2019**, 123C01 (2019). [Erratum: PTEP 2020, 029201 (2020)].

[147] A. Blondel, *et al.* (2013).

[148] K. Hayasaka, *et al.*, *Phys. Lett. B* **687**, 139 (2010).

[149] L. Bartoszek, *et al.* (2014).

[150] R. Abramishvili, *et al.*, *PTEP* **2020**, 033C01 (2020).

[151] A. Alekou, *et al.*, *Community Summer Study 2013: Snowmass on the Mississippi* (2013).

[152] A. Nehrkorn, *Nucl. Part. Phys. Proc.* **287-288**, 160 (2017).

[153] M. Dam, *SciPost Phys. Proc.* **1**, 041 (2019).

[154] R. Akers, *et al.*, *Z. Phys. C* **67**, 555 (1995).

[155] P. Abreu, *et al.*, *Z. Phys. C* **73**, 243 (1997).

[156] A. Atre, T. Han, S. Pascoli, B. Zhang, *JHEP* **05**, 030 (2009).

[157] A. de Gouvêa, A. Kobach, *Phys. Rev. D* **93**, 033005 (2016).

[158] E. Fernandez-Martinez, J. Hernandez-Garcia, J. Lopez-Pavon, *JHEP* **08**, 033 (2016).

[159] R. K. Ellis, *et al.* (2019).

[160] F. Bergsma, *et al.*, *Phys. Lett. B* **166**, 473 (1986).

[161] J. Badier, *et al.*, *Z. Phys. C* **31**, 21 (1986).

[162] C. Ahdida, *et al.*, *JHEP* **04**, 077 (2019).

[163] R. Acciarri, *et al.* (2016).

[164] I. Krasnov, *Phys. Rev. D* **100**, 075023 (2019).

[165] O. Adriani, *et al.*, *Phys. Lett. B* **295**, 371 (1992).

[166] P. Abreu, *et al.*, *Z. Phys. C* **74**, 57 (1997). [Erratum: Z.Phys.C 75, 580 (1997)].

[167] G. Aad, *et al.*, *JHEP* **10**, 265 (2019).

[168] G. Aad, *et al.*, *JHEP* **07**, 162 (2015).

[169] A. M. Sirunyan, *et al.*, *Phys. Rev. Lett.* **120**, 221801 (2018).

[170] A. M. Sirunyan, *et al.*, *JHEP* **01**, 122 (2019).

[171] A. Das, P. S. B. Dev, C. Kim, *Phys. Rev. D* **95**, 115013 (2017).

[172] S. Pascoli, R. Ruiz, C. Weiland, *JHEP* **06**, 049 (2019).

[173] A. Blondel, E. Graverini, N. Serra, M. Shaposhnikov, *Nucl. Part. Phys. Proc.* **273-275**, 1883 (2016).

[174] S. Banerjee, P. S. B. Dev, A. Ibarra, T. Mandal, M. Mitra, *Phys. Rev. D* **92**, 075002 (2015).

[175] D. Dercks, H. K. Dreiner, M. Hirsch, Z. S. Wang, *Phys. Rev. D* **99**, 055020 (2019).

[176] V. V. Gligorov, S. Knapen, M. Papucci, D. J. Robinson, *Phys. Rev. D* **97**, 015023 (2018).

[177] J. L. Feng, I. Galon, F. Kling, S. Trojanowski, *Phys. Rev. D* **97**, 035001 (2018).

[178] D. Curtin, *et al.*, *Rept. Prog. Phys.* **82**, 116201 (2019).

[179] M. Frank, *et al.*, *Phys. Lett. B* **802**, 135204 (2020).

[180] F. Kling, S. Trojanowski, *Phys. Rev. D* **97**, 095016 (2018).

[181] G. Anamiati, M. Hirsch, E. Nardi, *JHEP* **10**, 010 (2016).

[182] M. Drewes, J. Klarić, P. Klose, *JHEP* **19**, 032 (2020).

[183] F. del Aguila, J. de Blas, M. Perez-Victoria, *Phys. Rev. D* **78**, 013010 (2008).

[184] S. Antusch, C. Biggio, E. Fernandez-Martinez, M. Gavela, J. Lopez-Pavon, *JHEP* **10**, 084 (2006).

[185] E. Akhmedov, A. Kartavtsev, M. Lindner, L. Michaels, J. Smirnov, *JHEP* **05**, 081 (2013).

[186] S. Antusch, O. Fischer, *JHEP* **10**, 094 (2014).

[187] S. Antusch, O. Fischer pp. 83–92 (2017).

[188] M. Blennow, P. Coloma, E. Fernandez-Martinez, J. Hernandez-Garcia, J. Lopez-Pavon, *JHEP* **04**, 153 (2017).

[189] M. Blennow, E. Fernandez-Martinez, J. Lopez-Pavon, J. Menendez, *JHEP* **07**, 096 (2010).

[190] M. Mitra, G. Senjanovic, F. Vissani, *Nucl. Phys. B* **856**, 26 (2012).

[191] J. Lopez-Pavon, S. Pascoli, C.-f. Wong, *Phys. Rev. D* **87**, 093007 (2013).

[192] I. Girardi, A. Meroni, S. Petcov, *JHEP* **11**, 146 (2013).

[193] A. Abada, V. De Romeri, A. Teixeira, *JHEP* **09**, 074 (2014).

[194] J. Lopez-Pavon, E. Molinaro, S. Petcov, *JHEP* **11**, 030 (2015).

[195] A. Abada, A. Hernández-Cabezudo, X. Marcano, *JHEP* **01**, 041 (2019).

[196] K. Kannike, *Eur. Phys. J. C* **72**, 2093 (2012).

[197] A. Arhrib, R. Benbrik, M. El Kacimi, L. Rahili, S. Semlali, *Eur. Phys. J. C* **80**, 13 (2020).

[198] J. F. Gunion, H. E. Haber, *Phys. Rev. D* **67**, 075019 (2003).

[199] R. Alonso, M. Dhen, M. Gavela, T. Hambye, *JHEP* **01**, 118 (2013).

[200] T. Inami, C. Lim, *Prog. Theor. Phys.* **65**, 297 (1981). [Erratum: Prog.Theor.Phys. 65, 1772 (1981)].

[201] M. Beg, A. Sirlin, *Phys. Rept.* **88**, 1 (1982).

[202] T. Cheng, L.-F. Li, *Phys. Rev. Lett.* **45**, 1908 (1980).

[203] J. Bernabeu, J. Korner, A. Pilaftsis, K. Schilcher, *Phys. Rev. Lett.* **71**, 2695 (1993).

[204] J. I. Illana, M. Jack, T. Riemann, *2nd Workshop of the 2nd Joint ECFA / DESY Study on Physics and Detectors for a Linear Electron Positron Collider* (1999), pp. 490–524.

[205] J. F. Nieves, P. B. Pal, *Am. J. Phys.* **72**, 1100 (2004).

[206] C. Nishi, *Am. J. Phys.* **73**, 1160 (2005).

[207] A. Ilakovac, A. Pilaftsis, L. Popov, *Phys. Rev. D* **87**, 053014 (2013).

[208] A. Crivellin, S. Najjari, J. Rosiek, *JHEP* **04**, 167 (2014).

[209] J. Hisano, T. Moroi, K. Tobe, M. Yamaguchi, *Phys. Rev. D* **53**, 2442 (1996).

[210] E. Arganda, M. J. Herrero, *Phys. Rev. D* **73**, 055003 (2006).

[211] A. Abada, *et al.*, *JHEP* **11**, 048 (2014).

[212] A. Crivellin, *et al.*, *JHEP* **06**, 003 (2018).

[213] R. Kitano, M. Koike, Y. Okada, *Phys. Rev. D* **66**, 096002 (2002). [Erratum: Phys.Rev.D 76, 059902 (2007)].

[214] T. Kosmas, S. Kovalenko, I. Schmidt, *Phys. Lett. B* **511**, 203 (2001).

[215] G. Hernández-Tomé, J. Illana, M. Masip, G. López Castro, P. Roig, *Phys. Rev. D* **101**, 075020 (2020).

[216] G. Passarino, M. Veltman, *Nucl. Phys. B* **160**, 151 (1979).

[217] J. C. Romão, *Advanced Quantum Field Theory* (2020).

[218] B. He, T. Cheng, L.-F. Li, *Phys. Lett. B* **553**, 277 (2003).

[219] W. Grimus, L. Lavoura, *Phys. Rev. D* **66**, 014016 (2002).

[220] L. Lavoura, *Eur. Phys. J. C* **29**, 191 (2003).

Appendix A

Scalar sector

A.1 Scalar potential with soft-breaking terms

The Abelian symmetries that realise some of the maximally-restrictive textures of Section 3.2.1 were presented in Section 3.2.2, being the minimal scalar-field content required to implement those symmetry realisations given in Eq. (3.34), i.e., two Higgs doublets $\Phi_{1,2}$ and two complex singlets $S_{1,2}$:

$$\Phi_a = \begin{pmatrix} \phi_a^+ \\ \phi_a^0 \end{pmatrix} = \frac{1}{\sqrt{2}} \begin{pmatrix} \sqrt{2}\phi_a^+ \\ v_a e^{i\theta_a} + \rho_a + i\eta_a \end{pmatrix} \ , \ S_a = \frac{1}{\sqrt{2}} \left(u_a e^{i\xi_a} + \rho_{a+2} + i\eta_{a+2} \right) \ , \ a = 1, 2 \, , \tag{A.1}$$

where v_a and u_a are the VEVs of the Φ_a neutral component and of S_a, respectively. In the present case, only the phase difference $\theta = \theta_2 - \theta_1$ is relevant. The above fields transform under the Abelian symmetries as shown in Table 3.5. The most general potential invariant under those symmetries can be written as,

$$V_{\mathrm{U}(1)} = V_{\Phi\Phi} + V_{\Phi S} + V_{SS}, \tag{A.2}$$

with

$$\begin{aligned} V_{\Phi\Phi} &= \mu_{11}^2 \Phi_1^\dagger \Phi_1 + \mu_{22}^2 \Phi_2^\dagger \Phi_2 + \frac{\lambda_1}{2} \left(\Phi_1^\dagger \Phi_1 \right)^2 + \frac{\lambda_2}{2} \left(\Phi_2^\dagger \Phi_2 \right)^2 \\ &\quad + \lambda_3 \left(\Phi_1^\dagger \Phi_1 \right) \left(\Phi_2^\dagger \Phi_2 \right) + \lambda_4 \left(\Phi_1^\dagger \Phi_2 \right) \left(\Phi_2^\dagger \Phi_1 \right) , \\ V_{\Phi S} &= \left(\lambda_5 \Phi_1^\dagger \Phi_1 + \lambda_6 \Phi_2^\dagger \Phi_2 \right) |S_1|^2 + \left(\lambda_9 \Phi_1^\dagger \Phi_1 + \lambda_{10} \Phi_2^\dagger \Phi_2 \right) |S_2|^2 , \\ V_{SS} &= \mu_1^2 |S_1|^2 + \mu_2^2 |S_2|^2 + \frac{\lambda_7}{2} |S_1|^4 + \frac{\lambda_8}{2} |S_2|^4 + \lambda_{11} |S_1|^2 |S_2|^2 \ . \end{aligned} \tag{A.3}$$

For reasons that will become clear later, we consider all parameters to be real. To avoid massless Goldstone bosons, we add terms to the scalar potential, which break softly the Abelian flavour symmetries. Such terms could, for instance, originate from the spontaneous breaking of a larger symmetry at very high-energies. Possible soft-breaking terms are

$$V_{\mathrm{soft}}(\Phi_a, S_a) = \mu_{12}^2 \ \Phi_1^\dagger \Phi_2 + \mu_3^2 \ S_1^2 + \mu_4 \, |S_1|^2 \, S_1 + \mu_5 \ |S_2|^2 \, S_2 + \mathrm{H.c.} \, , \tag{A.4}$$

with all parameters real. This specific form of V_{soft} is chosen not only to avoid unwanted massless scalars, but also to open up the possibility for SCPV coming from the complex VEV of the scalar singlet S_1, as will be discussed later. The full scalar potential is then given by $V(\Phi_a, S_a) = V_{\text{U(1)}} + V_{\text{soft}}$.

As argued in Section 3.2.2, one of the motivations for adding two complex singlet scalars is to account for the mass hierarchy in the inverse-seesaw approximation through $u_1, v_1, v_2 \ll u_2$. In order to simplify the analysis, we will use that VEV hierarchy to consider the case in which S_2 is decoupled from the remaining scalars and, thus, the quartic term $\sim |S_2|^4$ will dominate over the terms $\sim \Phi_a^\dagger \Phi_a |S_2|^2$ and $\sim |S_1|^2 |S_2|^2$. The analysis is then simplified by taking

$$V_{\Phi S} \simeq \left(\lambda_5 \Phi_1^\dagger \Phi_1 + \lambda_6 \Phi_2^\dagger \Phi_2\right) |S_1|^2 \,, \; V_{SS} \simeq \mu_1^2 |S_1|^2 + \mu_2^2 |S_2|^2 + \frac{\lambda_7}{2} |S_1|^4 + \frac{\lambda_8}{2} |S_2|^4 \,. \tag{A.5}$$

In order to ensure vacuum stability, the scalar potential has to be bounded from below in any direction of the field space as the fields become large. This can be guaranteed by requiring the Hessian matrix of the quartic couplings in the potential to be copositive [196]. In the case under analysis, this is translated into the following conditions among λ_{1-8} [197]:

$$\begin{aligned}
&\lambda_1, \lambda_2, \lambda_7, \lambda_8 > 0 \,, \\
&\lambda_3 + \sqrt{\lambda_1 \lambda_2} > 0 \,, \; \lambda_3 + \lambda_4 + \sqrt{\lambda_1 \lambda_2} > 0 \,, \\
&\lambda_5 + \sqrt{\lambda_1 \lambda_7} > 0 \,, \; \lambda_6 + \sqrt{\lambda_2 \lambda_7} > 0, \\
&\lambda_3 \lambda_7 - \lambda_5 \lambda_6 + \sqrt{\left(\lambda_1 \lambda_7 - \lambda_5^2\right)\left(\lambda_2 \lambda_7 - \lambda_6^2\right)} > 0 \,, \\
&\left(\lambda_3 + \lambda_4\right) \lambda_7 - \lambda_5 \lambda_6 + \sqrt{\left(\lambda_1 \lambda_7 - \lambda_5^2\right)\left(\lambda_2 \lambda_7 - \lambda_6^2\right)} > 0 \,.
\end{aligned} \tag{A.6}$$

A.2 Spontaneous CP violation

Since we considered all Yukawa and scalar parameters to be real, the full Lagrangian is CP-conserving. Yet, CP can be spontaneously broken if some scalar field acquires a complex VEV. The main motivation for studying this possibility is to provide a dynamical explanation of CPV in the lepton sector manifested through non-trivial Dirac and Majorana phases δ and α, respectively (see Section 4.1). To show that this is indeed possible, we start by minimising

$$\begin{aligned}
V_0 = \; & \frac{\lambda_1}{8} v_1^4 + \frac{\lambda_2}{8} v_2^4 + \frac{\lambda_3}{4} v_1^2 v_2^2 + \frac{\lambda_4}{4} v_1^2 v_2^2 + \frac{\lambda_5}{4} u_1^2 v_1^2 + \frac{\lambda_6}{4} u_1^2 v_2^2 + \frac{\lambda_7}{8} u_1^4 + \frac{\lambda_8}{8} u_2^4 + \frac{\mu_{11}^2}{2} v_1^2 + \frac{\mu_{22}^2}{2} v_2^2 \\
& + \frac{\mu_1^2}{2} u_1^2 + \frac{\mu_2^2}{2} u_2^2 + \mu_{12}^2 v_1 v_2 \cos\theta + \frac{\mu_5}{\sqrt{2}} u_2^3 \cos\xi_2 + \frac{\mu_4}{\sqrt{2}} u_1^3 \cos\xi_1 + \mu_3^2 u_1^2 \cos\left(2\xi_1\right) ,
\end{aligned} \tag{A.7}$$

with respect to v_a, u_a, θ, ξ_1 and ξ_2. In particular, the extrema conditions for θ and ξ_2 lead to $\theta, \xi_2 = 0, \pi$. Two possible solutions for μ_{11}^2, μ_{22}^2 and μ_2^2 can be then obtained from the minimisation equations of $v_{1,2}$

and u_2, respectively. Namely,

$$\begin{aligned}
\theta = 0, \pi: \ \mu_{11}^2 &= -\frac{1}{2}\left[\lambda_1 v_1^2 + (\lambda_3+\lambda_4)\, v_2^2 + \lambda_5 u_1^2\right] \mp \frac{v_2}{v_1}\mu_{12}^2, \\
\mu_{22}^2 &= -\frac{1}{2}\left[\lambda_1 v_2^2 + (\lambda_3+\lambda_4)\, v_1^2 + \lambda_6 u_1^2\right] \mp \frac{v_1}{v_2}\mu_{12}^2\,, \\
\xi_2 = 0, \pi: \ \mu_2^2 &= -\frac{u_2}{2}\Big(\lambda_8 u_2 \pm 3\sqrt{2}\mu_5\Big)\,.
\end{aligned} \tag{A.8}$$

Instead, minimising with respect to ξ_1 leads to three solutions:

$$\begin{aligned}
\xi_1 = 0, \pi: \quad \mu_1^2 &= -\frac{1}{2}\left(\lambda_5 v_1^2 + \lambda_6 v_2^2 + \lambda_7 u_1^2 + 4\mu_3^2 \pm 3\sqrt{2}\mu_4 u_1\right), \\
\xi_1 = \arctan\left(\frac{\sqrt{32\mu_3^4 - \mu_4^2 u_1^2}}{\mu_4 u_1}\right): \quad \mu_1^2 &= \frac{\mu_4^2 u_1^2}{4\mu_3^2} - \frac{1}{2}\left(\lambda_5 v_1^2 + \lambda_6 v_2^2 + \lambda_7 u_1^2 - 4\mu_3^2\right)\,.
\end{aligned} \tag{A.9}$$

Notice that the last solution in (A.9) is the only one which provides a non-trivial phase ξ_1, leading to the possibility for SCPV. Setting $\theta, \xi_2 = 0, \pi$ in V_0, the value of the potential at each ξ_1 minimum ($V_{\rm min}$) is

$$\begin{aligned}
\xi_1 = 0, \pi: \quad V_{\rm min} &= \mp\frac{\mu_4 u_1^3}{2\sqrt{2}} - V', \\
\xi_1 = \arctan\left(\frac{\sqrt{32\mu_3^4 - \mu_4^2 u_1^2}}{\mu_4 u_1}\right): \quad V_{\rm min} &= \frac{\mu_4^2 u_1^4}{16\mu_3^2} - V',
\end{aligned} \tag{A.10}$$

with

$$V' = \frac{\lambda_1}{8}v_1^4 + \frac{\lambda_2}{8}v_2^4 + \frac{\lambda_3}{4}v_1^2 v_2^2 + \frac{\lambda_4}{4}v_1^2 v_2^2 + \frac{\lambda_5}{4}u_1^2 v_1^2 + \frac{\lambda_6}{4}u_1^2 v_2^2 + \frac{\lambda_7}{8}u_1^4 + \frac{\lambda_8}{8}u_2^4 \pm \frac{\mu_5}{2\sqrt{2}}u_2^3. \tag{A.11}$$

Therefore, the CPV solution with $\xi_1 \neq 0, \pi$ corresponds to the deepest minimum if $\mu_4 u_1 < \mp 4\sqrt{2}\,\mu_3^2$.

A.3 Scalar mass spectrum

We now briefly discuss the main features of the scalar mass spectrum of our model. In total we have two charged complex scalar fields $\phi_{1,2}^+$ and four neutral ones, $\phi_{1,2}^0$ and $S_{1,2}$. The mass matrix for the charged scalars is

$$\mathbf{M}_+^2 = -\frac{v_1 v_2 \lambda_4 \pm 2\mu_{12}^2}{2}\begin{pmatrix} \dfrac{v_2}{v_1} & \mp 1 \\ \mp 1 & \dfrac{v_1}{v_2} \end{pmatrix}, \tag{A.12}$$

where the upper (lower) sign corresponds to $\theta = 0\,(\pi)$. This matrix is diagonalised via the basis transformation

$$\mathbf{R} = \begin{pmatrix} c_\beta & \pm s_\beta \\ -s_\beta & \pm c_\beta \end{pmatrix} \to \begin{pmatrix} H_1 \\ H_2 \end{pmatrix} = \mathbf{R}\begin{pmatrix} \Phi_1 \\ \Phi_2 \end{pmatrix}, \tag{A.13}$$

with

$$c_\beta = \cos\beta = \frac{v_1}{v}, \quad s_\beta = \sin\beta = \frac{v_2}{v}, \tag{A.14}$$

where $v = \sqrt{v_1^2 + v_2^2} \simeq 246$ GeV. This leads to the SM massless Goldstone boson $G^\pm$ and massive charged states $H^\pm$ with mass

$$m_{H^\pm}^2 = -v^2 \frac{\lambda_4}{2} \mp \frac{2\mu_{12}^2}{\sin(2\beta)}. \tag{A.15}$$

The above rotation brings $\Phi_{1,2}$ into the Higgs basis with $H_{1,2}$ [74] given by

$$H_1 = \frac{1}{\sqrt{2}} \begin{pmatrix} \sqrt{2}G^+ \\ v + H^0 + iG^0 \end{pmatrix}, \quad H_2 = \frac{1}{\sqrt{2}} \begin{pmatrix} \sqrt{2}H^+ \\ R + iI \end{pmatrix}, \tag{A.16}$$

where $\langle H_1^0 \rangle = v/\sqrt{2}$, $\langle H_2^0 \rangle = 0$. Here, H^0 coincides with the 125 GeV SM Higgs in the alignment limit, $G^\pm$ and G^0 are the charged and neutral Goldstone bosons, and $H^\pm$ is the physical charged Higgs field. The neutral scalar mass matrix $\mathbf{M}_0^2$ is diagonalised through a unitary transformation $\mathbf{T}$ which relates weak and mass eigenstates through

$$\left(G^0, S_1^0, ..., S_7^0\right)^T = \mathbf{T} \left(\rho_1, \rho_2, \rho_3, \rho_4, \eta_1, \eta_2, \eta_3, \eta_4\right)^T. \tag{A.17}$$

As mentioned before, we assume that the mixing of the complex singlet S_2 with the remaining fields is negligible and, thus, η_4 and ρ_4 are decoupled. Furthermore, the CP-odd scalars $\eta_{1,2}$ from $\phi_{1,2}^0$ also do not mix with the other scalars. However, $\rho_{1,2,3}$ and η_3 do mix among themselves. For the SCPV solution in Eq. (A.9), the mixing among η_3, ρ_3 and $\rho_{1,2}$ will depend on the soft-breaking parameters $\mu_{3,4}$ and on VEV products u_1^2 and $u_1 v_a$ ($a = 1, 2$). Moreover, since the naturally small soft-breaking parameters must fulfil the SCPV condition $\mu_4 u_1 < \mp 4\sqrt{2}\,\mu_3^2$, and given that $u_1 \lesssim v_1, v_2$, it is reasonable to consider that the mixing among the $\phi_{1,2}^0$ and S_1 will be small. In this limit, the neutral mass matrix can be recast into a block-diagonal form composed of four 2×2 matrices: the CP-even $\mathbf{M}_{\text{CP-even}}^2$ for $\rho_{1,2}$, the CP-odd $\mathbf{M}_{\text{CP-odd}}^2$ for $\eta_{1,2}$, and the $S_{1,2}$ mass matrices $\mathbf{M}_{S_1}^2$ and $\mathbf{M}_{S_2}^2$. The former is given by

$$\mathbf{M}_{\text{CP-even}}^2 = \begin{pmatrix} v_1^2\lambda_1 \mp \dfrac{v_2\mu_{12}^2}{v_1} & \pm v_1 v_2 \left(\lambda_3 + \lambda_4\right) + \mu_{12}^2 \\ \pm v_1 v_2 \left(\lambda_3 + \lambda_4\right) + \mu_{12}^2 & v_2^2\lambda_2 \mp \dfrac{v_1\mu_{12}^2}{v_2} \end{pmatrix}, \tag{A.18}$$

being diagonalised by

$$\begin{pmatrix} S_1^0 \\ S_2^0 \end{pmatrix} = \begin{pmatrix} c_{\alpha_1-\beta} & s_{\alpha_1-\beta} \\ -s_{\alpha_1-\beta} & c_{\alpha_1-\beta} \end{pmatrix} \begin{pmatrix} H^0 \\ R \end{pmatrix}, \; \tan\left(2\alpha_1\right) = \frac{\pm v^2 \left(\lambda_3 + \lambda_4\right) \sin(2\beta) + 2\mu_{12}^2}{v^2(\lambda_1 c_\beta^2 - \lambda_2 s_\beta^2) \pm 2\mu_{12}^2 \tan(2\beta)}, \tag{A.19}$$

where, as before, the upper (lower) sign corresponds to $\theta = 0\,(\pi)$. The angle α_1 parameterises the mixing in the (ρ_1, ρ_2) sector. Throughout this work we set $\beta = \alpha_1 + \pi/2$, which is known as the alignment limit [198]. In this case, there is no mixing between H^0 and R and, thus, $S_1^0 = H^0$ and $S_2^0 = R$. As already mentioned, this allows us to identify H^0 with the 125 GeV Higgs boson discovered at the LHC [4].

For the CP-odd scalars we have

$$\mathbf{M}^2_{\text{CP-odd}} = \mu_{12}^2 \begin{pmatrix} \mp\dfrac{v_2}{v_1} & 1 \\ 1 & \mp\dfrac{v_1}{v_2} \end{pmatrix}, \tag{A.20}$$

which is diagonalised through the rotation matrix defined in Eq. (A.13), leading to the massless Goldstone boson G^0 and to the massive scalar $S_5^0 = I$ with mass

$$m_I^2 = m_{H^\pm}^2 + v^2 \frac{\lambda_4}{2} = \mp \frac{2\mu_{12}^2}{\sin(2\beta)}. \tag{A.21}$$

The S_1 mass matrix is

$$\mathbf{M}^2_{S_1} = \begin{pmatrix} \dfrac{u_1^2\mu_4^2}{32\mu_3^4}\left(u_1^2\lambda_7 - 16\mu_3^2\right) + 4\mu_3^2 & \dfrac{u_1\mu_4}{32\mu_3^4}\sqrt{32\mu_3^4 - \mu_4^2u_1^2}\left(u_1^2\lambda_7 - 8\mu_3^2\right) \\ \dfrac{u_1\mu_4}{32\mu_3^4}\sqrt{32\mu_3^4 - \mu_4^2u_1^2}\left(u_1^2\lambda_7 - 8\mu_3^2\right) & u_1^2\lambda_7\left(1 - \dfrac{u_1^2\mu_4^2}{32\mu_3^4}\right) \end{pmatrix}, \tag{A.22}$$

which is diagonalised by a rotation with an angle α_2 given by,

$$\tan(2\alpha_2) = \frac{u_1\mu_4\sqrt{32\mu_3^4 - \mu_4^2u_1^2}\left(u_1^2\lambda_7 - 8\mu_3^2\right)}{16\mu_3^4\left(4\mu_3^2 - u_1^2\lambda_7\right) + u_1^2\mu_4^2\left(u_1^2\lambda_7 - 8\mu_3^2\right)}. \tag{A.23}$$

After diagonalising the mass matrix $\mathbf{M}^2_{S_1}$ there remains a very small mixing in the (ρ_3, η_3) sector, which depends on the soft-breaking couplings. The mass terms for the resulting physical fields, $S_3^0 \simeq \rho_3$ and $S_6^0 \simeq \eta_3$, are given by

$$\xi_1 = \arctan\left(\frac{\sqrt{32\mu_3^4 - \mu_4^2u_1^2}}{\mu_4 u_1}\right),\ m^2_{S_3^0} \simeq m^2_{S_6^0} \simeq 2\mu_3^2 - \frac{u_1^2\left(\mu_4^2 - 2\lambda_7\mu_3^2\right)}{4\mu_3^2}, \tag{A.24}$$

which are approximately degenerate for the SCPV solution. Notice that in the absence of soft-breaking terms proportional to μ_3 and μ_4, unwanted massless Goldstone bosons appear. SCPV originated from the complex VEV of the singlet S_1 is possible if the masses above are positive and the condition for the global minimum is satisfied. Lastly, the matrix $\mathbf{M}^2_{S_2}$ is diagonal and the corresponding scalar masses for $S_4^0 = \rho_4$ and $S_7^0 = \eta_4$ are

$$m^2_{\eta_4} = \mp\frac{\mu_5 u_2}{\sqrt{2}},\ m^2_{\rho_4} = u_2^2\left(\lambda_8 \pm \frac{3\mu_5}{\sqrt{2}u_2}\right), \tag{A.25}$$

for ξ_2 equal 0 or π, respectively. Once again, if the soft-breaking term proportional to μ_5 vanishes, η_4 would be a massless Goldstone boson. Since u_2 can be naturally large, the scalar fields η_4 and ρ_4 can have a large mass, which further justifies the decoupling behaviour of the singlet S_2.

Appendix B

Interactions in the mass-eigenstate basis

In this appendix we collect the interactions relevant for our work in the mass-eigenstate basis of fermions, scalars and gauge bosons. We consider an arbitrary number of Majorana neutrinos ν_i ($i = 1, \ldots, n_f$) with masses m_i, so that the results can be applied for scenarios with any number of sterile neutrinos. In the ISS(2,2) considered in this work $n_f = 7$, being $\nu_{1,2,3}$ the three light active neutrinos, and ν_{4-7} the heavy sterile ones.

B.1 Charged-current and neutral-current interactions

In the Feynman-'t Hooft gauge and mass-eigenstate basis, the charged-current, weak neutral-current and Goldstone-boson interactions read:

$$\mathcal{L}_{W^\pm} = \frac{g}{\sqrt{2}} W_\mu^- \sum_{\alpha=1}^{3} \sum_{j=1}^{n_f} \mathbf{B}_{\alpha j}\, \overline{e_\alpha} \gamma^\mu P_L \nu_j + \text{H.c.}, \tag{B.1}$$

$$\mathcal{L}_Z = \frac{g}{2c_W} Z_\mu \sum_{i,j=1}^{n_f} \boldsymbol{\mathcal{C}}_{ij}\, \overline{\nu_i} \gamma^\mu P_L \nu_j = \frac{g}{4c_W} Z_\mu \sum_{i,j=1}^{n_f} \overline{\nu_i} \gamma^\mu \left(\boldsymbol{\mathcal{C}}_{ij} P_L - \boldsymbol{\mathcal{C}}_{ij}^* P_R \right) \nu_j, \tag{B.2}$$

$$\mathcal{L}_{G^\pm} = -\frac{g}{\sqrt{2} M_W} G^- \sum_{\alpha=1}^{3} \sum_{j=1}^{n_f} \mathbf{B}_{\alpha j}\, \overline{e_\alpha} \left(m_\alpha P_L - m_j P_R \right) \nu_j + \text{H.c.}, \tag{B.3}$$

$$\begin{aligned} \mathcal{L}_{G^0} &= -\frac{ig}{2M_W} G^0 \sum_{i,j=1}^{n_f} \boldsymbol{\mathcal{C}}_{ij} \overline{\nu_i} \left(P_L m_i - P_R m_j \right) \nu_j \\ &= -\frac{ig}{4M_W} G^0 \sum_{i,j=1}^{n_f} \overline{\nu_i} \left[\boldsymbol{\mathcal{C}}_{ij} \left(P_L m_i - P_R m_j \right) - \boldsymbol{\mathcal{C}}_{ij}^* \left(P_R m_i - P_L m_j \right) \right] \nu_j, \end{aligned} \tag{B.4}$$

where we have followed closely the notation of Refs. [127, 199]. The $\mathbf{B}$ and $\boldsymbol{\mathcal{C}}$ matrices have been defined in Eq. (3.20). The last equalities in Eqs. (B.2) and (B.4) result from the Majorana character of neutrinos ($\nu = \nu^c$). Therefore, for Majorana neutrinos, the coupling $Z\, \overline{\nu_i}\, \nu_j$ is non-diagonal and involves both chiralities.

B.2 Scalar-fermion interactions

In this section we present the scalar-fermion interactions extracted from the Yukawa Lagrangian in Eq. (3.35), using the notation for the scalar fields introduced in Section A.3. For charged and neutral scalars $S_a^{\pm}$ and S_a^0 we have:

$$\begin{aligned}\mathcal{L}_{S_a^{\pm}} = S_a^- \Bigg\{ & \sum_{\alpha=1}^{3}\sum_{j=1}^{n_f} \overline{e_\alpha}\left[\left(\mathbf{\Gamma}_e^a\right)_{\alpha j} P_L - \left(\mathbf{\Gamma}_\nu^a\right)_{\alpha j} P_R\right]\nu_j \\ & + \sum_{\substack{u_i=u,c,t \\ d_i=d,s,b}} \overline{d_i}\left[\left(\mathbf{\Gamma}_d^a\right)_{d_i u_j} P_L - \left(\mathbf{\Gamma}_u^a\right)_{d_i u_j} P_R\right] u_j \Bigg\} + \text{H.c.},\end{aligned} \tag{B.5}$$

$$\mathcal{L}_{S_a^0} = S_a^0 \left[\sum_{\alpha,\beta=1}^{3} \overline{e_\alpha}\left(\mathbf{\Delta}_e^a\right)_{\alpha\beta} P_R e_\beta + \sum_{i,j=1}^{n_f} \overline{\nu_i}\left(\mathbf{\Delta}_\nu^a\right)_{ij} P_R \nu_j\right] + \text{H.c.}, \tag{B.6}$$

respectively, where $\mathbf{\Gamma}$ and $\mathbf{\Delta}$ are general Yukawa matrices. In this work, the scalar sector contains two Higgs doublets and two neutral scalar singlets, which we will consider to obey the alignment and decoupling limits discussed in Appendix A. In such case, the Yukawa coupling matrices between the fermions and the charged Higgs $S_1^{\pm} = H^{\pm}$ are given by

$$\begin{aligned}\mathbf{\Gamma}_e^1 &= \frac{g}{\sqrt{2}M_W}\mathbf{N}_e^\dagger \mathbf{B}\ ,\ \mathbf{\Gamma}_\nu = \frac{g}{\sqrt{2}M_W}\mathbf{B}\mathbf{N}_\nu\ , \\ \mathbf{\Gamma}_d^1 &= \frac{g}{\sqrt{2}M_W}\mathbf{N}_d^\dagger \mathbf{V}^\dagger\ ,\ \mathbf{\Gamma}_u^1 = \frac{g}{\sqrt{2}M_W}\mathbf{V}^\dagger \mathbf{N}_u\,,\end{aligned} \tag{B.7}$$

where $\mathbf{B}$ is defined in Eq. (3.20) and

$$\mathbf{N}_e = \mathbf{V}_L^\dagger \mathbf{N}_e^0 \mathbf{V}_R,\ \mathbf{N}_e^0 = \frac{v}{\sqrt{2}}\left(s_\beta \mathbf{Y}_\ell^1 - c_\beta \mathbf{Y}_\ell^2 e^{i\theta}\right), \tag{B.8}$$

$$(\mathbf{N}_\nu)_{ij} = \sum_{\alpha=1}^{3}\sum_{k=4}^{3+n_R} \boldsymbol{\mathcal{U}}_{\alpha i}^*\left(\mathbf{N}_\nu^0\right)_{\alpha k}\boldsymbol{\mathcal{U}}_{kj}^*,\ \mathbf{N}_\nu^0 = \frac{v}{\sqrt{2}}\left(s_\beta \mathbf{Y}_D^1 - c_\beta \mathbf{Y}_D^2 e^{-i\theta}\right), \tag{B.9}$$

$$\mathbf{N}_d = \mathbf{V}_L^{d\dagger} \mathbf{N}_d^0 \mathbf{V}_R^d,\ \mathbf{N}_d^0 = \frac{v}{\sqrt{2}}\left(s_\beta \mathbf{Y}_d^1 - c_\beta \mathbf{Y}_d^2 e^{i\theta}\right), \tag{B.10}$$

$$\mathbf{N}_u = \mathbf{V}_L^{u\dagger} \mathbf{N}_u^0 \mathbf{V}_R^u,\ \mathbf{N}_u^0 = \frac{v}{\sqrt{2}}\left(s_\beta \mathbf{Y}_u^1 - c_\beta \mathbf{Y}_u^2 e^{-i\theta}\right). \tag{B.11}$$

where the unitary matrices $\mathbf{V}_{L,R}$, $\mathbf{V}_{L,R}^{d,u}$ and $\boldsymbol{\mathcal{U}}$ are respectively defined in Eqs. (2.24) and (3.6). Additionally, the quark mixing matrix $\mathbf{V}$ is defined in Eq. (2.25). We explicitly present the interaction Lagrangian involving the $H^{\pm}$ charged scalar since it has been extensively used, for instance, in the computation of the cLFV amplitudes (see Appendices C and D). Namely,

$$\begin{aligned}\mathcal{L}_{H^{\pm}} = -\frac{g}{\sqrt{2}M_W}\Bigg\{ & \sum_{\alpha,\beta=1}^{3}\sum_{i,j=1}^{n_f} \overline{e_\alpha}\left[\left(\mathbf{B}\mathbf{N}_\nu\right)_{\alpha j} P_R - \left(\mathbf{N}_e^\dagger \mathbf{B}\right)_{\alpha j} P_L\right]\nu_j \\ & + \sum_{\substack{u_i=u,c,t \\ d_i=d,s,b}} \overline{d_i}\left[\left(\mathbf{V}^\dagger \mathbf{N}_u\right)_{d_i u_j} P_R - \left(\mathbf{N}_d^\dagger \mathbf{V}^\dagger\right)_{d_i u_j} P_L\right] u_j \Bigg\} H^- + \text{H.c.}.\end{aligned} \tag{B.12}$$

The Yukawa matrices entering the interaction terms (B.6) among leptons and the the neutral scalars $S_1^0 = H^0$, $S_2^0 = R$ and $S_5^0 = I$ (those stemming from the Higgs doublets) are

$$\begin{aligned}
&\left(\mathbf{\Delta}_e^1\right)_{\alpha\beta} = -\frac{g}{2M_W}\delta_{\alpha\beta}m_\alpha \ , \ \left(\mathbf{\Delta}_\nu^1\right)_{ij} = -\frac{g}{4M_W}\left(\boldsymbol{\mathcal{C}}_{ij}m_j + \boldsymbol{\mathcal{C}}_{ij}^* m_i\right), \\
&\left(\mathbf{\Delta}_e^2\right)_{\alpha\beta} = \frac{g}{2M_W}(\mathbf{N}_e)_{\alpha\beta} = -i\left(\mathbf{\Delta}_e^5\right)_{\alpha\beta} \ , \ \left(\mathbf{\Delta}_\nu^2\right)_{ij} = \frac{g}{4M_W}\left[(\mathbf{N}_\nu)_{ij} + \left(\mathbf{N}_\nu^T\right)_{ij}\right] = i\left(\mathbf{\Delta}_\nu^5\right)_{ij},
\end{aligned} \tag{B.13}$$

where the matrix $\boldsymbol{\mathcal{C}}$ is defined in Eq. (3.20). We explicitly present the Lagrangians involving the above neutral scalars and ν_i since they were useful in our calculations of the radiative corrections to light neutrino masses performed in Section 4.2. We have,

$$\begin{aligned}
\mathcal{L}_{H^0} &= -\frac{g}{2M_W}H^0\sum_{i,j=1}^{n_f}\boldsymbol{\mathcal{C}}_{ij}\overline{\nu_i}\left(P_L m_i + P_R m_j\right)\nu_j \\
&= -\frac{g}{4M_W}H^0\sum_{i,j=1}^{n_f}\overline{\nu_i}\left[\boldsymbol{\mathcal{C}}_{ij}\left(P_L m_i + P_R m_j\right) + \boldsymbol{\mathcal{C}}_{ij}^*\left(P_R m_i + P_L m_j\right)\right]\nu_j,
\end{aligned} \tag{B.14}$$

$$\mathcal{L}_R = \frac{g}{4M_W}R\sum_{i,j=1}^{n_f}\overline{\nu_i}\left\{\left[(\mathbf{N}_\nu)_{ij} + \left(\mathbf{N}_\nu^T\right)_{ij}\right]P_R + \left[\left(\mathbf{N}_\nu^\dagger\right)_{ij} + (\mathbf{N}_\nu^*)_{ij}\right]P_L\right\}\nu_j, \tag{B.15}$$

$$\mathcal{L}_I = -\frac{ig}{4M_W}I\sum_{i,j=1}^{n_f}\overline{\nu_i}\left\{\left[(\mathbf{N}_\nu)_{ij} + \left(\mathbf{N}_\nu^T\right)_{ij}\right]P_R - \left[\left(\mathbf{N}_\nu^\dagger\right)_{ij} + (\mathbf{N}_\nu^*)_{ij}\right]P_L\right\}\nu_j. \tag{B.16}$$

Lastly, the coupling matrices appearing in interaction terms between the neutrinos and the neutral scalars $S_3^0 \simeq \rho_3$, $S_6^0 \simeq \eta_3$, $S_4^0 = \rho_4$ and $S_7^0 = \eta_4$ (coming from the complex scalar singlets $S_{1,2}$) are,

$$\begin{aligned}
&\left(\mathbf{\Delta}_\nu^3\right)_{ij} = -\frac{1}{4u_1}\left[\left(\tilde{\mathbf{N}}_s^\dagger\right)_{ij} + \left(\tilde{\mathbf{N}}_s^*\right)_{ij}\right], \ \left(\mathbf{\Delta}_\nu^6\right)_{ij} = \frac{i}{4u_1}\left[\left(\tilde{\mathbf{N}}_s^\dagger\right)_{ij} + \left(\tilde{\mathbf{N}}_s^*\right)_{ij}\right], \\
&\left(\mathbf{\Delta}_\nu^4\right)_{ij} = -\frac{1}{2u_2}\left[\left(\mathbf{N}_R^\dagger\right)_{ij} + (\mathbf{N}_R^*)_{ij}\right] \ , \ \left(\mathbf{\Delta}_\nu^7\right)_{ij} = \frac{i}{2u_2}\left[\left(\mathbf{N}_R^\dagger\right)_{ij} + (\mathbf{N}_R^*)_{ij}\right],
\end{aligned} \tag{B.17}$$

where

$$(\tilde{\mathbf{N}}_s)_{ij} = \sum_{k,l=4+n_R}^{n_f}\boldsymbol{\mathcal{U}}_{ki}\left(\tilde{\mathbf{N}}_s^0\right)_{kl}\boldsymbol{\mathcal{U}}_{lj} \ , \ \tilde{\mathbf{N}}_s^0 = \frac{u_1}{\sqrt{2}}\left(\mathbf{Y}_s^1 + \mathbf{Y}_s^2\right), \tag{B.18}$$

$$(\mathbf{N}_s)_{ij} = \sum_{k,l=4+n_R}^{n_f}\boldsymbol{\mathcal{U}}_{ki}\left(\mathbf{N}_s^0\right)_{kl}\boldsymbol{\mathcal{U}}_{lj} \ , \ \mathbf{N}_s^0 = \frac{u_1}{\sqrt{2}}\left(\mathbf{Y}_s^1 - \mathbf{Y}_s^2\right), \tag{B.19}$$

$$(\mathbf{N}_R)_{ij} = \sum_{k=4}^{3+n_R}\sum_{l=4+n_R}^{n_f}\boldsymbol{\mathcal{U}}_{ki}\left(\mathbf{N}_R^0\right)_{kl}\boldsymbol{\mathcal{U}}_{lj} \ , \ \mathbf{N}_R^0 = \frac{u_2}{\sqrt{2}}\mathbf{Y}_R. \tag{B.20}$$

Note that, in order to obtain the Feynman rules using the interactions between ν_i and the Z-boson or S^0 neutral scalars, one must multiply by a factor of 2 since Majorana neutrinos are self-conjugate fields.

Appendix C

Charged-lepton flavour violation

In this appendix we present the amplitudes and decay rates for the cLFV processes $\ell_\alpha \to \ell_\beta \gamma$, $Z \to \ell_\alpha^\pm \ell_\beta^\mp$, $\ell_\alpha^- \to \ell_\beta^- \ell_\gamma^+ \ell_\delta^-$ and coherent $\mu - e$ conversion in heavy nuclei. The corresponding current experimental bounds and future sensitivities are given in Table 4.2. We included in our calculations the $W^\pm$-boson and charged Higgs $H^\pm$ contributions. The one-loop Feynman diagrams are summarised in Figs. C.1, C.2 and C.3. Furthermore, the computations were performed in the Feynman-'t Hooft gauge following the interaction Lagrangians in the mass-eigenstate basis given in Appendix B. We provide the results for the amplitudes and branching ratios in terms of the form factors collected in Appendix D.

C.1 The radiative decay $\ell_\alpha \to \ell_\beta \gamma$

In Fig. C.1 we show the diagrams contributing to the effective vertex $\overline{\ell_\beta} \ell_\alpha \gamma$ ($\beta \neq \alpha$) at one-loop level. The transition amplitude can be written in the form

$$\mathcal{A}_\gamma^{\alpha\beta} = -\frac{e\,\alpha_W}{8\pi M_W^2} \varepsilon_\gamma^\mu \, \overline{\ell_\beta} \left[\left(q^2 \gamma_\mu - \not{q} q_\mu\right) \left(F_{\gamma,L}^{\alpha\beta} P_L + F_{\gamma,R}^{\alpha\beta} P_R \right) - i \sigma_{\mu\nu} q^\nu \left(G_{\gamma,L}^{\alpha\beta} P_L + G_{\gamma,R}^{\alpha\beta} P_R \right) \right] \ell_\alpha, \tag{C.1}$$

where $\alpha_W = g^2/(4\pi)$, ε_γ^μ is the photon polarisation four-vector and $q = p_\alpha - p_\beta$ is the photon momentum. F_γ is the local monopole contribution for an off-shell photon ($q^2 \neq 0$), while G_γ stands for the non-local dipole contribution for an on-shell photon ($q^2 = 0$). The expressions for $F_{\gamma,L(R)}^{\alpha\beta}$ and $G_{\gamma,L(R)}^{\alpha\beta}$ are given in Section D.2. The former contributes to $\ell_\alpha^- \to \ell_\beta^- \ell_\gamma^+ \ell_\delta^-$ and $\mu - e$ conversion in nuclei, while the latter encodes the only contribution to $\ell_\alpha \to \ell_\beta \gamma$. In particular, for this process one has

$$\text{BR}(\ell_\alpha^- \to \ell_\beta^- \gamma) = \frac{3\alpha_e}{2\pi m_\alpha^2} \left(\left| G_{\gamma,L}^{\alpha\beta} \right|^2 + \left| G_{\gamma,R}^{\alpha\beta} \right|^2 \right) \text{BR}\left(\ell_\alpha \to \ell_\beta \nu_\alpha \overline{\nu_\beta}\right), \tag{C.2}$$

where $\alpha_e = e^2/(4\pi)$ and the values of $\text{BR}\left(\ell_\alpha \to \ell_\beta \nu_\alpha \overline{\nu_\beta}\right)$ are given by [89]

$$\text{BR}\left(\mu \to e \nu_\mu \overline{\nu_e}\right) \simeq 1.0 \;,\; \text{BR}\left(\tau \to e \nu_\tau \overline{\nu_e}\right) \simeq 0.18 \;,\; \text{BR}\left(\tau \to \mu \nu_\tau \overline{\nu_\mu}\right) \simeq 0.17. \tag{C.3}$$

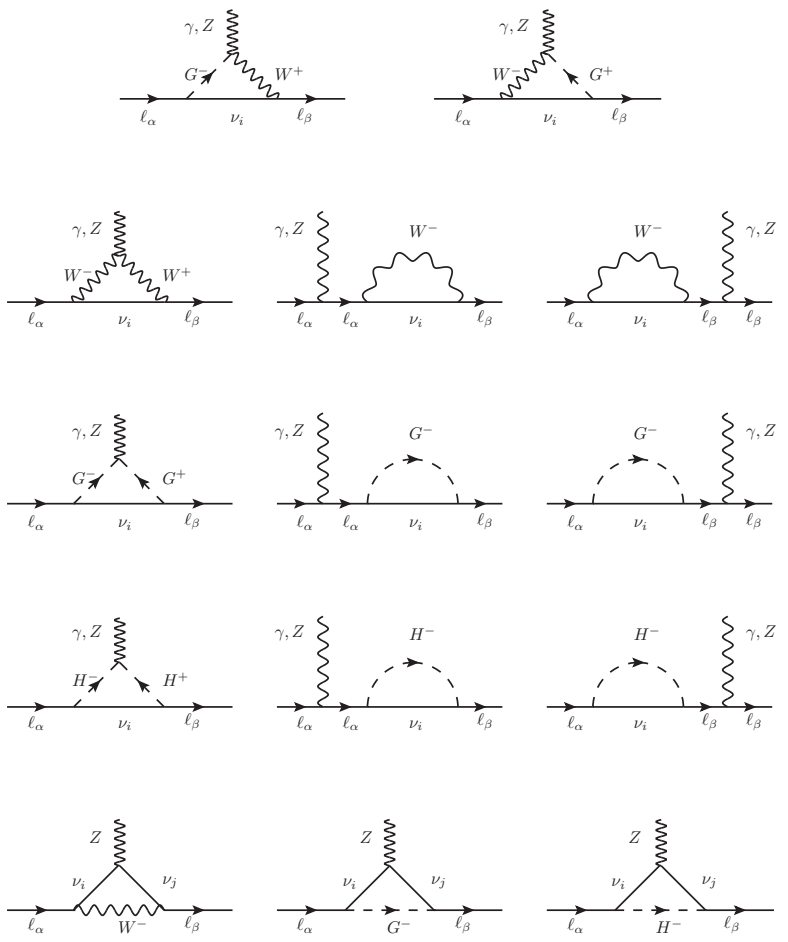

Figure C.1: The γ-penguin and Z-penguin diagrams that contribute to the effective vertices $\overline{\ell_\beta}\ell_\alpha\gamma$ and $\overline{\ell_\beta}\ell_\alpha Z$, respectively.

In the limit where there is no charged scalar contribution, the branching ratio given in Eq. (C.2) is consistent with the results of Refs. [19, 200–202].

C.2 The radiative decay $Z \to \ell_\alpha^\pm \ell_\beta^\mp$

The one-loop diagrams for the effective vertex $\overline{\ell_\beta}\ell_\alpha Z$ ($\beta \neq \alpha$) are also shown in Fig. C.1. In this case, the transition amplitude is

$$\mathcal{A}_Z^{\alpha\beta} = \frac{g\,\alpha_W}{8\pi c_W}\varepsilon_Z^\mu\ \overline{\ell_\beta}\left(F_{Z,L}^{\alpha\beta}\gamma_\mu P_L + F_{Z,R}^{\alpha\beta}\gamma_\mu P_R\right)\ell_\alpha, \tag{C.4}$$

where ε_Z^μ is the Z-boson polarisation four-vector. The branching ratio for the LFV decay $Z \to \ell_\alpha^-\ell_\beta^+ + \ell_\alpha^+\ell_\beta^-$ is

$$\mathrm{BR}(Z \to \ell_\alpha^-\ell_\beta^+ + \ell_\alpha^+\ell_\beta^-) = \frac{\alpha_W^3}{192\ \pi^2 c_W^2}\frac{M_Z}{\Gamma_Z}\left(\left|F_{Z,L}^{\alpha\beta}\right|^2 + \left|F_{Z,R}^{\alpha\beta}\right|^2\right), \tag{C.5}$$

where $F_{Z,L}^{\alpha\beta}$ and $F_{Z,R}^{\alpha\beta}$, are given in Section D.3 and the Z-boson total decay width is $\Gamma_Z = 2.4952$ GeV [89]. Note that, in the limit where the scalar content coincides with the SM one, the above branching ratio is consistent with the results of Refs. [203, 204].

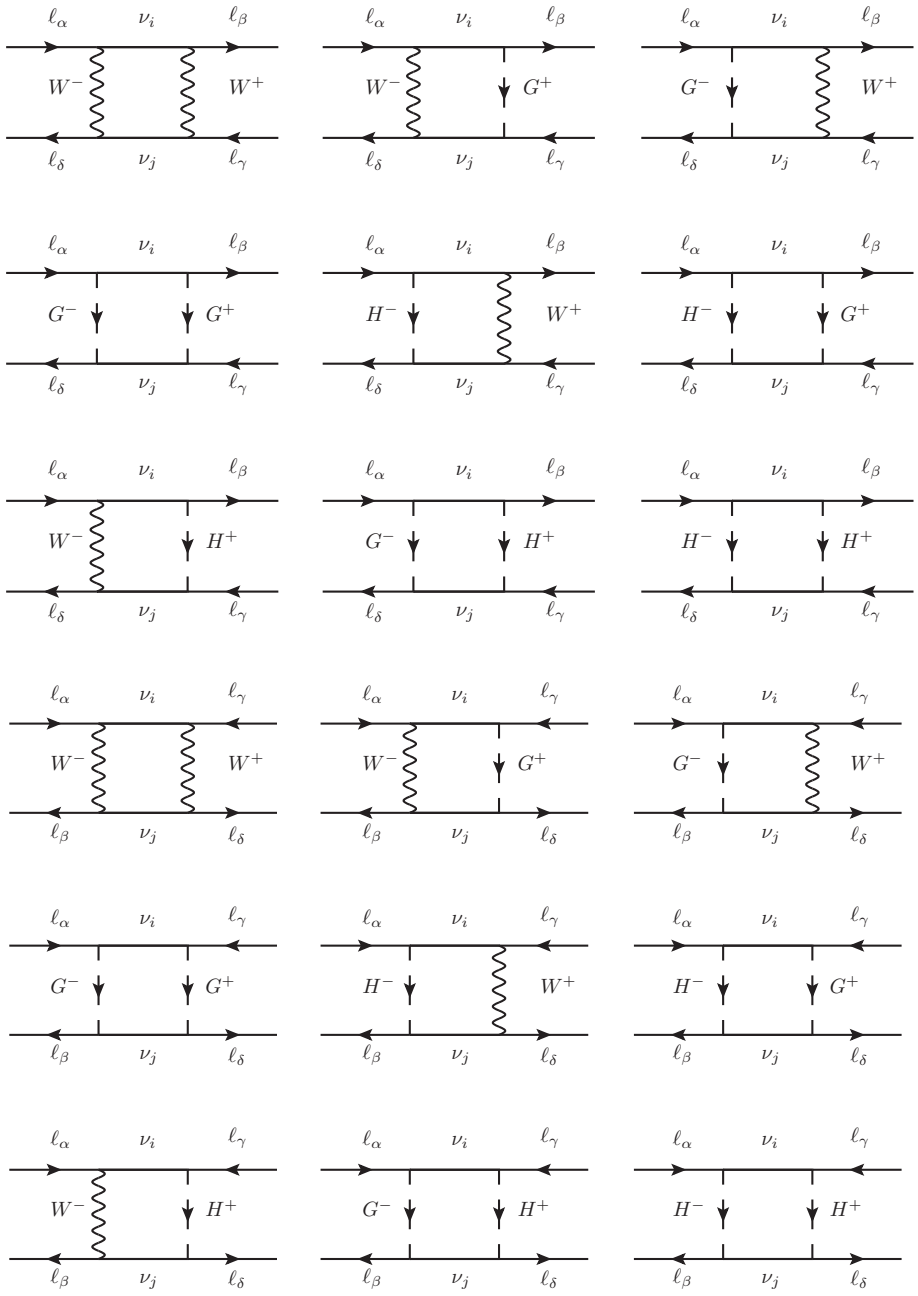

Figure C.2: Leptonic box diagrams contributing to the three-body decay $\ell_\alpha^- \to \ell_\beta^- \ell_\gamma^+ \ell_\delta^-$.

C.3 The three-body decay $\ell_\alpha^- \to \ell_\beta^- \ell_\gamma^+ \ell_\delta^-$

The $\ell_\alpha^- \to \ell_\beta^- \ell_\gamma^+ \ell_\delta^-$ amplitude receives contributions from the γ-penguin, Z-penguin and leptonic box diagrams shown in Figs. C.1 and C.2, which we write as

$$\begin{aligned}\mathcal{A}_\gamma^{\alpha\beta\gamma\delta} = &-\frac{\alpha_W^2 s_W^2}{2M_W^2}\,\Big\{\delta_{\gamma\delta}\,\overline{\ell_\beta}\Big[\left(F_{\gamma,L}^{\alpha\beta}\gamma_\mu P_L + F_{\gamma,R}^{\alpha\beta}\gamma_\mu P_R\right)\\ &- i\sigma_{\mu\nu}\frac{q^\nu}{q^2}\left(G_{\gamma,L}^{\alpha\beta}P_L + G_{\gamma,R}^{\alpha\beta}P_R\right)\Big]\ell_\alpha\,\overline{\ell_\delta}\gamma^\mu\ell_\gamma^c - (\beta\leftrightarrow\delta)\Big\}, \qquad \text{(C.6)}\\ \mathcal{A}_Z^{\alpha\beta\gamma\delta} = &\frac{\alpha_W^2}{2M_W^2}\left[\delta_{\gamma\delta}\,\overline{\ell_\beta}\left(F_{Z,L}^{\alpha\beta}\gamma_\mu P_L + F_{Z,R}^{\alpha\beta}\gamma_\mu P_R\right)\ell_\alpha\,\overline{\ell_\delta}\left(g_L^\ell\gamma^\mu P_L + g_R^\ell\gamma^\mu P_R\right)\ell_\gamma^c - (\beta\leftrightarrow\delta)\right], \qquad \text{(C.7)}\end{aligned}$$

$$\mathcal{A}_{\rm Box}^{\alpha\beta\gamma\delta} = -\frac{\alpha_W^2}{4M_W^2} \sum_{X,Y=L,R} \sum_{A=S,V,T} B_{A,XY}^{\alpha\beta\gamma\delta}\ \overline{\ell_\beta}\Lambda_A^X \ell_\alpha\ \overline{\ell_\delta}\Lambda_A^Y \ell_\gamma^c\,, \tag{C.8}$$

where the Z-boson charged-lepton couplings are $g_L^\ell = s_W^2 - 1/2$ and $g_R^\ell = s_W^2$ [see Table 2.1 and Eq. (2.15)]. The $\Lambda_A^{X,Y}$ are given by the following combinations of Dirac matrices and chiral projectors:

$$\left(\Lambda_S^L, \Lambda_S^R, \Lambda_V^L, \Lambda_V^R, \Lambda_T^L, \Lambda_T^R\right) \equiv \left(P_L, P_R, \gamma_\mu P_L, \gamma_\mu P_R, \sigma_{\mu\nu} P_L, \sigma_{\mu\nu} P_R\right), \tag{C.9}$$

with $\sigma_{\mu\nu} = i\left[\gamma_\mu, \gamma_\nu\right]/2$. From the generic leptonic box diagrams presented in Fig. C.2 we obtain the transition amplitude (C.8) involving the form factor $B_{A,XY}^{\alpha\beta\gamma\delta}$, written in terms of the spinorial structure $\overline{\ell_\beta}\Lambda_A^X\ell_\alpha\ \overline{\ell_\delta}\Lambda_A^Y\ell_\gamma^c$. Since we are in the presence of Majorana neutrinos, LNV diagrams must be also considered, together with cross-diagrams with interchanged lepton indices ($\beta \leftrightarrow \delta$). All these contributions can be written in the form (C.8) by using Fierz transformations [205, 206]. In Section D.5, the form factors $B_{A,XY}^{\alpha\beta\gamma\delta}$ are presented. In particular, $B_{T,LR}^{\alpha\beta\gamma\delta} = B_{T,RL}^{\alpha\beta\gamma\delta} = 0$, which can be readily seen from the identity $\sigma_{\mu\nu}\gamma_5 = -i\varepsilon_{\mu\nu\rho\lambda}\ \sigma^{\rho\lambda}/2$.

The calculation of the decay rate for each process is done, whenever possible, assuming vanishing masses for the final lepton states, since $m_{\beta,\gamma,\delta} \ll m_\alpha$. However, an exception is made for terms involving the photon amplitude, where light lepton masses must be treated with care. As well known, the three-body phase space integrals for the photon contribution are singular in the limit $q^2 \to 0$. Therefore, one must first perform the phase space integration and only after take the limit $m_{\beta,\gamma,\delta} \to 0$ for non-divergent terms. This will lead to the logarithmic term $\ln(m_\alpha^2/m_{\beta,\gamma,\delta}^2)$ appearing in the pure photonic dipole contributions. Also, a symmetry factor of 1/2 has to be taken into account in the case of two identical charged leptons in the final state. The branching ratio for the 3-body LFV decays can be written in the general form:

$$\begin{aligned}\frac{\mathrm{BR}(\ell_\alpha^- \to \ell_\beta^-\ell_\gamma^+\ell_\delta^-)}{\mathrm{BR}\left(\ell_\alpha \to \ell_\beta \nu_\alpha \overline{\nu_\beta}\right)} = \frac{k_1\alpha_W^2}{64\pi^2}\Big\{ & k_2\left|F_{V,LL}\right|^2 + \left|F_{V,LR}\right|^2 + \frac{1}{4}\Big(\left|F_{S,LL}\right|^2 + \left|F_{S,LR}\right|^2\Big) + 12\left|F_{T,LL}\right|^2 \\ & + k_3\frac{8s_W^2}{m_\alpha}\mathrm{Re}\left[\left(k_2 F_{V,LL} + F_{V,LR}\right)G_{\gamma,R}^*\right] \\ & + k_3\frac{32s_W^4}{m_\alpha^2}\left|G_{\gamma,L}\right|^2\left(\ln\frac{m_\alpha^2}{m_\delta^2} - k_4\right) + (L \leftrightarrow R)\Big\}\,,\end{aligned} \tag{C.10}$$

where the values for the branching ratios $\mathrm{BR}\left(\ell_\alpha \to \ell_\beta \nu_\alpha \overline{\nu_\beta}\right)$ are given in Eq. (C.3). The k_i coefficients and the form factors F depend on the charged-lepton final states, for which three combinations are possible. Namely,

(i) Two different flavours of leptons, where leptons with the same flavour have opposite charge ($\beta \neq \gamma \wedge \delta = \gamma$)

$$\begin{aligned}& k_1 = k_2 = k_3 = 1\ ,\ k_4 = 3\,, \\ & F_{V,LL} = B_{V,LL} - 2g_L^\ell F_{Z,L} + 2s_W^2 F_{\gamma,L}\ ,\ F_{V,LR} = B_{V,LR} - 2g_R^\ell F_{Z,L} + 2s_W^2 F_{\gamma,L}, \\ & F_{S,LL} = B_{S,LL}\ ,\ F_{S,LR} = B_{S,LR}\ ,\ F_{T,LL} = B_{T,LL};\end{aligned} \tag{C.11}$$

Nucleus ${}^{A}_{Z}$N	$Dm_\mu^{-5/2}$	$S^{(p)}m_\mu^{-5/2}$	$S^{(n)}m_\mu^{-5/2}$	$V^{(p)}m_\mu^{-5/2}$	$V^{(n)}m_\mu^{-5/2}$	$\Gamma_{\rm capt}$ $(10^6 s^{-1})$
${}^{27}_{13}$Al	0.0362	0.0155	0.0167	0.0161	0.0173	0.7054
${}^{48}_{22}$Ti	0.0864	0.0368	0.0435	0.0396	0.0468	2.59
${}^{197}_{79}$Au	0.189	0.0614	0.0918	0.0974	0.146	13.07
${}^{208}_{82}$Pb	0.161	0.0488	0.0749	0.0834	0.128	13.45

Table C.1: Nuclear form factors and muon capture rate for the $\mu - e$ conversion process [213].

(ii) Three leptons with the same flavour ($\beta = \gamma = \delta$)

$$\begin{aligned} &k_1 = k_3 = 1\ ,\ k_2 = 2\ ,\ k_4 = 11/4\,, \\ &F_{V,LL} = \frac{1}{2}B_{V,LL} - 2g_L^\ell F_{Z,L} + 2s_W^2 F_{\gamma,L}\ ,\ F_{V,LR} = B_{V,LR} - 2g_R^\ell F_{Z,L} + 2s_W^2 F_{\gamma,L}, \\ &F_{S,LL} = \frac{1}{\sqrt{2}}B_{S,LL}\ ,\ F_{S,LR} = 0\ ,\ F_{T,LL} = \frac{1}{\sqrt{2}}B_{T,LL}; \end{aligned} \tag{C.12}$$

(iii) Two distinct flavours, where leptons with same flavour have the same charge ($\delta \neq \gamma \wedge \beta \neq \gamma$)

$$\begin{aligned} &k_1 = 1/2\ ,\ k_2 = 1\ ,\ k_3 = k_4 = 0\,, \\ &F_{V,LL} = B_{V,LL}\ ,\ F_{V,LR} = B_{V,LR}\ ,\ F_{S,LL} = B_{S,LL}\ ,\ F_{S,LR} = B_{S,LR}\ ,\ F_{T,LL} = B_{T,LL}. \end{aligned} \tag{C.13}$$

Our results agree with those obtained in Ref. [207, 208] (see also Refs. [209–212]). We have also checked that the BRs match the well-known results in the limit of a SM scalar content [127].

C.4 Coherent $\mu - e$ conversion in nuclei

Following Ref. [213], the operators relevant for coherent $\mu - e$ conversion in nuclei have the general form

$$\begin{aligned} \mathcal{L}_{\rm int.}^{\mu-e} = \frac{G_{\rm F}}{\sqrt{2}\pi}\Bigg[\frac{e}{8\pi}G_{\gamma,L}^{\mu e}\ \overline{e}\sigma_{\lambda\rho}P_L\mu\ F^{\lambda\rho} + \alpha_W \sum_{q=u,d,s}\Big(F_{S,L}^{\mu e,q}\ \overline{e}P_L\mu\ \overline{q}q + F_{V,L}^{\mu e,q}\ \overline{e}\gamma^\rho P_L\mu\ \overline{q}\gamma_\rho q\Big)\Bigg] \\ + (L \leftrightarrow R) + \text{H.c.}\,, \end{aligned} \tag{C.14}$$

where $G_{\rm F}$ is the Fermi constant [89]. The form factors receive contributions from γ-penguin and Z-penguin diagrams as shown in Fig. C.1, the expression for their amplitudes are similar to the ones in Eqs. (C.6) and (C.7), respectively. The transition amplitude for the semi-leptonic box diagrams in Fig. C.3 is given by,

$$\mathcal{A}_{\rm Box}^{\mu eqq} = \frac{\alpha_W^2}{4M_W^2}\sum_{X,Y=L,R}\ \sum_{A=S,V,T} B_{A,XY}^{\mu eqq}\ \overline{\ell_\beta}\Lambda_A^X\ell_\alpha\ \overline{q}\Lambda_A^Y q\,, \tag{C.15}$$

leading to,

$$\begin{aligned} F_{V,X}^{\mu e,q} &= Q_q s_W^2 F_{\gamma,X}^{\mu e} + \left(\frac{T_3^q}{2} - Q_q s_W^2\right)F_{Z,X}^{\mu e} + \frac{1}{4}\left(B_{V,XX}^{\mu eqq} + B_{V,XY}^{\mu eqq}\right), \\ F_{S,X}^{\mu e,q} &= \frac{1}{4}\left(B_{S,XX}^{\mu eqq} + B_{S,XY}^{\mu eqq}\right),\ \text{for } X,Y = L,R \text{ and } X \neq Y\,, \end{aligned} \tag{C.16}$$

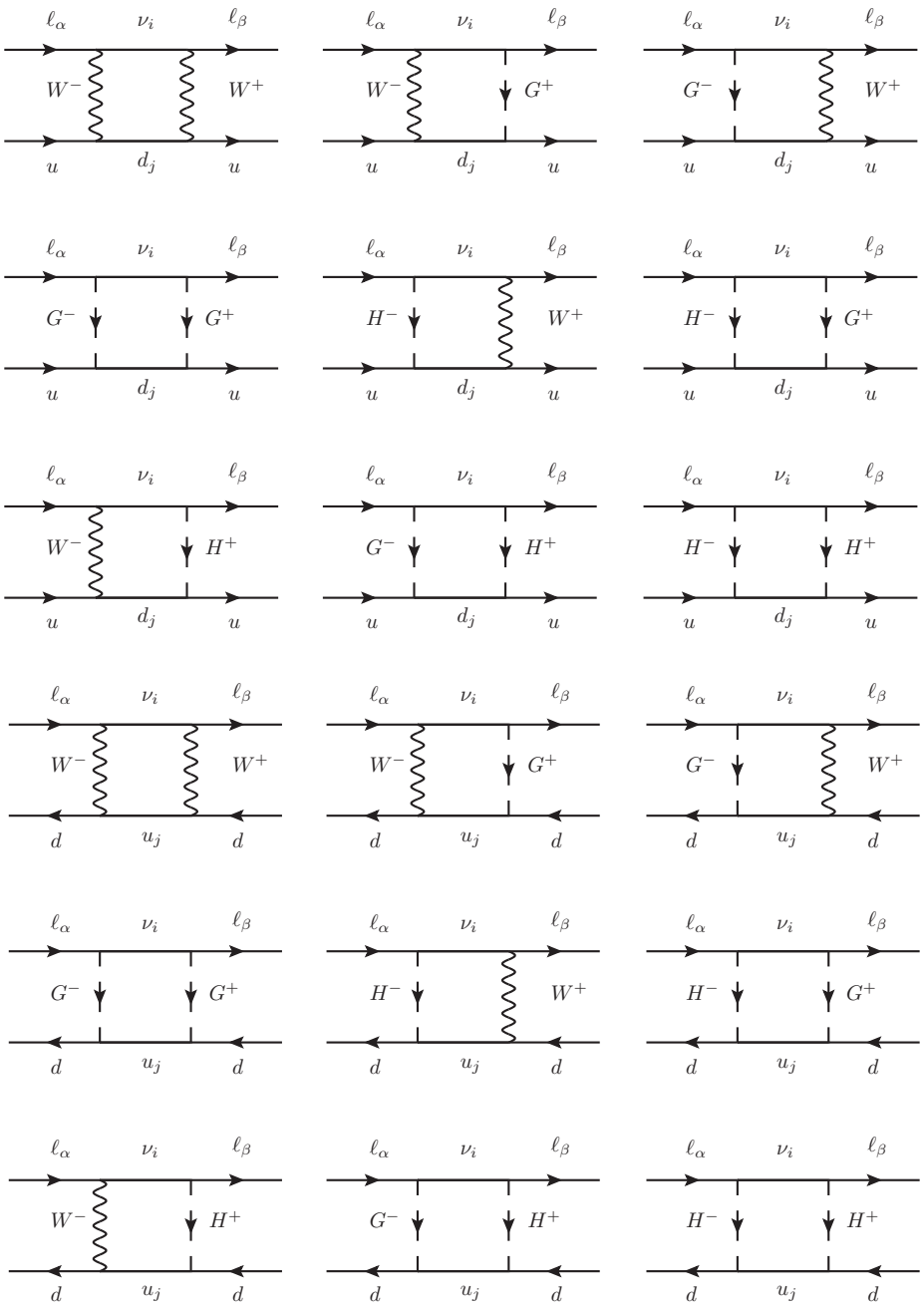

Figure C.3: Semi-leptonic u and d-type box diagrams contributing to the $\mu - e$ conversion process, where $\ell_\alpha = \mu$, $\ell_\beta = e$, $u_j = u, c, t$ and $d_j = d, s, b$.

with $T_3^u = -T_3^d = 1/2$, $Q_u = 2/3$, $Q_d = -1/3$ (see Table 2.1) and the semi-leptonic box form factors $B_{A,XY}^{\alpha\beta qq}$ ($\alpha = \mu$ and $\beta = e$) are given in Section D.4. From the Lagrangian (C.14) we obtain the coherent $\mu - e$ conversion rate

$$\begin{aligned} \mathrm{CR}(\mu \to e, \mathrm{N}) = \frac{G_\mathrm{F}^2 \alpha_W^2 m_\mu^5}{8\pi^2\, \Gamma_{\mathrm{capt}}(Z)} \Bigg[\Bigg| & 4V^{(p)} \left(2F_{V,L}^{\mu e,u} + F_{V,L}^{\mu e,d}\right) + 4V^{(n)} \left(F_{V,L}^{\mu e,u} + 2F_{V,L}^{\mu e,d}\right) \\ & + \frac{G_{\gamma,R}^{\mu e}}{m_\mu} s_w^2 \left(\frac{D}{2e}\right) + 4 \sum_{q=u,d,s} \left(S^{(p)} G_S^{(q,p)} + S^{(n)} G_S^{(q,n)}\right) F_{S,R}^{\mu e,q} \Bigg|^2 + (L \leftrightarrow R) \Bigg], \end{aligned} \tag{C.17}$$

where the values for the nuclear form factors D, $S^{(p)}$, $S^{(n)}$, $V^{(p)}$ and $V^{(n)}$, as well as the muon capture rates $\Gamma_{\rm capt}(Z)$ are reported in Table C.1 for the nuclei relevant to this work. The scalar-operator coefficients $G_S^{(q,n)}$ and $G_S^{(q,p)}$ are [214]

$$G_S^{(u,p)} = G_S^{(d,n)} = 5.1,\ G_S^{(d,p)} = G_S^{(u,n)} = 4.3,\ G_S^{(s,p)} = G_S^{(s,n)} = 2.5. \tag{C.18}$$

The above expressions are general and thus can be applied to several models in which $\mu - e$ conversion is studied. We have also verified that with only the SM Higgs doublet the above CR coincides with that given in [199].

Appendix D

Form factors and loop functions

We now provide the form factors and loop functions entering the amplitudes for the cLFV observables analysed in Appendix C. All contributions with $W^\pm$ and $H^\pm$ in the loops were included, being the form factors given at leading order in the momenta and masses of the external charged leptons. Note that, we have checked that in the limit where there are no charged-scalar contributions, i.e., for a scalar sector matching the SM one, our results are in agreement with Refs. [127, 199] (see also [45, 49, 215]).

D.1 Passarino-Veltman integrals

In this section we collect explicit analytical expressions for the Passarino-Veltman integrals [216, 217], relevant for our work. We will present the results stemming form the evaluation of the integrals, for vanishing external momenta, containing the two, three and four-point functions used during our calculations of the self-energy, penguin and box-type diagrams, respectively. The notation for momenta and masses in these diagrams is shown in Fig. D.1.

Two-point functions: The types of integrals we will need to evaluate for the two-point functions are the following

$$\frac{i}{16\pi^2}\{B_0, B^\mu\}(\text{args}) = \mu^\epsilon \int \frac{d^d k}{(2\pi)^d} \frac{\{1, k^\mu\}}{[k^2 - m_0^2]\,[(k+p)^2 - m_1^2]}, \tag{D.1}$$

where the mass scale μ provides the correct dimension to the integral in space-time dimensions $d = 4 - \epsilon$ (dimensional regularisation). In the above (args) $= (p^2; m_0^2, m_1^2)$ containing invariant quantities. We are interested in the case where $p = 0$. Hence, we evaluate the above integrals for the function $B \equiv B(0; m_0^2, m_1^2)$. Using the mass ratio $x = m_0^2/m_1^2$ we get

$$B_0 \equiv \Delta_\epsilon - b_0(x)\ ,\ b_0(x) = -\frac{x}{1-x}\ln x - 1, \tag{D.2}$$

$$B_1 \equiv -\frac{\Delta_\epsilon}{2} + b_1(x)\ ,\ b_1(x) = -\frac{1 - 4x + 3x^2 - 2x^2 \ln x}{4(1-x)^2}, \tag{D.3}$$

where the divergence is $\Delta_\epsilon = \dfrac{2}{\epsilon} - \gamma + \ln 4\pi$ with $\gamma \approx 0.57721$ being the Euler-Mascheroni constant.

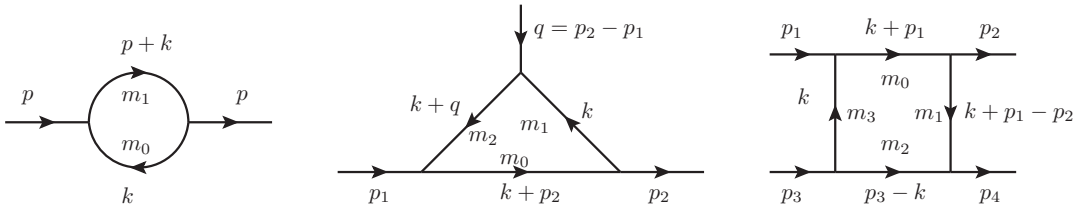

Figure D.1: Generic one-loop diagrams with two legs (self-energy) [Left], three legs (penguin) [Centre] and four legs (box) [Right]. The arrow indicates the momentum orientation.

Three-point functions: The integrals of interest for the three-point functions are

$$\frac{i}{16\pi^2}\{C_0, C^\mu, C^{\mu\nu}\}(\text{args}) = \mu^\epsilon \int \frac{d^dk}{(2\pi)^d} \frac{\{1, k^\mu, k^\mu k^\nu\}}{[(k+p_2)^2 - m_0^2]\,[k^2 - m_1^2]\,[(k+q)^2 - m_2^2]}, \tag{D.4}$$

where $(\text{args}) = (p_1^2, q^2, p_2^2; m_0^2, m_1^2, m_2^2)$. We start with $C \equiv C(0, q^2, 0; m_0^2, m_1^2, m_1^2)$ where two masses are equal $m_1 = m_2$. Using the mass ratio $x = m_0^2/m_1^2$ we obtain the results up to $\mathcal{O}(q^2)$

$$-m_1^2 C_0 \equiv c_0(x) + \frac{q^2}{m_1^2}\Delta c_0(x) = \frac{1 - x + x\ln x}{(1-x)^2} + \frac{q^2}{m_1^2}\frac{1 - 6x + 3x^2 + 2x^3 - 6x^2\ln x}{12(1-x)^4}, \tag{D.5}$$

$$c_1(x) \equiv m_1^2 C_1 = m_1^2 C_2 = \frac{1 - 4x + 3x^2 - 2x^2\ln x}{4(1-x)^3}, \tag{D.6}$$

$$c_{11}(x) \equiv -m_1^2 C_{11,(22)} = -2m_1^2 C_{12} = \frac{2 - 9x + 18x^2 - 11x^3 + 6x^3\ln x}{18(1-x)^4}, \tag{D.7}$$

$$-2C_{00} \equiv -\frac{\Delta_\epsilon}{2} + c_{00}(x) + \frac{q^2}{m_1^2}\Delta c_{00}(x) = -\frac{\Delta_\epsilon}{2} + b_1(x) - \frac{q^2}{m_1^2}\,\frac{c_{11}(x)}{2}. \tag{D.8}$$

Furthermore, we are interested in the case of $\overline{C} \equiv C(0, 0, 0; m_0^2, m_1^2, m_2^2)$ where all the masses are different. For the mass ratios $x = m_1^2/m_0^2$ and $y = m_2^2/m_0^2$ we get

$$c_0(x, y) \equiv -m_0^2\overline{C}_0 = -\frac{1}{x-y}\left(\frac{x}{1-x}\ln x - \frac{y}{1-y}\ln y\right), \tag{D.9}$$

$$-2\overline{C}_{00} \equiv -\frac{\Delta_\epsilon}{2} + c_{00}(x, y) = -\frac{\Delta_\epsilon}{2} - \frac{1}{2\,(x-y)}\left(\frac{x^2}{1-x}\ln x - \frac{y^2}{1-y}\ln y\right) - \frac{3}{4}. \tag{D.10}$$

Four-point functions: The relevant integrals for the four-point functions are

$$\frac{i}{16\pi^2}\{D_0, D^\mu, D^{\mu\nu}\}(\text{args}) = \int \frac{d^4k}{(2\pi)^4} \frac{\{1, k^\mu, k^\mu k^\nu\}}{[(k+p_1)^2 - m_0^2]\,[(k+p_1-p_2)^2 - m_1^2]\,[(p_3-k)^2 - m_2^2]\,[k^2 - m_3^2]}, \tag{D.11}$$

where $(\text{args}) = (p_1^2, p_2^2, (p_1-p_2)^2, \ldots; m_0^2, m_1^2, m_2^2, m_3^2)$ with "…" standing for invariant quantities constructed with the momenta $p_{1,2,3,4}$. However, we will work in the limit of zero external momenta where $p_{1,2,3,4} = 0$ and therefore $D \equiv D(0; m_0^2, m_1^2, m_2^2, m_3^2)$. Hence, we only need to evaluate the following integrals

$$\frac{i}{16\pi^2} D_0 = \int \frac{d^4k}{(2\pi)^4} \frac{1}{[k^2 - m_0^2]\,[k^2 - m_1^2]\,[k^2 - m_2^2]\,[k^2 - m_3^2]}, \tag{D.12}$$

$$\frac{i}{16\pi^2} D_{00} = \frac{1}{4} \int \frac{d^4k}{(2\pi)^4} \frac{k^2}{[k^2 - m_0^2]\,[k^2 - m_1^2]\,[k^2 - m_2^2]\,[k^2 - m_3^2]}. \tag{D.13}$$

For the case where all the masses are distinct and with the notation $x = m_0^2/m_3^2$, $y = m_1^2/m_3^2$ and $z = m_2^2/m_3^2$, for the mass ratios, we obtain

$$d_0(x,y,z) \equiv m_3^4 D_0 = \frac{x \ln x}{(1-x)(x-y)(x-z)} + \frac{y \ln y}{(1-y)(y-x)(y-z)} + \frac{z \ln z}{(1-z)(z-x)(z-y)}, \tag{D.14}$$

$$\widetilde{d_0}(x,y,z) \equiv 4m_3^2 D_{00} = \frac{x^2 \ln x}{(1-x)(x-y)(x-z)} + \frac{y^2 \ln y}{(1-y)(y-x)(y-z)} + \frac{z^2 \ln z}{(1-z)(z-x)(z-y)}. \tag{D.15}$$

Additionally, for two equal masses $m_3 = m_1$, we have

$$d_0(x,y) = -\frac{1}{(x-y)} \left[\frac{1}{1-x} + \frac{x}{(1-x)^2} \ln x - \frac{1}{1-y} - \frac{y}{(1-y)^2} \ln y \right], \tag{D.16}$$

$$\widetilde{d_0}(x,y) = -\frac{1}{(x-y)} \left[\frac{1}{1-x} + \frac{x^2}{(1-x)^2} \ln x - \frac{1}{1-y} - \frac{y^2}{(1-y)^2} \ln y \right]. \tag{D.17}$$

Note that, we will express the upcoming loop functions in terms of the results presented in this section.

D.2 Photon form factors

The photon form factors coming from the γ-penguin diagrams, generically presented in Fig. C.1, are given by

$$F^{\alpha\beta}_{\gamma,L(R)} = F^{\alpha\beta(1)}_{\gamma,L(R)} + F^{\alpha\beta(2)}_{\gamma,L(R)} \quad , \quad G^{\alpha\beta}_{\gamma,L(R)} = G^{\alpha\beta(1)}_{\gamma,L(R)} + G^{\alpha\beta(2)}_{\gamma,L(R)}\,, \tag{D.18}$$

where the superscript (1) and (2) correspond to the contributions stemming from $W^\pm$ and $H^\pm$, respectively. Looking at the general form of the amplitude $\mathcal{A}^{\alpha\beta}_\gamma$ in Eq. (C.1), we notice that due to electromagnetic gauge invariance these photon form factors vanish in the limit of zero external lepton momenta and masses. Therefore, to obtain a non-vanishing result we must expand the loop integrals up to next order in q^2 [see Eqs.(D.5) and (D.8)]. The $W^\pm$-boson contribution yields

$$F^{\alpha\beta(1)}_{\gamma,L} = \sum_{i=1}^{n_f} \mathbf{B}_{\beta i} \mathbf{B}^*_{\alpha i} F^{(1)}_\gamma(\lambda_i)\,, \tag{D.19}$$

$$F^{\alpha\beta(1)}_{\gamma,R} = 0\,, \tag{D.20}$$

$$G^{\alpha\beta(1)}_{\gamma,L} = m_\beta \sum_{i=1}^{n_f} \mathbf{B}_{\beta i} \mathbf{B}^*_{\alpha i} G^{(1)}_\gamma(\lambda_i)\,, \tag{D.21}$$

$$G^{\alpha\beta(1)}_{\gamma,R} = m_\alpha \sum_{i=1}^{n_f} \mathbf{B}_{\beta i} \mathbf{B}^*_{\alpha i} G^{(1)}_\gamma(\lambda_i)\,,\ \lambda_i = \frac{m_i^2}{M_W^2}\,, \tag{D.22}$$

where $\mathbf{B}$ has been defined in Eq. (3.20). The $H^\pm$ scalar contribution yields

$$F^{\alpha\beta(2)}_{\gamma,L} = \frac{1}{m^2_{H^\pm}} \sum_{i=1}^{n_f} \left(\mathbf{B}\mathbf{N}_\nu\right)_{\beta i} \left(\mathbf{N}^\dagger_\nu \mathbf{B}^\dagger\right)_{i\alpha} F^{(2)}_\gamma(\omega_i), \tag{D.23}$$

$$F_{\gamma,R}^{\alpha\beta(2)} = \frac{1}{m_{H^\pm}^2}\sum_{i=1}^{n_f}\left(\mathbf{N}_e^\dagger\mathbf{B}\right)_{\beta i}\left(\mathbf{B}^\dagger\mathbf{N}_e\right)_{i\alpha}F_\gamma^{(2)}(\omega_i), \tag{D.24}$$

$$\begin{aligned} G_{\gamma,L}^{\alpha\beta(2)} = -\frac{1}{m_{H^\pm}^2}\sum_{i=1}^{n_f}\Big\{ &\left[m_i\left(\mathbf{N}_e^\dagger\mathbf{B}\right)_{\beta i}\left(\mathbf{N}_\nu^\dagger\mathbf{B}^\dagger\right)_{i\alpha} + m_i\left(\mathbf{B}\mathbf{N}_\nu\right)_{\beta i}\left(\mathbf{B}^\dagger\mathbf{N}_e\right)_{i\alpha}\right]G_\gamma^{(2)}(\omega_i) \\ &- \left[m_\alpha\left(\mathbf{N}_e^\dagger\mathbf{B}\right)_{\beta i}\left(\mathbf{B}^\dagger\mathbf{N}_e\right)_{i\alpha} + m_\beta\left(\mathbf{B}\mathbf{N}_\nu\right)_{\beta i}\left(\mathbf{N}_\nu^\dagger\mathbf{B}^\dagger\right)_{i\alpha}\right]G_\gamma^{(3)}(\omega_i)\Big\}, \end{aligned} \tag{D.25}$$

$$\begin{aligned} G_{\gamma,R}^{\alpha\beta(2)} = -\frac{1}{m_{H^\pm}^2}\sum_{i=1}^{n_f}\Big\{ &\left[m_i\left(\mathbf{N}_e^\dagger\mathbf{B}\right)_{\beta i}\left(\mathbf{N}_\nu^\dagger\mathbf{B}^\dagger\right)_{i\alpha} + m_i\left(\mathbf{B}\mathbf{N}_\nu\right)_{\beta i}\left(\mathbf{B}^\dagger\mathbf{N}_e\right)_{i\alpha}\right]G_\gamma^{(2)}(\omega_i) \\ &- \left[m_\alpha\left(\mathbf{B}\mathbf{N}_\nu\right)_{\beta i}\left(\mathbf{N}_\nu^\dagger\mathbf{B}^\dagger\right)_{i\alpha} + m_\beta\left(\mathbf{N}_e^\dagger\mathbf{B}\right)_{\beta i}\left(\mathbf{B}^\dagger\mathbf{N}_e\right)_{i\alpha}\right]G_\gamma^{(3)}(\omega_i)\Big\}\,,\ \omega_i = \frac{m_i^2}{m_{H^\pm}^2}\,, \end{aligned} \tag{D.26}$$

where the scalar-lepton couplings $\mathbf{N}_e$ and $\mathbf{N}_\nu$ are given in Eqs. (B.8) and (B.9). The loop functions $F_\gamma^{(i)}$ and $G_\gamma^{(i)}$ read

$$\begin{aligned} F_\gamma^{(1)}(x) &= 4c_1(x) - c_{11}(x) - 2x\Delta c_0(x) + (6+x)\Delta c_{00}(x) - \frac{5}{9} \\ &= -\frac{x\left(12+x-7x^2\right)}{12(1-x)^3} - \frac{x^2\left(12-10x+x^2\right)}{6(1-x)^4}\ln x\,, \end{aligned} \tag{D.27}$$

$$F_\gamma^{(2)}(x) = \Delta c_{00}(x) = \frac{-2+7x-11x^2}{36(1-x)^3} - \frac{x^3\ln x}{6(1-x)^4}, \tag{D.28}$$

$$\begin{aligned} G_\gamma^{(1)}(x) &= -xc_0(x) - (2-3x)c_1(x) - \frac{3}{2}(2+x)c_{11}(x) + \frac{5}{6} \\ &= \frac{x\left(1-5x-2x^2\right)}{4(1-x)^3} - \frac{3x^3}{2(1-x)^4}\ln x\,, \end{aligned} \tag{D.29}$$

$$G_\gamma^{(2)}(x) = c_0(x) - 2c_1(x) = \frac{(1+x)}{2(1-x)^2} + \frac{x\ln x}{(1-x)^3}, \tag{D.30}$$

$$G_\gamma^{(3)}(x) = c_1(x) - \frac{3}{2}c_{11}(x) = \frac{1-5x-2x^2}{12(1-x)^3} - \frac{x^2\ln x}{2(1-x)^4}\,. \tag{D.31}$$

The charged Higgs form factors and loop functions given above are consistent with the results of Refs. [218–220].

D.3 Z-boson form factors

The Z-penguin diagrams displayed in Fig. C.1 lead to the form factors:

$$F_{Z,L(R)}^{\alpha\beta} = F_{Z,(R)}^{\alpha\beta(1)} + F_{Z,L(R)}^{\alpha\beta(2)}\,, \tag{D.32}$$

where the $W^\pm$-boson contributions are

$$F_{Z,L}^{\alpha\beta(1)} = \sum_{i,j=1}^{n_f}\mathbf{B}_{\beta i}\mathbf{B}_{\alpha j}^*\left[\delta_{ij}F_Z^{(1)}(\lambda_i) + \boldsymbol{\mathcal{C}}_{ij}G_Z^{(1)}(\lambda_i,\lambda_j) + \boldsymbol{\mathcal{C}}_{ij}^*H_Z(\lambda_i,\lambda_j)\right]\,, \tag{D.33}$$

$$F_{Z,R}^{\alpha\beta(1)} = 0\,, \tag{D.34}$$

with the matrix $\boldsymbol{\mathcal{C}}$ defined in Eq. (3.20), while the $H^\pm$ scalar contribution is

$$F_{Z,L}^{\alpha\beta(2)} = \frac{1}{M_W^2}\sum_{i,j=1}^{n_f}\left(\mathbf{B}\mathbf{N}_\nu\right)_{\beta i}\left(\mathbf{N}_\nu^\dagger\mathbf{B}^\dagger\right)_{j\alpha}\left[\boldsymbol{\mathcal{C}}_{ij}\; G_Z^{(2)}(\omega_i,\omega_j) - \boldsymbol{\mathcal{C}}_{ij}^* G_Z^{(3)}(\omega_i,\omega_j)\right], \tag{D.35}$$

$$F_{Z,R}^{\alpha\beta(2)} = \frac{1}{M_W^2}\sum_{i,j=1}^{n_f}\left(\mathbf{N}_e^\dagger\mathbf{B}\right)_{\beta i}\left(\mathbf{B}^\dagger\mathbf{N}_e\right)_{j\alpha}\left[\delta_{ij}F_Z^{(2)}(\omega_i) + \boldsymbol{\mathcal{C}}_{ij}G_Z^{(3)}(\omega_i,\omega_j) - \boldsymbol{\mathcal{C}}_{ij}^* G_Z^{(2)}(\omega_i,\omega_j)\right]. \tag{D.36}$$

The loop functions entering the above form factors are given by

$$F_Z^{(1)}(x) = -3b_1(x) - xc_0(x) - \frac{3}{4} = -\frac{5x}{2(1-x)} - \frac{5x^2}{2(1-x)^2}\ln x, \tag{D.37}$$

$$F_Z^{(2)}(x) = -\frac{1}{2}b_1(x) = -\frac{x}{4(1-x)} - \frac{x^2\ln x}{4(1-x)^2} + \frac{1}{8}, \tag{D.38}$$

$$\begin{aligned} G_Z^{(1)}(x,y) &= -\frac{xy}{2}c_0(x,y) + c_{00}(x,y) + \frac{3}{4} \\ &= -\frac{1}{2(x-y)}\left[\frac{x^2(1-y)}{(1-x)}\ln x - \frac{y^2(1-x)}{(1-y)}\ln y\right], \end{aligned} \tag{D.39}$$

$$G_Z^{(2)}(x,y) = \frac{\sqrt{xy}}{2}c_0(x,y) = -\frac{\sqrt{xy}}{2(x-y)}\left[\frac{x\ln x}{(1-x)} - \frac{y\ln y}{(1-y)}\right], \tag{D.40}$$

$$G_Z^{(3)}(x,y) = -\frac{1}{2}c_{00}(x,y) = \frac{1}{4(x-y)}\left[\frac{x^2\ln x}{(1-x)} - \frac{y^2\ln y}{(1-y)}\right] + \frac{3}{8}, \tag{D.41}$$

$$\begin{aligned} H_Z(x,y) &= \sqrt{xy}\left[2c_0(x,y) - c_{00}(x,y) - \frac{3}{4}\right] \\ &= \frac{\sqrt{xy}}{4(x-y)}\left[\frac{x^2-4x}{(1-x)}\ln x - \frac{y^2-4y}{(1-y)}\ln y\right]. \end{aligned} \tag{D.42}$$

The charged Higgs form factors and loop functions given above are consistent with the results of Ref. [219].

D.4 Semi-leptonic box form factors

Here we present the form factors and loop functions relevant for the amplitudes (C.15) corresponding to the semi-leptonic u-type and d-type diagrams presented in Fig. C.3. We write [1]

$$B_{V,LL}^{\alpha\beta qq} = B_{V,LL}^{\alpha\beta qq(1)} + B_{V,LL}^{\alpha\beta qq(2)}, \tag{D.43}$$

where $W^\pm$-boson contributes only to $B_{V,LL}^{\alpha\beta qq(1)}$, while the $H^\pm$ loops produces all types of form factors in (C.15), including $B_{V,LL}^{\alpha\beta qq(2)}$. We now present the various $B_{A,XY}^{\alpha\beta qq}$ for the u and d-type diagrams shown in Fig. C.3.

***u*-type diagrams:** The only $W^\pm$-boson contribution is

$$B_{V,LL}^{\alpha\beta uu(1)} = \sum_{i=1}^{n_f}\sum_{d_j=d,s,b}\mathbf{V}_{ud_j}\mathbf{V}_{ud_j}^*\mathbf{B}_{\beta i}\mathbf{B}_{\alpha i}^* F_{\text{Box}}^{(1)}(\lambda_i,\lambda_{d_j}), \tag{D.44}$$

[1] Although we use general α and β indices, for $\mu - e$ conversion one obviously has $\alpha = \mu$ and $\beta = e$.

while the diagrams with $H^{\pm}$ lead to [2,3]

$$B_{V,LL}^{\alpha\beta uu(2)} = \frac{1}{M_W^2 m_{H^\pm}^2}\sum_{i=1}^{n_f}\sum_{d_j=d,s,b}\Bigg\{(\mathbf{B}\mathbf{N}_\nu)_{\beta i}\left(\mathbf{N}_\nu^\dagger\mathbf{B}^\dagger\right)_{i\alpha}(\mathbf{V}\mathbf{N}_d)_{ud_j}\left(\mathbf{N}_d^\dagger\mathbf{V}^\dagger\right)_{d_ju} F_{\rm Box}^{(3)}(\omega_i,\omega_{d_j}) + \left[\mathbf{V}_{ud_j}^*\mathbf{B}_{\alpha i}^*(\mathbf{B}\mathbf{N}_\nu)_{\beta i}(\mathbf{V}\mathbf{N}_d)_{ud_j} + \mathbf{V}_{ud_j}\mathbf{B}_{\beta i}\left(\mathbf{N}_\nu^\dagger\mathbf{B}^\dagger\right)_{i\alpha}\left(\mathbf{N}_d^\dagger\mathbf{V}^\dagger\right)_{d_ju}\right] \times m_{H^\pm}^2 H_{\rm Box}^{(1)}(\lambda_i,\lambda_{d_j},\lambda_\pm)\Bigg\}, \tag{D.45}$$

$$B_{V,LR}^{\alpha\beta uu} = \frac{1}{M_W^2 m_{H^\pm}^2}\sum_{i=1}^{n_f}\sum_{d_j=d,s,b}(\mathbf{B}\mathbf{N}_\nu)_{\beta i}\left(\mathbf{N}_\nu^\dagger\mathbf{B}^\dagger\right)_{i\alpha}\left(\mathbf{N}_u^\dagger\mathbf{V}\right)_{ud_j}\left(\mathbf{V}^\dagger\mathbf{N}_u\right)_{d_ju} F_{\rm Box}^{(3)}(\omega_i,\omega_{d_j}), \tag{D.46}$$

$$B_{V,RL}^{\alpha\beta uu} = \frac{1}{M_W^2 m_{H^\pm}^2}\sum_{i=1}^{n_f}\sum_{d_j=d,s,b}\left(\mathbf{N}_e^\dagger\mathbf{B}\right)_{\beta i}\left(\mathbf{B}^\dagger\mathbf{N}_e\right)_{i\alpha}(\mathbf{V}\mathbf{N}_d)_{ud_j}\left(\mathbf{N}_d^\dagger\mathbf{V}^\dagger\right)_{d_ju} F_{\rm Box}^{(3)}(\omega_i,\omega_{d_j}), \tag{D.47}$$

$$B_{V,RR}^{\alpha\beta uu} = \frac{1}{M_W^2 m_{H^\pm}^2}\sum_{i=1}^{n_f}\sum_{d_j=d,s,b}\left(\mathbf{N}_e^\dagger\mathbf{B}\right)_{\beta i}\left(\mathbf{B}^\dagger\mathbf{N}_e\right)_{i\alpha}\left(\mathbf{N}_u^\dagger\mathbf{V}\right)_{ud_j}\left(\mathbf{V}^\dagger\mathbf{N}_u\right)_{d_ju} F_{\rm Box}^{(3)}(\omega_i,\omega_{d_j}), \tag{D.48}$$

$$B_{S,LL}^{\alpha\beta uu} = \sum_{i=1}^{n_f}\sum_{d_j=d,s,b}\frac{\left(\mathbf{N}_e^\dagger\mathbf{B}\right)_{\beta i}\left(\mathbf{N}_u^\dagger\mathbf{V}\right)_{ud_j}}{M_W^2}\Bigg[\mathbf{V}_{ud_j}^*\mathbf{B}_{\alpha i}^* H_{\rm Box}^{(2)}(\lambda_i,\lambda_{d_j},\lambda_\pm) + \left(\mathbf{N}_\nu^\dagger\mathbf{B}^\dagger\right)_{i\alpha}\left(\mathbf{N}_d^\dagger\mathbf{V}^\dagger\right)_{d_ju}\frac{F_{\rm Box}^{(4)}(\omega_i,\omega_{d_j})}{m_{H^\pm}^2}\Bigg], \tag{D.49}$$

$$B_{S,LR}^{\alpha\beta uu} = \frac{1}{M_W^2 m_{H^\pm}^2}\sum_{i=1}^{n_f}\sum_{d_j=d,s,b}\left(\mathbf{N}_e^\dagger\mathbf{B}\right)_{\beta i}\left(\mathbf{N}_\nu^\dagger\mathbf{B}^\dagger\right)_{i\alpha}(\mathbf{V}\mathbf{N}_d)_{ud_j}\left(\mathbf{V}^\dagger\mathbf{N}_u\right)_{d_ju} F_{\rm Box}^{(4)}(\omega_i,\omega_{d_j}), \tag{D.50}$$

$$B_{S,RL}^{\alpha\beta uu} = \frac{1}{M_W^2 m_{H^\pm}^2}\sum_{i=1}^{n_f}\sum_{d_j=d,s,b}(\mathbf{B}\mathbf{N}_\nu)_{\beta i}\left(\mathbf{B}^\dagger\mathbf{N}_e\right)_{i\alpha}\left(\mathbf{N}_u^\dagger\mathbf{V}\right)_{ud_j}\left(\mathbf{N}_d^\dagger\mathbf{V}^\dagger\right)_{d_ju} F_{\rm Box}^{(4)}(\omega_i,\omega_{d_j}), \tag{D.51}$$

$$B_{S,RR}^{\alpha\beta uu} = \sum_{i=1}^{n_f}\sum_{d_j=d,s,b}\frac{\left(\mathbf{B}^\dagger\mathbf{N}_e\right)_{i\alpha}\left(\mathbf{V}^\dagger\mathbf{N}_u\right)_{d_ju}}{M_W^2}\Bigg[\mathbf{V}_{ud_j}\mathbf{B}_{\beta i} H_{\rm Box}^{(2)}(\lambda_i,\lambda_{d_j},\lambda_\pm) + (\mathbf{B}\mathbf{N}_\nu)_{\beta i}(\mathbf{V}\mathbf{N}_d)_{ud_j}\frac{F_{\rm Box}^{(4)}(\omega_i,\omega_{d_j})}{m_{H^\pm}^2}\Bigg], \tag{D.52}$$

$$B_{T,LL}^{\alpha\beta uu} = -\frac{1}{M_W^2}\sum_{i=1}^{n_f}\sum_{d_j=d,s,b}\mathbf{V}_{ud_j}^*\mathbf{B}_{\alpha i}^*\left(\mathbf{N}_e^\dagger\mathbf{B}\right)_{\beta i}\left(\mathbf{N}_u^\dagger\mathbf{V}\right)_{ud_j} H_{\rm Box}^{(3)}(\lambda_i,\lambda_{d_j},\lambda_\pm), \tag{D.53}$$

$$B_{T,RR}^{\alpha\beta uu} = -\frac{1}{M_W^2}\sum_{i=1}^{n_f}\sum_{d_j=d,s,b}\mathbf{V}_{ud_j}\mathbf{B}_{\beta i}\left(\mathbf{B}^\dagger\mathbf{N}_e\right)_{i\alpha}\left(\mathbf{V}^\dagger\mathbf{N}_u\right)_{d_ju} H_{\rm Box}^{(3)}(\lambda_i,\lambda_{d_j},\lambda_\pm) \quad , \tag{D.54}$$

where $\lambda_{d_j} = m_{d_j}^2/M_W^2$ and $\omega_{d_j} = m_{d_j}^2/m_{H^\pm}^2$. $\mathbf{N}_d$ and $\mathbf{N}_u$ are defined in Eqs. (B.10) and (B.11), respectively.

***d*-type diagrams:** The form factor for the d-type diagrams coming from the $W^\pm$-boson contribution is

$$B_{V,LL}^{\alpha\beta dd(1)} = \sum_{i=1}^{n_f}\sum_{u_j=u,c,t}\mathbf{V}_{du_j}\mathbf{V}_{du_j}^*\mathbf{B}_{\beta i}\mathbf{B}_{\alpha i}^* F_{\rm Box}^{(2)}(\lambda_i,\lambda_{u_j}), \tag{D.55}$$

[2]Note that the form factors $B_{T,LL(RR)}$ do not contribute to the $\mu - e$ conversion process.

[3]Since for our numerical analysis we have considered diagonal quark mass matrices and $\tan\beta = 1$ we will have $\mathbf{N}_{u,d} \equiv 0$ and, therefore, the semi-leptonic box form factors involving $H^\pm$ in the loop will not contribute to the rates in that case.

while for the $H^\pm$ loops:

$$B_{V,LL}^{\alpha\beta dd(2)} = -\frac{1}{M_W^2 m_{H^\pm}^2}\sum_{i=1}^{n_f}\sum_{u_j=u,c,t}\Bigg\{ (\mathbf{B}\mathbf{N}_\nu)_{\beta i}\left(\mathbf{N}_\nu^\dagger\mathbf{B}^\dagger\right)_{i\alpha}\left(\mathbf{V}^\dagger\mathbf{N}_u\right)_{du_j}\left(\mathbf{N}_u^\dagger\mathbf{V}\right)_{u_j d}\ F_{\rm Box}^{(3)}(\omega_i,\omega_{u_j}) + \left[\mathbf{V}_{du_j}\mathbf{B}_{\alpha i}^*(\mathbf{B}\mathbf{N}_\nu)_{\beta i}\left(\mathbf{N}_u^\dagger\mathbf{V}\right)_{u_j d} + \mathbf{B}_{\beta i}\mathbf{V}_{du_j}^*\left(\mathbf{N}_\nu^\dagger\mathbf{B}^\dagger\right)_{i\alpha}\left(\mathbf{V}^\dagger\mathbf{N}_u\right)_{du_j}\right] \times m_{H^\pm}^2 H_{\rm Box}^{(1)}(\lambda_i,\lambda_{u_j},\lambda_\pm)\Bigg\}, \tag{D.56}$$

$$B_{V,LR}^{\alpha\beta dd} = -\frac{1}{M_W^2 m_{H^\pm}^2}\sum_{i=1}^{n_f}\sum_{u_j=u,c,t}(\mathbf{B}\mathbf{N}_\nu)_{\beta i}\left(\mathbf{N}_\nu^\dagger\mathbf{B}^\dagger\right)_{i\alpha}\left(\mathbf{N}_d^\dagger\mathbf{V}^\dagger\right)_{du_j}(\mathbf{V}\mathbf{N}_d)_{u_j d}\ F_{\rm Box}^{(3)}(\omega_i,\omega_{u_j}), \tag{D.57}$$

$$B_{V,RL}^{\alpha\beta dd} = -\frac{1}{M_W^2 m_{H^\pm}^2}\sum_{i=1}^{n_f}\sum_{u_j=u,c,t}\left(\mathbf{N}_e^\dagger\mathbf{B}\right)_{\beta i}\left(\mathbf{B}^\dagger\mathbf{N}_e\right)_{i\alpha}\left(\mathbf{V}^\dagger\mathbf{N}_u\right)_{du_j}\left(\mathbf{N}_u^\dagger\mathbf{V}\right)_{u_j d}\ F_{\rm Box}^{(3)}(\omega_i,\omega_{u_j}), \tag{D.58}$$

$$B_{V,RR}^{\alpha\beta dd} = -\frac{1}{M_W^2 m_{H^\pm}^2}\sum_{i=1}^{n_f}\sum_{u_j=u,c,t}\left(\mathbf{N}_e^\dagger\mathbf{B}\right)_{\beta i}\left(\mathbf{B}^\dagger\mathbf{N}_e\right)_{i\alpha}\left(\mathbf{N}_d^\dagger\mathbf{V}^\dagger\right)_{du_j}(\mathbf{V}\mathbf{N}_d)_{u_j d}\ F_{\rm Box}^{(3)}(\omega_i,\omega_{u_j}), \tag{D.59}$$

$$B_{S,LL}^{\alpha\beta dd} = \frac{1}{M_W^2 m_{H^\pm}^2}\sum_{i=1}^{n_f}\sum_{u_j=u,c,t}\left(\mathbf{N}_e^\dagger\mathbf{B}\right)_{\beta i}\left(\mathbf{N}_\nu^\dagger\mathbf{B}^\dagger\right)_{i\alpha}\left(\mathbf{N}_d^\dagger\mathbf{V}^\dagger\right)_{du_j}\left(\mathbf{N}_u^\dagger\mathbf{V}\right)_{u_j d}\ F_{\rm Box}^{(4)}(\omega_i,\omega_{u_j}), \tag{D.60}$$

$$B_{S,LR}^{\alpha\beta dd} = \sum_{i=1}^{n_f}\sum_{u_j=u,c,t}\frac{\left(\mathbf{N}_e^\dagger\mathbf{B}\right)_{\beta i}(\mathbf{V}\mathbf{N}_d)_{u_j d}}{M_W^2}\Bigg[\mathbf{V}_{du_j}\mathbf{B}_{\alpha i}^* H_{\rm Box}^{(2)}(\lambda_i,\lambda_{u_j},\lambda_\pm) + \left(\mathbf{N}_\nu^\dagger\mathbf{B}^\dagger\right)_{i\alpha}\left(\mathbf{V}^\dagger\mathbf{N}_u\right)_{du_j}\frac{F_{\rm Box}^{(4)}(\omega_i,\omega_{u_j})}{m_{H^\pm}^2}\Bigg],$$

$$B_{S,RL}^{\alpha\beta dd} = \sum_{i=1}^{n_f}\sum_{u_j=u,c,t}\frac{\left(\mathbf{B}^\dagger\mathbf{N}_e\right)_{i\alpha}\left(\mathbf{N}_d^\dagger\mathbf{V}^\dagger\right)_{du_j}}{M_W^2}\Bigg[\mathbf{V}_{du_j}^*\mathbf{B}_{\beta i} H_{\rm Box}^{(2)}(\lambda_i,\lambda_{u_j},\lambda_\pm) + (\mathbf{B}\mathbf{N}_\nu)_{\beta i}\left(\mathbf{N}_u^\dagger\mathbf{V}\right)_{u_j d}\frac{F_{\rm Box}^{(4)}(\omega_i,\omega_{u_j})}{m_{H^\pm}^2}\Bigg],$$

$$B_{S,RR}^{\alpha\beta dd} = \frac{1}{M_W^2 m_{H^\pm}^2}\sum_{i=1}^{n_f}\sum_{u_j=u,c,t}(\mathbf{B}\mathbf{N}_\nu)_{\beta i}\left(\mathbf{B}^\dagger\mathbf{N}_e\right)_{i\alpha}\left(\mathbf{V}^\dagger\mathbf{N}_u\right)_{du_j}(\mathbf{V}\mathbf{N}_d)_{u_j d}\,F_{\rm Box}^{(4)}(\omega_i,\omega_{u_j}), \tag{D.61}$$

with $\lambda_{u_j} = m_{u_j}^2/M_W^2$ and $\omega_{u_j} = m_{u_j}^2/m_{H^\pm}^2$. The loop functions entering the semi-leptonic box form factors are

$$\begin{aligned} F_{\rm Box}^{(1)}(x,y) &= -\left(4+\frac{xy}{4}\right)\ \widetilde{d}_0(x,y) + 2xy\ d_0(x,y) \\ &= \frac{1}{x-y}\left\{\left(4+\frac{xy}{4}\right)\left[\frac{1}{1-x}+\frac{x^2}{(1-x)^2}\ln x - \frac{1}{1-y} - \frac{y^2}{(1-y)^2}\ln y\right]\right. \\ &\left. -2xy\left[\frac{1}{1-x}+\frac{x}{(1-x)^2}\ln x - \frac{1}{1-y} - \frac{y}{(1-y)^2}\ln y\right]\right\}, \end{aligned} \tag{D.62}$$

$$\begin{aligned} F_{\rm Box}^{(2)}(x,y) &= \left(1+\frac{xy}{4}\right)\ \widetilde{d}_0(x,y) - 2xy\ d_0(x,y) \\ &= -\frac{1}{x-y}\left\{\left(1+\frac{xy}{4}\right)\left[\frac{1}{1-x}+\frac{x^2}{(1-x)^2}\ln x - \frac{1}{1-y} - \frac{y^2}{(1-y)^2}\ln y\right]\right. \\ &\left. -2xy\left[\frac{1}{1-x}+\frac{x}{(1-x)^2}\ln x - \frac{1}{1-y} - \frac{y}{(1-y)^2}\ln y\right]\right\}, \end{aligned} \tag{D.63}$$

$$F_{\rm Box}^{(3)}(x,y) = -\frac{\widetilde{d}_0(x,y)}{4} = \frac{1}{4(x-y)}\left[\frac{1}{1-x}+\frac{x^2}{(1-x)^2}\ln x - \frac{1}{1-y} - \frac{y^2}{(1-y)^2}\ln y\right], \tag{D.64}$$

$$F^{(4)}_{\rm Box}(x,y) = \sqrt{xy}\; d_0(x,y) = -\frac{\sqrt{xy}}{(x-y)}\left[\frac{1}{1-x} + \frac{x}{(1-x)^2}\ln x - \frac{1}{1-y} - \frac{y}{(1-y)^2}\ln y\right], \tag{D.65}$$

$$\begin{aligned} H^{(1)}_{\rm Box}(x,y,z) &= \frac{\sqrt{xy}}{4}\left[4d_0(x,y,z) - \widetilde{d}_0(x,y,z)\right] \\ &= \frac{\sqrt{xy}}{4}\left[\frac{x(4-x)\ln x}{(1-x)(x-y)(x-z)} + \frac{y(4-y)\ln y}{(1-y)(y-x)(y-z)} + \frac{z(4-z)\ln z}{(1-z)(z-x)(z-y)}\right], \end{aligned} \tag{D.66}$$

$$\begin{aligned} H^{(2)}_{\rm Box}(x,y,z) &= -\widetilde{d}_0(x,y,z) + xy\; d_0(x,y,z) \\ &= -\left[\frac{x^2(1-y)\ln x}{(1-x)(x-y)(x-z)} + \frac{y^2(1-x)\ln y}{(1-y)(y-x)(y-z)} + \frac{z(z-xy)\ln z}{(1-z)(z-x)(z-y)}\right], \end{aligned} \tag{D.67}$$

$$\begin{aligned} H^{(3)}_{\rm Box}(x,y,z) &= -\frac{\widetilde{d}_0(x,y,z)}{4} \\ &= -\frac{1}{4}\left[\frac{x^2\ln x}{(1-x)(x-y)(x-z)} + \frac{y^2\ln y}{(1-y)(y-x)(y-z)} + \frac{z^2\ln z}{(1-z)(z-x)(z-y)}\right]. \end{aligned} \tag{D.68}$$

D.5 Leptonic box form factors

Finally, we present the form factors in $\mathcal{A}^{\alpha\beta\gamma\delta}_{\rm Box}$ of Eq. (C.8), corresponding to the leptonic one-loop box diagrams generically presented in Fig. C.2. As explained in Appendix C, we consider all contributions, including those stemming from LNV and cross diagrams ($\beta \leftrightarrow \delta$) with spinorial structure $\overline{\ell^c_\alpha}\Lambda^X_A \ell^c_\gamma\; \overline{\ell_\delta}\Lambda^Y_A \ell^c_\beta$ and $\overline{\ell_\delta}\Lambda^X_A \ell_\alpha\; \overline{\ell_\beta}\Lambda^Y_A \ell^c_\gamma$, respectively. The Fierz rearrangements [205, 206] we use to bring these contributions into the canonical structure $\overline{\ell_\beta}\Lambda^X_A \ell_\alpha\; \overline{\ell_\delta}\Lambda^Y_A \ell^c_\gamma$ in Eq. (C.8) are the following

$$\begin{aligned}
\overline{\ell^c_\alpha}\Lambda^{L,R}_V \ell^c_\gamma\; \overline{\ell_\delta}\Lambda^{L,R}_V \ell^c_\beta &= -\overline{\ell_\beta}\Lambda^{R,L}_V \ell_\alpha\; \overline{\ell_\delta}\Lambda^{L,R}_V \ell^c_\gamma, \\
\overline{\ell^c_\alpha}\Lambda^{L,R}_V \ell^c_\gamma\; \overline{\ell_\delta}\Lambda^{R,L}_V \ell^c_\beta &= -2\;\overline{\ell_\beta}\Lambda^{R,L}_S \ell_\alpha\; \overline{\ell_\delta}\Lambda^{L,R}_S \ell^c_\gamma, \\
\overline{\ell^c_\alpha}\Lambda^{L,R}_S \ell^c_\gamma\; \overline{\ell_\delta}\Lambda^{L,R}_S \ell^c_\beta &= -\frac{1}{2}\;\overline{\ell_\beta}\Lambda^{L,R}_S \ell_\alpha\; \overline{\ell_\delta}\Lambda^{L,R}_S \ell^c_\gamma + \frac{1}{8}\;\overline{\ell_\beta}\Lambda^{L,R}_T \ell_\alpha\; \overline{\ell_\delta}\Lambda^{L,R}_T \ell^c_\gamma, \\
\overline{\ell^c_\alpha}\Lambda^{L,R}_S \ell^c_\gamma\; \overline{\ell_\delta}\Lambda^{R,L}_S \ell^c_\beta &= \frac{1}{2}\overline{\ell_\beta}\Lambda^{L,R}_V \ell_\alpha\; \overline{\ell_\delta}\Lambda^{L,R}_V \ell^c_\gamma, \\
\overline{\ell^c_\alpha}\Lambda^{L,R}_T \ell^c_\gamma\; \overline{\ell_\delta}\Lambda^{L,R}_T \ell^c_\beta &= -6\;\overline{\ell_\beta}\Lambda^{L,R}_S \ell_\alpha\; \overline{\ell_\delta}\Lambda^{L,R}_S \ell^c_\gamma - \frac{1}{2}\;\overline{\ell_\beta}\Lambda^{L,R}_T \ell_\alpha\; \overline{\ell_\delta}\Lambda^{L,R}_T \ell^c_\gamma,
\end{aligned} \tag{D.69}$$

and,

$$\begin{aligned}
\overline{\ell_\beta}\Lambda^{L,R}_V \ell_\alpha\; \overline{\ell_\delta}\Lambda^{L,R}_V \ell^c_\gamma &= \overline{\ell_\delta}\Lambda^{L,R}_V \ell_\alpha\; \overline{\ell_\beta}\Lambda^{L,R}_V \ell^c_\gamma, \\
\overline{\ell_\beta}\Lambda^{L,R}_V \ell_\alpha\; \overline{\ell_\delta}\Lambda^{R,L}_V \ell^c_\gamma &= -2\;\overline{\ell_\delta}\Lambda^{L,R}_S \ell_\alpha\; \overline{\ell_\beta}\Lambda^{R,L}_S \ell^c_\gamma, \\
\overline{\ell_\beta}\Lambda^{L,R}_S \ell_\alpha\; \overline{\ell_\delta}\Lambda^{L,R}_S \ell^c_\gamma &= -\frac{1}{2}\;\overline{\ell_\delta}\Lambda^{L,R}_S \ell_\alpha\; \overline{\ell_\beta}\Lambda^{L,R}_S \ell^c_\gamma - \frac{1}{8}\;\overline{\ell_\delta}\Lambda^{L,R}_T \ell_\alpha\; \overline{\ell_\beta}\Lambda^{L,R}_T \ell^c_\gamma, \\
\overline{\ell_\beta}\Lambda^{L,R}_S \ell_\alpha\; \overline{\ell_\delta}\Lambda^{R,L}_S \ell^c_\gamma &= -\frac{1}{2}\;\overline{\ell_\delta}\Lambda^{L,R}_V \ell_\alpha\; \overline{\ell_\beta}\Lambda^{R,L}_V \ell^c_\gamma, \\
\overline{\ell_\beta}\Lambda^{L,R}_T \ell_\alpha\; \overline{\ell_\delta}\Lambda^{L,R}_T \ell^c_\gamma &= -6\;\overline{\ell_\delta}\Lambda^{L,R}_S \ell_\alpha\; \overline{\ell_\beta}\Lambda^{L,R}_S \ell^c_\gamma + \frac{1}{2}\;\overline{\ell_\delta}\Lambda^{L,R}_T \ell_\alpha\; \overline{\ell_\beta}\Lambda^{L,R}_T \ell^c_\gamma,
\end{aligned} \tag{D.70}$$

where the different Λ^X_A with $A \equiv S,V,T$ and $X \equiv L,R$ are defined in Eq. (C.9).

The form factor $B^{\alpha\beta\gamma\delta}_{V,LL}$ has two types of contributions, coming from the $W^\pm$ boson and $H^\pm$ scalar. The remaining form factors are due to box diagrams with $H^\pm$. We write

$$B^{\alpha\beta\gamma\delta}_{V,LL} = B^{\alpha\beta\gamma\delta(1)}_{V,LL} + B^{\alpha\beta\gamma\delta(2)}_{V,LL}. \tag{D.71}$$

where the $W^\pm$ contribution is

$$B_{V,LL}^{\alpha\beta\gamma\delta(1)} = \sum_{i,j=1}^{n_f} \left[\mathbf{B}_{\alpha i}^* \mathbf{B}_{\gamma i}^* \mathbf{B}_{\beta j} \mathbf{B}_{\delta j} G_{\rm Box}(\lambda_i, \lambda_j) - \mathbf{B}_{\alpha i}^* \mathbf{B}_{\gamma j}^* \left(\mathbf{B}_{\beta i} \mathbf{B}_{\delta j} + \mathbf{B}_{\beta j} \mathbf{B}_{\delta i} \right) F_{\rm Box}^{(2)}(\lambda_i, \lambda_j) \right] . \tag{D.72}$$

For the box form factors with $H^\pm$ we have:

$$\begin{aligned} B_{V,LL}^{\alpha\beta\gamma\delta(2)} = \frac{1}{M_W^2} \sum_{i,j=1}^{n_f} \Bigg\{ & \frac{1}{m_{H^\pm}^2} \left(\mathbf{N}_\nu^\dagger \mathbf{B}^\dagger \right)_{i\alpha} \left(\mathbf{B} \mathbf{N}_\nu \right)_{\beta j} \left(\mathbf{N}_\nu^\dagger \mathbf{B}^\dagger \right)_{i\gamma} \left(\mathbf{B} \mathbf{N}_\nu \right)_{\delta j} F_{\rm Box}^{(4)}(\omega_i, \omega_j) \\ & + \frac{1}{m_{H^\pm}^2} \left(\mathbf{N}_\nu^\dagger \mathbf{B}^\dagger \right)_{i\alpha} \left(\mathbf{N}_\nu^\dagger \mathbf{B}^\dagger \right)_{j\gamma} \left[\left(\mathbf{B} \mathbf{N}_\nu \right)_{\beta j} \left(\mathbf{B} \mathbf{N}_\nu \right)_{\delta i} + (\beta \leftrightarrow \delta) \right] F_{\rm Box}^{(3)}(\omega_i, \omega_j) \\ & + \left[\mathbf{B}_{\alpha i}^* \left(\mathbf{N}_\nu^\dagger \mathbf{B}^\dagger \right)_{i\gamma} + (\alpha \leftrightarrow \gamma) \right] \left[\mathbf{B}_{\beta j} \left(\mathbf{B} \mathbf{N}_\nu \right)_{\delta j} + (\beta \leftrightarrow \delta) \right] \frac{J_{\rm Box}^{(2)}(\lambda_i, \lambda_j, \lambda_\pm)}{2} \\ & + \left[\mathbf{B}_{\alpha i}^* \left(\mathbf{N}_\nu^\dagger \mathbf{B}^\dagger \right)_{j\gamma} + (\alpha \leftrightarrow \gamma) \right] \left[\mathbf{B}_{\beta i} \left(\mathbf{B} \mathbf{N}_\nu \right)_{\delta j} + (\beta \leftrightarrow \delta) \right] H_{\rm Box}^{(1)}(\lambda_i, \lambda_j, \lambda_\pm) \Bigg\}, \end{aligned} \tag{D.73}$$

$$\begin{aligned} B_{V,LR}^{\alpha\beta\gamma\delta} = -\frac{1}{M_W^2} \sum_{i,j=1}^{n_f} \Bigg\{ & \mathbf{B}_{\beta j} \mathbf{B}_{\alpha i}^* \Bigg[\left(\mathbf{N}_e^\dagger \mathbf{B} \right)_{\delta j} \left(\mathbf{B}^\dagger \mathbf{N}_e \right)_{i\gamma} J_{\rm Box}^{(1)}(\lambda_i, \lambda_j, \lambda_\pm) \\ & - \left(\mathbf{B}^\dagger \mathbf{N}_e \right)_{j\gamma} \left(\mathbf{N}_e^\dagger \mathbf{B} \right)_{\delta i} \frac{H_{\rm Box}^{(2)}(\lambda_i, \lambda_j, \lambda_\pm)}{2} \Bigg] - \frac{1}{m_{H^\pm}^2} \left(\mathbf{N}_\nu^\dagger \mathbf{B}^\dagger \right)_{i\alpha} \left(\mathbf{B}^\dagger \mathbf{N}_e \right)_{j\gamma} \\ & \times \left[\left(\mathbf{B} \mathbf{N}_\nu \right)_{\beta i} \left(\mathbf{N}_e^\dagger \mathbf{B} \right)_{\delta j} F_{\rm Box}^{(3)}(\omega_i, \omega_j) + \left(\mathbf{B} \mathbf{N}_\nu \right)_{\beta j} \left(\mathbf{N}_e^\dagger \mathbf{B} \right)_{\delta i} \frac{F_{\rm Box}^{(4)}(\omega_i, \omega_j)}{2} \right] \Bigg\}, \end{aligned} \tag{D.74}$$

$$\begin{aligned} B_{V,RL}^{\alpha\beta\gamma\delta} = -\frac{1}{M_W^2} \sum_{i,j=1}^{n_f} \Bigg\{ & \left(\mathbf{B}^\dagger \mathbf{N}_e \right)_{i\alpha} \left(\mathbf{N}_e^\dagger \mathbf{B} \right)_{\beta j} \Bigg[\mathbf{B}_{\delta j} \mathbf{B}_{\gamma i}^* J_{\rm Box}^{(1)}(\lambda_i, \lambda_j, \lambda_\pm) \\ & - \mathbf{B}_{\delta i} \mathbf{B}_{\gamma j}^* \frac{H_{\rm Box}^{(2)}(\lambda_i, \lambda_j, \lambda_\pm)}{2} \Bigg] - \frac{1}{m_{H^\pm}^2} \left(\mathbf{B}^\dagger \mathbf{N}_e \right)_{i\alpha} \left(\mathbf{N}_\nu^\dagger \mathbf{B}^\dagger \right)_{j\gamma} \\ & \times \left[\left(\mathbf{N}_e^\dagger \mathbf{B} \right)_{\beta i} \left(\mathbf{B} \mathbf{N}_\nu \right)_{\delta j} F_{\rm Box}^{(3)}(\omega_i, \omega_j) + \left(\mathbf{N}_e^\dagger \mathbf{B} \right)_{\beta j} \left(\mathbf{B} \mathbf{N}_\nu \right)_{\delta i} \frac{F_{\rm Box}^{(4)}(\omega_i, \omega_j)}{2} \right] \Bigg\}, \end{aligned} \tag{D.75}$$

$$\begin{aligned} B_{V,RR}^{\alpha\beta\gamma\delta} = \frac{1}{M_W^2 m_{H^\pm}^2} \sum_{i,j=1}^{n_f} \Bigg\{ & \left(\mathbf{B}^\dagger \mathbf{N}_e \right)_{i\alpha} \left(\mathbf{N}_e^\dagger \mathbf{B} \right)_{\beta j} \left(\mathbf{B}^\dagger \mathbf{N}_e \right)_{i\gamma} \left(\mathbf{N}_e^\dagger \mathbf{B} \right)_{\delta j} F_{\rm Box}^{(4)}(\omega_i, \omega_j) \\ & + \left(\mathbf{B}^\dagger \mathbf{N}_e \right)_{i\alpha} \left(\mathbf{B}^\dagger \mathbf{N}_e \right)_{j\gamma} \left[\left(\mathbf{N}_e^\dagger \mathbf{B} \right)_{\beta j} \left(\mathbf{N}_e^\dagger \mathbf{B} \right)_{\delta i} + \left(\mathbf{N}_e^\dagger \mathbf{B} \right)_{\beta i} \left(\mathbf{N}_e^\dagger \mathbf{B} \right)_{\delta j} \right] F_{\rm Box}^{(3)}(\omega_i, \omega_j) \Bigg\}, \end{aligned} \tag{D.76}$$

$$\begin{aligned} B_{S,LL}^{\alpha\beta\gamma\delta} = -\frac{1}{M_W^2 m_{H^\pm}^2} \sum_{i,j=1}^{n_f} \Bigg\{ & \Bigg[\left(\mathbf{N}_\nu^\dagger \mathbf{B}^\dagger \right)_{i\alpha} \left(\mathbf{N}_\nu^\dagger \mathbf{B}^\dagger \right)_{j\gamma} \Big(\left(\mathbf{N}_e^\dagger \mathbf{B} \right)_{\beta i} \left(\mathbf{N}_e^\dagger \mathbf{B} \right)_{\delta j} \\ & - \frac{1}{2} \left(\mathbf{N}_e^\dagger \mathbf{B} \right)_{\beta j} \left(\mathbf{N}_e^\dagger \mathbf{B} \right)_{\delta i} \Big) + \left(\mathbf{N}_\nu^\dagger \mathbf{B}^\dagger \right)_{i\alpha} \left(\mathbf{N}_e^\dagger \mathbf{B} \right)_{\beta j} \left(\mathbf{N}_\nu^\dagger \mathbf{B}^\dagger \right)_{i\gamma} \left(\mathbf{N}_e^\dagger \mathbf{B} \right)_{\delta j} \Bigg] F_{\rm Box}^{(4)}(\omega_i, \omega_j) \Bigg\}, \end{aligned} \tag{D.77}$$

$$\begin{aligned} B_{S,LR}^{\alpha\beta\gamma\delta} = \frac{1}{M_W^2} \sum_{i,j=1}^{n_f} \Bigg\{ & \mathbf{B}_{\delta j} \mathbf{B}_{\alpha i}^* \Bigg[\left(\mathbf{N}_e^\dagger \mathbf{B} \right)_{\beta j} \left(\mathbf{B}^\dagger \mathbf{N}_e \right)_{i\gamma} 2 J_{\rm Box}^{(1)}(\lambda_i, \lambda_j, \lambda_\pm) \\ & - \left(\mathbf{B}^\dagger \mathbf{N}_e \right)_{j\gamma} \left(\mathbf{N}_e^\dagger \mathbf{B} \right)_{\beta i} H_{\rm Box}^{(2)}(\lambda_i, \lambda_j, \lambda_\pm) \Bigg] - \frac{1}{m_{H^\pm}^2} \left(\mathbf{N}_\nu^\dagger \mathbf{B}^\dagger \right)_{i\alpha} \left(\mathbf{B}^\dagger \mathbf{N}_e \right)_{j\gamma} \\ & \left[\left(\mathbf{B} \mathbf{N}_\nu \right)_{\delta i} \left(\mathbf{N}_e^\dagger \mathbf{B} \right)_{\beta j} 2 F_{\rm Box}^{(3)}(\omega_i, \omega_j) + \left(\mathbf{B} \mathbf{N}_\nu \right)_{\delta j} \left(\mathbf{N}_e^\dagger \mathbf{B} \right)_{\beta i} F_{\rm Box}^{(4)}(\omega_i, \omega_j) \right] \Bigg\}, \end{aligned} \tag{D.78}$$

$$B_{S,RL}^{\alpha\beta\gamma\delta} = \frac{1}{M_W^2} \sum_{i,j=1}^{n_f} \Bigg\{ \left(\mathbf{B}^\dagger \mathbf{N}_e \right)_{i\alpha} \left(\mathbf{N}_e^\dagger \mathbf{B} \right)_{\delta j} \Bigg[\mathbf{B}_{\beta j} \mathbf{B}_{\gamma i}^* 2 J_{\rm Box}^{(1)}(\lambda_i, \lambda_j, \lambda_\pm)$$

$$- \mathbf{B}_{\beta i}\mathbf{B}^{*}_{\gamma j} H^{(2)}_{\rm Box}(\lambda_i,\lambda_j,\lambda_\pm)\Big] - \frac{1}{m^2_{H^\pm}} \left(\mathbf{N}^\dagger_\nu \mathbf{B}^\dagger\right)_{j\gamma} \left(\mathbf{B}^\dagger \mathbf{N}_e\right)_{i\alpha}$$
$$\left[\left(\mathbf{B}\mathbf{N}_\nu\right)_{\beta j} \left(\mathbf{N}^\dagger_e \mathbf{B}\right)_{\delta i} 2F^{(3)}_{\rm Box}(\omega_i,\omega_j) + \left(\mathbf{B}\mathbf{N}_\nu\right)_{\beta i} \left(\mathbf{N}^\dagger_e \mathbf{B}\right)_{\delta j} F^{(4)}_{\rm Box}(\omega_i,\omega_j)\right]\Bigg\}, \tag{D.79}$$

$$B^{\alpha\beta\gamma\delta}_{S,RR} = -\frac{1}{M^2_W m^2_{H^\pm}} \sum_{i,j=1}^{n_f} \Bigg\{ \Bigg[\left(\mathbf{B}^\dagger \mathbf{N}_e\right)_{i\alpha} \left(\mathbf{B}^\dagger \mathbf{N}_e\right)_{j\gamma} \Big(\left(\mathbf{B}\mathbf{N}_\nu\right)_{\beta i} \left(\mathbf{B}\mathbf{N}_\nu\right)_{\delta j}$$
$$- \frac{1}{2} \left(\mathbf{B}\mathbf{N}_\nu\right)_{\beta j} \left(\mathbf{B}\mathbf{N}_\nu\right)_{\delta i} \Big) + \left(\mathbf{B}^\dagger \mathbf{N}_e\right)_{i\alpha} \left(\mathbf{B}\mathbf{N}_\nu\right)_{\beta j} \left(\mathbf{B}^\dagger \mathbf{N}_e\right)_{i\gamma} \left(\mathbf{B}\mathbf{N}_\nu\right)_{\delta j} \Bigg] F^{(4)}_{\rm Box}(\omega_i,\omega_j) \Bigg\}, \tag{D.80}$$

$$B^{\alpha\beta\gamma\delta}_{T,LL} = \frac{1}{M^2_W m^2_{H^\pm}} \sum_{i,j=1}^{n_f} \Bigg\{ \left(\mathbf{N}^\dagger_\nu \mathbf{B}^\dagger\right)_{i\alpha} \left(\mathbf{N}^\dagger_e \mathbf{B}\right)_{\beta j} \Big[\left(\mathbf{N}^\dagger_\nu \mathbf{B}^\dagger\right)_{i\gamma} \left(\mathbf{N}^\dagger_e \mathbf{B}\right)_{\delta j}$$
$$+ \frac{1}{2} \left(\mathbf{N}^\dagger_\nu \mathbf{B}^\dagger\right)_{j\gamma} \left(\mathbf{N}^\dagger_e \mathbf{B}\right)_{\delta i} \Big] \frac{F^{(4)}_{\rm Box}(\omega_i,\omega_j)}{4} \Bigg\}, \tag{D.81}$$

$$B^{\alpha\beta\gamma\delta}_{T,RR} = \frac{1}{M^2_W m^2_{H^\pm}} \sum_{i,j=1}^{n_f} \Bigg\{ \left(\mathbf{B}^\dagger \mathbf{N}_e\right)_{i\alpha} \left(\mathbf{B}\mathbf{N}_\nu\right)_{\beta j} \Big[\left(\mathbf{B}^\dagger \mathbf{N}_e\right)_{i\gamma} \left(\mathbf{B}\mathbf{N}_\nu\right)_{\delta j}$$
$$+ \frac{1}{2} \left(\mathbf{B}^\dagger \mathbf{N}_e\right)_{j\gamma} \left(\mathbf{B}\mathbf{N}_\nu\right)_{\delta i} \Big] \frac{F^{(4)}_{\rm Box}(\omega_i,\omega_j)}{4} \Bigg\}, \tag{D.82}$$

where $\mathbf{N}_e$ and $\mathbf{N}_\nu$ have been defined in Eqs. (B.8) and (B.9), respectively. The loop functions relevant for the leptonic box form factors are

$$\begin{aligned} G_{\rm Box}(x,y) &= \sqrt{xy}\left[(4+xy)d_0(x,y) - 2\widetilde{d}_0(x,y)\right] \\ &= -\frac{\sqrt{xy}}{x-y}\left\{(4+xy)\left[\frac{1}{1-x} + \frac{x}{(1-x)^2}\ln x - \frac{1}{1-y} - \frac{y}{(1-y)^2}\ln y\right]\right. \\ &\left. -2\left[\frac{1}{1-x} + \frac{x^2}{(1-x)^2}\ln x - \frac{1}{1-y} - \frac{y^2}{(1-y)^2}\ln y\right]\right\}, \end{aligned} \tag{D.83}$$

$$\begin{aligned} J^{(1)}_{\rm Box}(x,y,z) &= -\frac{\sqrt{xy}}{4}\left[\widetilde{d}_0(x,y,z) + 4d_0(x,y,z)\right] \\ &= -\frac{\sqrt{xy}}{4}\left[\frac{x(x+4)\ln x}{(1-x)(x-y)(x-z)} + \frac{y(y+4)\ln y}{(1-y)(y-x)(y-z)} + \frac{z(z+4)\ln z}{(1-z)(z-x)(z-y)}\right], \end{aligned} \tag{D.84}$$

$$\begin{aligned} J^{(2)}_{\rm Box}(x,y,z) &= -\widetilde{d}_0(x,y,z) - xy\; d_0(x,y,z) \\ &= -\left[\frac{x^2(1+y)\ln x}{(1-x)(x-y)(x-z)} + \frac{y^2(1+x)\ln y}{(1-y)(y-x)(y-z)} + \frac{z(z+xy)\ln z}{(1-z)(z-x)(z-y)}\right]. \end{aligned} \tag{D.85}$$

The contributions to the box form factors stemming from $H^\pm$ in the loop are consistent with the derivation performed in Ref. [219]. We refer the reader to Refs. [207, 211] where charged-Higgs contributions were considered in the context of low-scale seesaw SUSY. This enabled us to check the types of loop functions and of matrix and chiral structures that enter the resulting form factors. However, to the best of our knowledge, the box form factors and loop functions presented in a compact form in this work within the framework of a seesaw type model and 2HDM scalar sector have not been presented elsewhere.